Deep Sea Mining In Soft Clay: An Adhesion Problem

Mitigating Adhesion on Deep Sea Harvester

by

Zeid Bitar

in fulfilment of the requirements for the degree of
Master of Science
at the Delft University of Technology,
to be defended publicly in February 2021.

Confidential: Repository Version

Student number:	4435877	
Project duration:	February 17, 2020 – February, 2021	
Thesis Committee:	Dominique Ngan-Tillard	*TU Delft, CEG*
	Yenigul Buket	*Allseas*
	Wout Broere	*CEG*
	Sape Miediema	*3mE*

Delft University of Technology
Faculty of Civil Engineering and Geo-Sciences
Master Applied Earth Sciences

Abstract

The clay adhesion phenomenon has been problematic in multiple engineering projects involving soft cohesive soils. In this dissertation, the adhesive characteristics of offshore high plasticity clay will be analyzed in support to deep sea mining applications. Adhesion of clays are particularly relevant in 2:1 swelling clays, where the magnitude of the force is highly dependant on the clay properties itself, working conditions and the soil engaging component surface material. The most prevalent force in offshore saturated conditions arises from the suction forces between micro-channels in the clay and the soil engaging component. Methods to reduce this adhesive force were assessed, ranging from solutions such as vibrations and electro-osmosis, to modifying the soil engaging surface to break continuous contacts between the clay and component. The natural adhesion of two typical offshore clays were experimentally determined by interface shear tests for the shear adhesion and pull-out tests for tensile adhesion. Interfacial shear strength was measured for typical materials found in the offshore industry, that being steel, aluminium, rubber and a polymer coating. Results from the tests showed that materials do have an impact on adhesive stresses. Similarly, pull-out tests showed this variation pattern. The influence of pull-out rates and contact time on adhesive tensile strength were also assessed and showed to increase with faster rates and longer contact times, respectively. In application to a typical rotational cutterwheel in deep sea mining, a scaled test-setup of a rack of cutter-teeth was dragged through the test clay to acquire horizontal cutting forces with the utilization of the experimentally found natural adhesion in the interface tests. The found adhesion value for the test clays were utilized to validate the cutting clay model from "The Delft Sand, Clay & Rock Cutting Model" (Miedema, 2019). Practical results from the scaled experiment seemed to coincide relatively well with the theoretical model. It is therefore recommended to further investigate the use of experimental means to determine adhesion of clays to develop an even more accurate empirical model.

Contents

List of Figures

List of Tables

1 Introduction

The phenomenon of soil adhesion is an often disregarded in many engineering calculations when dealing with fine grained cohesive soil. In recent times, the study of soil adhesion has been increasingly sought out due to contribution to unwanted resistive forces such as in tillage tools and clogging of flow ducts and chambers such as in TBM's. Researchers such as (Thewes, 1954), (Fountaine, 1954), and (Burbaum, 2009) have established a basis of understanding of the mechanism of adhesion in relation to soil properties and soil disturbance methods. Most of past research on adhesion were in relation to TBM excavation, as this excavation method has been popularized by increasing urban development due to the lack of space to transport the masses. However, the implementation of this engineering knowledge can be scoped out into offshore (saturated) conditions. The ever growing demand for the increase in infrastructure, global trade, and mineral resources in recent times have pushed engineering construction from continental grounds into the ocean. The offshore industry is expected to grow profusely over the coming years, particularly constructions such as monopile wind turbines, pipelines, cable routes and deep sea mining harvesters. In this dissertation, the fundamentals of clay adhesion will be explored in the application of deep sea mining harvesters.

Allseas, in collaboration with Deep Green, are set to deploy a pilot mining test of a new deep sea harvester in the Clarion-Clipperton submarine fracture zone in the Pacific Ocean. On the surface of the seabed lies an estimated 21 billion tons of polymetallic nodules laying on a very soft high plasticity clay sea bed. For the collection of nodules, a number of offshore companies have been developing a concept design of a mechanical rotating cutter wheel to scoop the nodules from the seabed and pump the nodules through a vertical transport system (VTS) onto the supplementary barge. The nodules are then to be taken to a processing plant to extract and concentrate the valuable metals. A schematic overview of the deep sea mining process is shown on Figure 1.1:

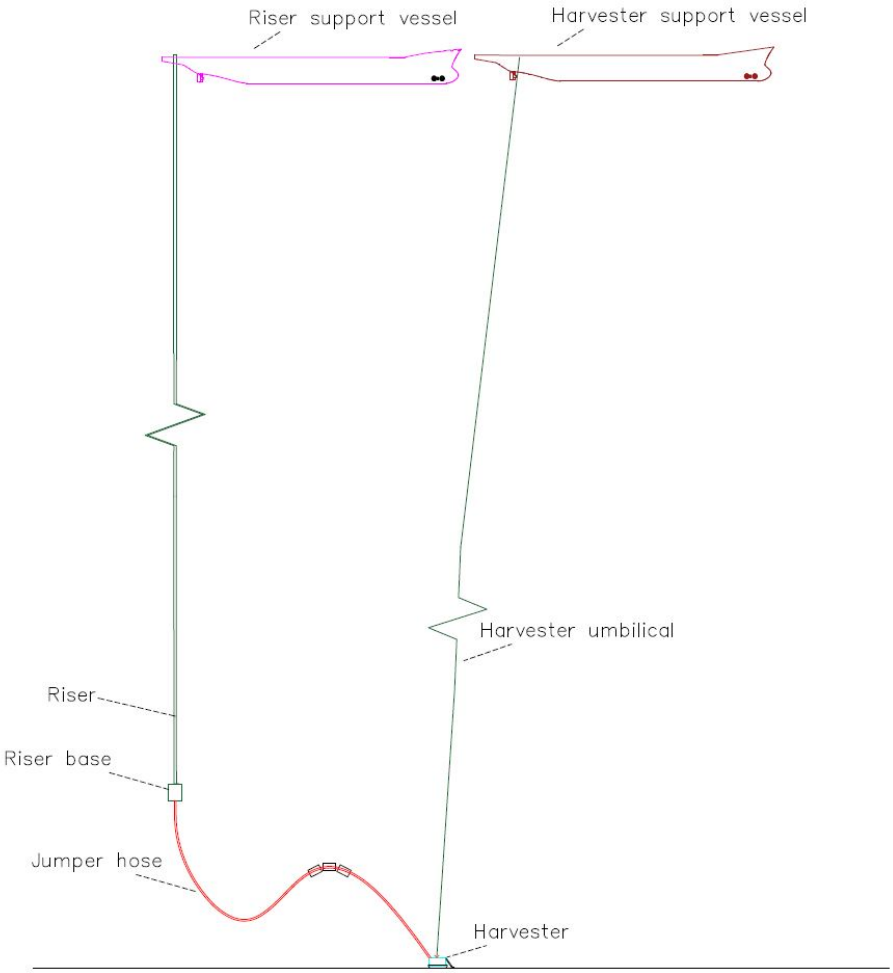

Figure 1.1: DSM Overview

The harvester will run on tracks and thrusters which will consist of a rotating cutter wheel in the front that will act as scoops to pick up the nodules. The picked up nodules along with an inevitable amount of seabed sediment will then be pumped through tubes into a hopper container, where the nodules are transferred to the VTS and the clay sediment is ejected out by a diffuser behind the harvester trailing direction. The general process of a deep sea crawler is shown as a schematic sketch on Figure 1.2:

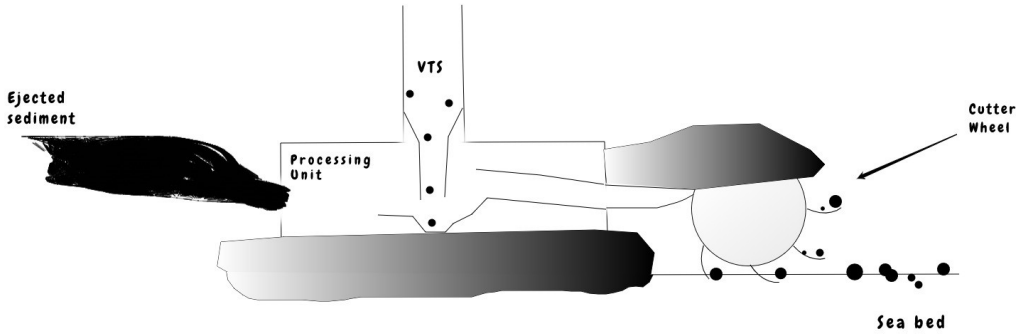

Figure 1.2: Conceptual Harvester Drawing

The design objectives of the harvester for the pilot mining system are listed below:

- Capable of picking nodules up to 10 cm below the seafloor
- Reject nodules with an axis diameter greater than 80 mm
- Capable of separating nodules from clay sediment before transport to the VTS
- Capable of dispersing the separated sediment from the nodules

To be able to efficiently achieve these objectives, an in-depth study of the mechanical and geotechnical aspects of the collection system needs to be set. As part of this in-depth study, this dissertation will focus on the geotechnical side of the collection system, which will entail the soil interaction with the cutter-wheel. With a theoretical basis of adhesion mechanisms and clay cutting, a more qualitative understanding of clay adhesion interactions with soil engaging components can be drawn. A qualitative understanding of the adhesion phenomenon leads to more insight on how engineers can predict the impact adhesive forces in a particular project. In other words, more qualitative understanding leads to more developments in analysing clay adhesion quantitatively by experimental means.

1.1 Introduction to Deep Sea Mining

Deep sea mining is a retrieval process of minerals on or in the ocean floor. In recent years, with the rapid development of technologies and infrastructure, the need for mineral and metal supplies are increasing exponentially. New technological advancements and commercial projects are under immense pressure to adhere to eco-friendly regulations due to growing concerns of global warming and diminishing viable ore deposits. Using wind, solar, and other renewable energy sources increases the demand of many metal minerals for the use of advanced technologies such as energy storage batteries. According to the report "The Growing Role of Minerals and Metals for a Low-Carbon Future" (Arrobas, Hund, Mccormick, Ningthoujam, & Drexhage, 2017), minerals and metals expected to see a heightened demand in the future include: aluminium, copper, lead, lithium, manganese, cobalt, nickel, silver, steel, zinc and rare earth minerals. Whether the need for these minerals are for high-end technological developments or a geopolitical tool in an increasingly unstable global market, the necessity is quite evident. Large mining cooperation's will tend to mine commercially profitable regions rather than deal with low grade ores. Therefore, the shift of focus is slowly turning deep sea mining. Deep sea mining entails retrieving mineral rich resources on the sea floor. The main type of these mineral rich resources are cobalt-rich manganese crusts, polymetallic manganese nodules, and polymetallic massive sulphides (SMS deposits).

1.2 The Offshore environment

One of the most challenging aspects of offshore engineering is acquiring and interpreting geotechnical data due to the complexity of the geological history of submarine sediments. Issues with operating in such deep waters include:

- Site investigations are extremely expensive (right vessels, mobilisation etc)
- Soil conditions are unusual and highly variable. However, in abyssal plains this is less so.
- Applied loads are very large, highly variable environmental loads
- Design modifications are not possible or will cost a lot of money and time to achieve

Characteristic soil conditions arise from a long history of complex geological and geomorphological processes prior to, during and after deposition. The earth is an ever moving and dynamic body which creates, erodes, and destroys matter in a never-ending rock cycle. In engineering practices, it is only the more recent history of the encountered sediments that are of concern which entail the most significant geotechnical properties due to the presence on the surface. Understanding the recent geological history helps build an environmental ground regime which in combination with mass properties and imposed changes will formulate the total ground response.

The earth's continental plates vary in thickness between 80 km and 400 km where the top layer of the continental plates is referred to as the crust. Simplistically, crust located underneath the ocean are 'oceanic crusts' while the crust above sea level are referred to as the 'continental crust'. Due to tectonic movements, the oceanic crust is continuously being created at various mid-oceanic ridges with new crust being pushed up into the seabed at 'spreading centres' and pushed down into the mantle at subduction zones. Spreading can occur at a rate of up to 100 mm/year, but often less than 30 mm/year (Randolph & Gourvenec, 2011). The tectonic activity in the oceanic crusts not only produce new sediment material but also multiple fracture zones due to plate collisions or seabed extension such as that observed in the Clarion Clipperton Zone. Due to weathering and erosion processes, there is an increase in inclination from deep abyssal plain regions to the continental shelf. The geology common to all oceans consists of the continental margin, the continental rise and abyssal plains of the deep ocean.

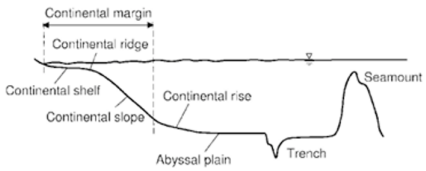

Figure 1.3: Topigraphical features of ocean floors (Poulos, 1988)

The continental margin is underlain by continental crust and can be classified as a relatively high energy environment. The impact submarine slides, turbidity currents, and slope failures cause sediments to have very low lateral continuity. Going deeper into the ocean the continental rise has a much more gently dipping slope and is underlain by a transition from continental to oceanic crust. The continental rise usually has soft underconsolidated sediments. At the deepest ocean depths lies the abyssal plain. These plains lie about 5000 meters of ocean depth and has a smooth and flat seafloor. It is underlain solely by the oceanic crust, and has little to no offshore activity.

Marine clay is a type of soil that largely exists at the coastal corridors, low lands and offshore areas as well as other parts of the earth. It is a soft sensitive soil that usually exhibits unfavourable engineering properties such as high settlement capacity, low shear strength, uncertainty of performance, low unconfined compressive strength and high adhesive potential. Marine clay often display high natural moisture contents (39% to about 175%) so therefore this type of clay has

the tendency to absorb large quantities of water until it loses its shape and is often found in a slurry form (Al-Bared & Marto, 2017). In the abyssal plain, the clay deposits on the seabed are a result of a continuum of processes including pelagic settling, reworking by bottom currents, and resedimentation by mass (Shephard & Rutledge, 1991). In the deep ocean currents are driven by thermohaline circulation – meaning circulation driven by density variations in the water due to temperature (thermo) and salinity (haline). Sediments from the debris flow from the continental slope are dispersed into turbidites which eventually settle and flocculate over a long period of time to form a mainly clay abyssal sea bed.

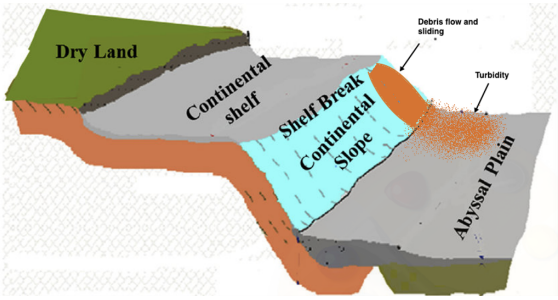

Figure 1.4: Marine geology: Turbidity formation

In deep ocean depths, pelagic sediments are typically found. Pelagic sediments are generally fine grained and range in color from white to a dark reddish-brown. These sediments may be either inorganic or organic in origin. Those pelagic sediments which contain less than about 30% of organic remains are called red clay and those which contain more than about 30% are known as oozes (Mero, 1965). Red clay consists of hydrated aluminium-silicate minerals resulting from the end product of weathering of terrestrial igneous rocks which have been deposited in the water column, mixed with iron oxides and settled on the ocean bottom. Oozes can be calcareous or siliceous. Both ooze types are formed from skeletal remains of planktonic plants and animals.

1.3 Polymetallic Nodules

Polymetallic nodules are rock concretions that are usually spherical in shape with axis lengths ranging from 0.2 cm to larger than 10 cm. The nodules are composed of concentric layers of manganese and iron around a nuclei source. The development of these nodules are very slow, growing a few millimeters in a million years. Polymetallic nodules are attractive to exploit due to their shear abundance in deep sea basins and the growing demand of metal minerals. Manganese nodules are particularly abundant in the Clarion-Clipperton Fracture Zone (CCZ), the Peru Basin, the Penrhyn-Samoa Basin, and the Central Indian Ocean Basin (Hein, Mizell, Koschinsky, & Conrad, 2013). The primary sources of metals for the nodule deposits are terrigenous or volcanogenic sources on North and Central American continents and the East Specific Rise. According to the ISA research center (ISA, 2010), six factors are believed to be important to nodule formation:

- Supply of metals to growing surface
- Presence of nucleus
- The corrosive and erosive forces caused by benthic currents of the Antarctic Bottom water
- Occurrence of semi-liquid surface layer on the seafloor (sediment water interface)
- Bioturbation; and
- Internal Stratigraphy of individual nodules.

During collection, the nodules will preferably have an axial length of less than 8 cm to avoid damaging the harvester tubes. Shipboard taken properties of the nodules such as volumetric density

and water content can be measured immediately after the samples are retrieved. Other physical properties such as dry nodule density, porosity, void ratio, and specific nodule density can be subsequently calculated. While these properties are of concern when processing the nodules, they are not of interest during the collection phase. However, one particular property, the Uniaxial Compressive strength (UCS), is important to know when designing a collection system. Unnecessary breakage of the nodules could lead to significant losses of nodule concentrations from being lost through the collection wheel or pumped in suspension out of the harvester. The UCS test itself is rather simple and can be performed on board after retrieving the nodules, such as the use of the Schmidt hammer. The UCS is a simple measure of how much compressive force the nodule can sustain before breaking. This is not a standardized test because it is impossible to cut a standard shape (such as cylinder for rocks) due to the surface irregularities. Generally, the UCS values differ according to the size, shape, and location of the stress applied. However, Dreseitl (Dreiseitl, 2017) generalized the nodule strength from 127 measurements to have a UCS of 1.02 to 1.34 MPa for medium sized nodules and < 1 MPa for larger ones (above 8 cm). This was plotted in a graph showing the size relation with the UCS:

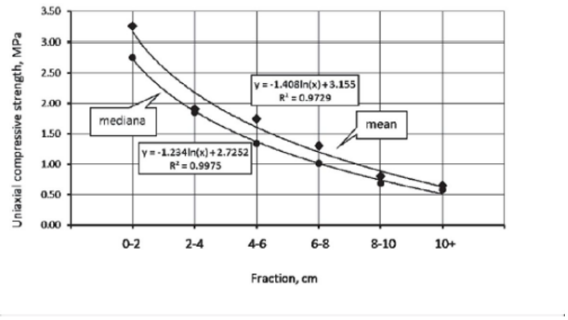

Fig. 4 Nodule strength and the fractions

Figure 1.5: UCS vs Nodule size (Dreiseitl, 2017)

1.4 Site Investigation Review

Due to the discovery of polymetallic nodules concentrated in the Clarion-Clipperton Zone, the area has been investigated relatively thoroughly compared to other abyssal regions.

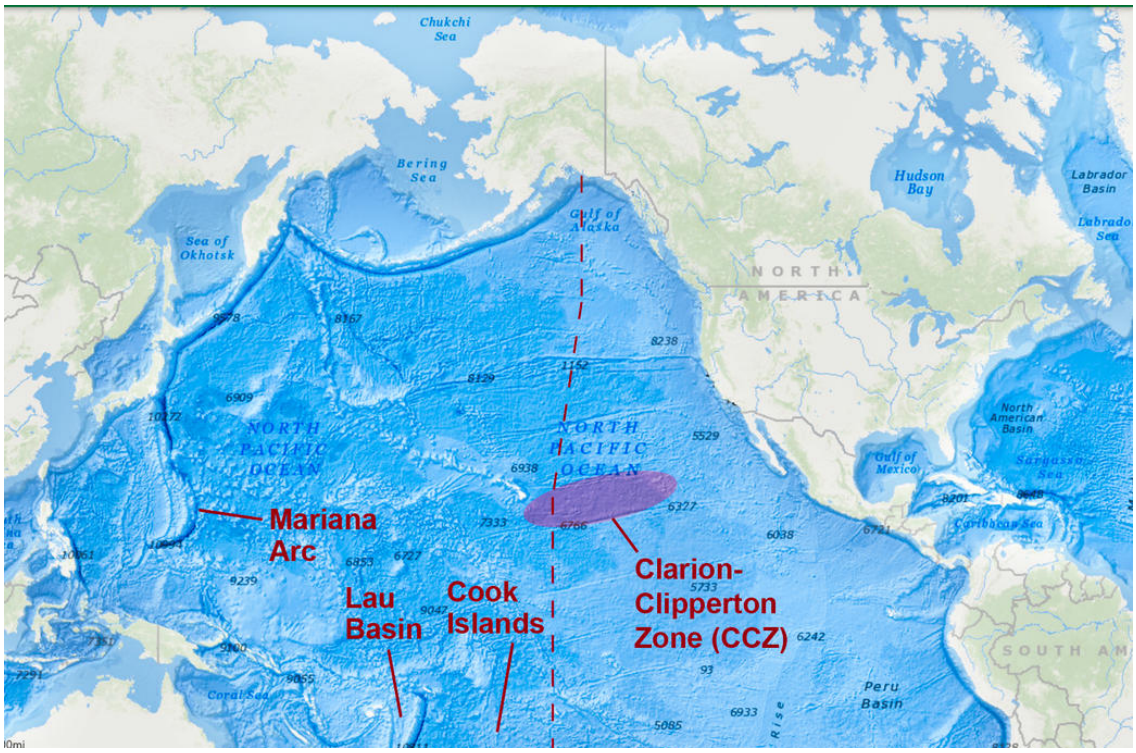

Figure 1.6: Clarion-Clipperton Fracture Zone Location

The Clarion-Clipperton Fracture Zone is a submarine fracture zone on the Pacific plate formed on the western flank of the East Pacific Rise between the Cretaceous and the Miocene. The CCZ is defined by two major WSW-ENE trending fracture zones, the Clipperton to the south and the Clarion to the north as shown on Figure 1.7 (Matthew, 2012). The area spans approximately 5.5 million km^2, extending 5200 km between 116° W and 155° W, and 1000 km between 5° N and 15° N.

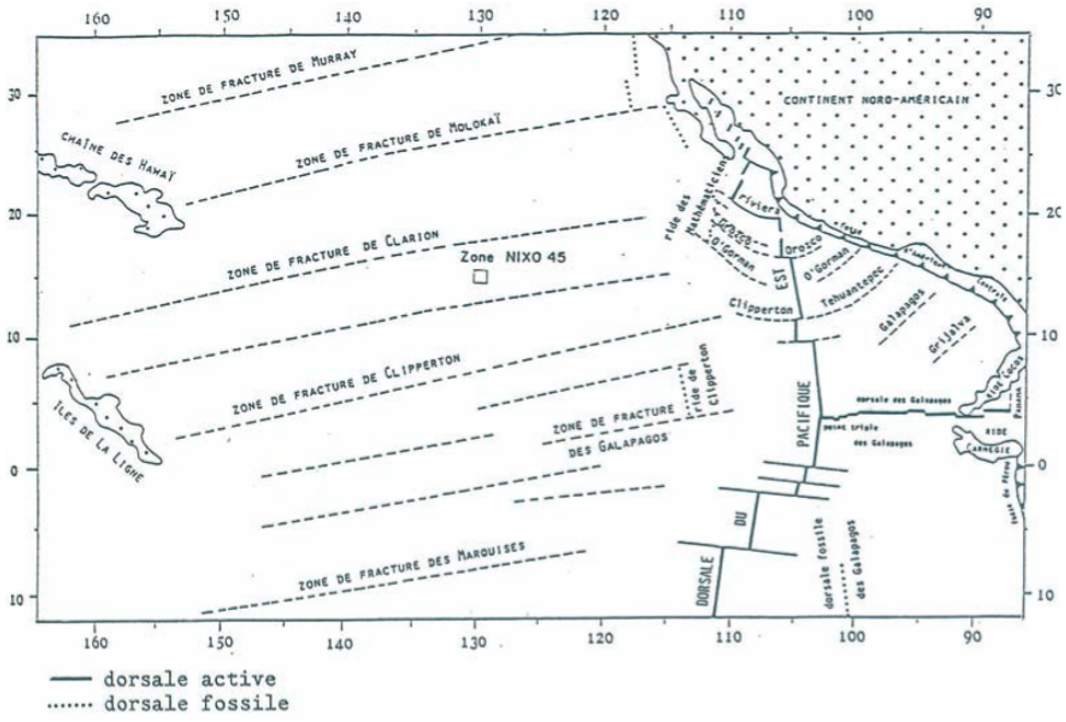

Figure 1.7: CCZ Regional Geological setting (Tilot, 2006)

According to recent studies, particularly the ISA report of the geology of the Clarion Clipperton region, a general overview of the bathymetry and sediments can be established. The CCZ geomorpholigical structure conforms to the pattern of a typical seabed structure of mid-ocean ridges and adjacent basins. To the North and south, the Clairon Clipperton fractures form part of major oceanic structures which carve the Pacific abyssal plain into large parallel strips, oriented E-W for more than 5000 km and reaching 5,500 m depth (Tilot, 2006). During the time of the formation of the CCZ, the Pacific plate saw significant changes in its plate motion which are reflected in changes of strike directions of the seafloor spreading anomalies as well as in bends of the fracture zones (Barckhausen, Bagge, & Wilson, 2013).

The bathymetric characteristics within the CCZ follow a pronounced order, most commonly consisting of trends that line up with the overall movement of the Pacific Plate and trends perpendicular to this direction. Generally water depths and crustal age increases with distance from the East Pacific Rise. The ocean floor is a hilly plain plateau crossed by a strictly north-south system of horst and graben structures (ISA, 2010). The Clarion Clipperton fractures form part of major oceanic structures which carve the Pacific abyssal plain.

The sediment facies show a trend of predominantly carbonate sediments in the south-east to reddish brown clay in the northwest. The surface sediments consist of Pleistocene-Holocene siliceous clay underlain by Miocene to Pliocene pelagic clay, zeolitic clay and crust. The most common sediment types in this region include reddish brown clay zeolitic clay (less than 5% amorphous silica content), slightly siliceous (with 5-10% amorphous silica content), siliceous (10-30%) amorphous silica content) silty clay as well as slightly calcareous (5-10% calcium carbonate content) and calcareous (10-30% calcium carbonate content) silty clay (ISA, 2010). Mixtures of these types dominate the vast majority of the CCZ seabed. (Zawadzki, Maciag, Abramowski, & McCartney, 2020) classified the sediment deposit in the eastern CCZ region from exploration projects covering 75,000 km^2 of the Interoceanmetal Joint Organisation (IOM) which is consortium of six

states: Bulgaria, Cuba, Czech Republic, Poland, Russia, and Slovakia. A total of 135 box core samples were collected from 45 different sampling sites. The lithology is consistent with previous research of the area. The top 32 cm of each box-core was divided into four horizons based on the consistency, water content, and sediment color shown in Figure 1.8.

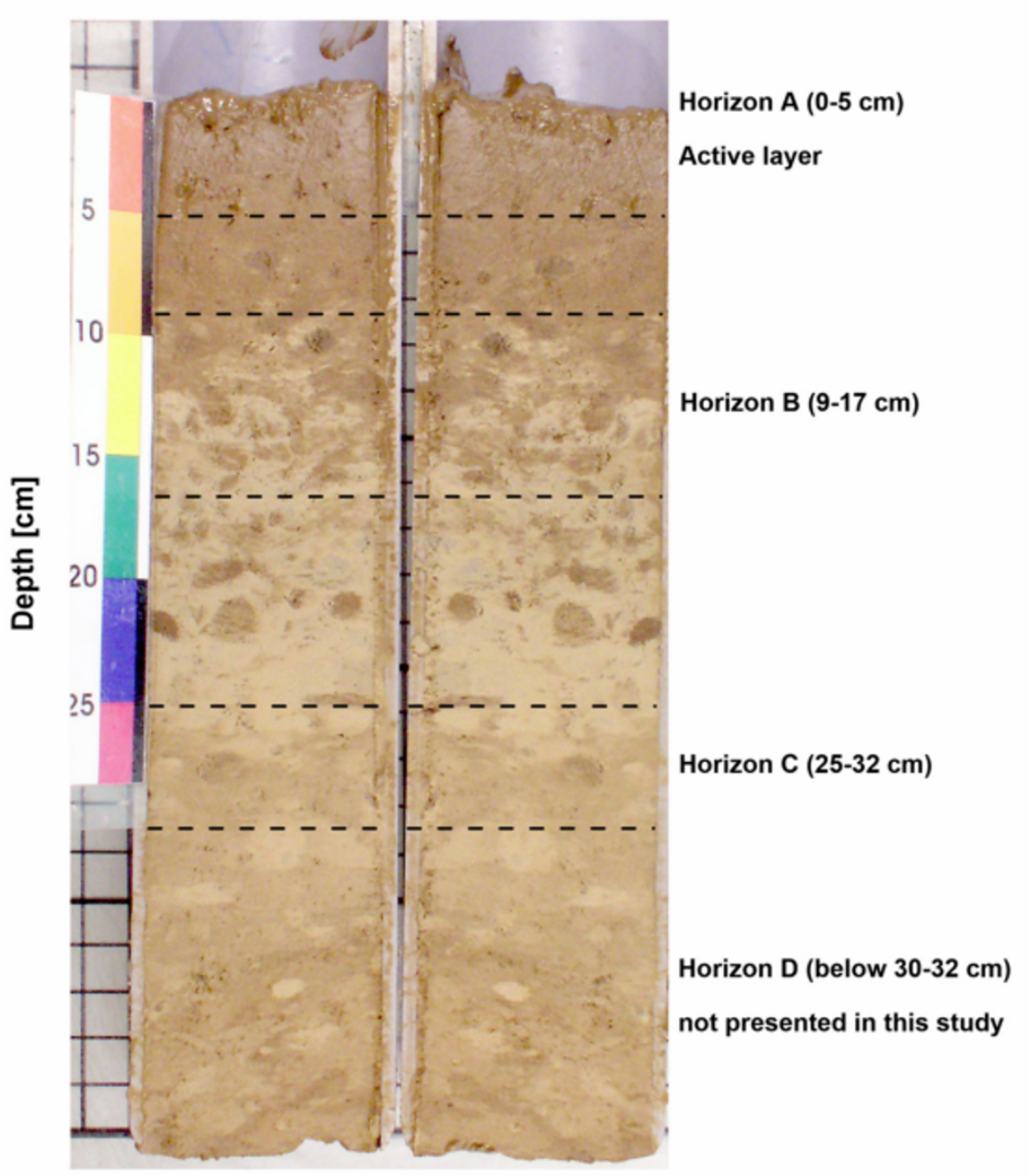

Figure 1.8: Typical Lithology from Box Core Samples in the CCZ (Zawadzki et al., 2020)

.

The description of the four horizons are as follows:

- horizon A: semiliquid geochemically active surface layer (0-5 cm). This layer contains the highest amount of polymetallic nodules.

- horizon B: (9-17 cm) Transitional layer, highly plastic more firm than horizon A.
- horizon C: (25-32 cm) Dark beige with brownish bioturbation, moderate water content and more firm than A and B.
- horizon D: (30-32 cm) lowest water content and greatest firmness

During mining operations, it is hoped that the harvester will not penetrate more than 18 centimeters. This means that horizon A and B will be of main concern. XRD tests was done on 41 selected samples. It was found that the clay content was consistent across all horizons of a mean of around 32%. The clay minerals were dominated by dioctahedral Fe-smectite, illite and mixed-layered ilite-smectite. Smectite was the the main constituent (mean about 16.3% of clay content) and was more dominant in horizons B and C. As discussed previously, smectite is a water adsorbing mineral and is associated with a high cation exchange capacity and therefore larger plasticity index. This could explain why previous pilot mining harvesters failed to perform under these very sticky conditions.

1.5 Jurisdiction, Laws and Regulations

The United Convention of the Law of the Sea (UNCLOS) is the international agreement which dictates the rights and responsibilities of nations when dealing with oceans including establishing guidelines for environmental and socio-economic policies. Generally, marine beach deposits lie within the jurisdiction of the coastal nation in which the beach is located. However, deposits of the deep sea, such as polymetallic nodules, have entirely different set of laws. For access and guidelines to these nodules is governed by the International Seabed Authority (ISA). The ISA (Part XI of UNCLOS) - is an organisation responsible for dictating the rules for mining in seabed areas that are outside national jurisdiction. The ISA has appointed 18 contractors for the exploration of polymetallic nodules in the Clarion Clipperton Zone as displayed on Figure 1.9.

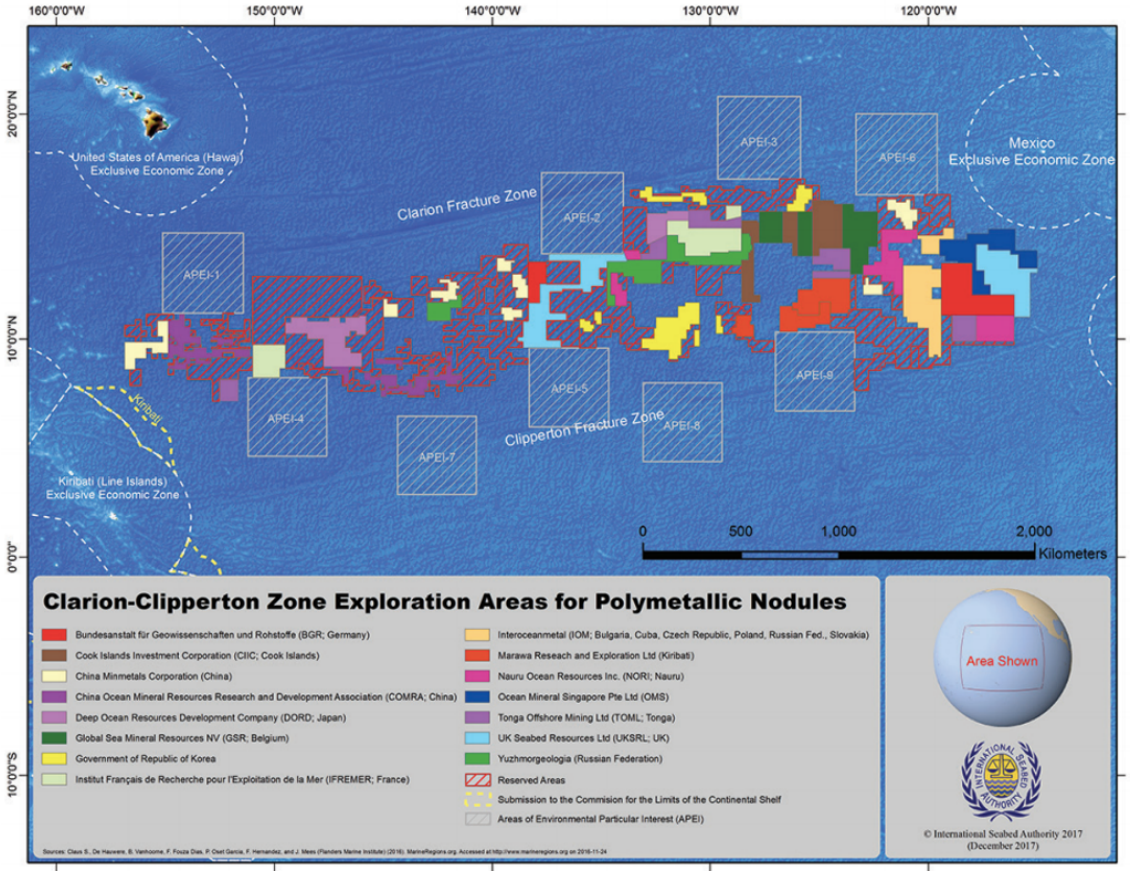

Figure 1.9: Clarion-Clipperton Zone Division (ISA, 2010)

A confining restraint on the operation of harvesters when mining nodules is the environmental impact. The seabed containing nodules are inhabited by sessile and mobile megafauna ($> 2cm$), macrofauna ($1 - 2cm$), meiofauna ($< 1cm$), and bacteria (Koschinsky et al., 2018). Many of these organisms depend on nutrients that settle down to the seafloor such as fecal pellets. This makes the present organisms one of the most food limited creatures on earth. It is easy to understand the sensitivity of these organisms to changes in water fluxes and temperature. This is particularly concerning when designing a deep sea harvester, as ejected sediment could span a significantly large area. Plume productions should be limited which in turn adds restraints in production speed. Clay particles take ages to settle on the seafloor which can disturb the natural habitat of the present flora and fauna. UNCLOS article 145 states that pollution should be controlled to utmost care and to prevent any harm to the ecological balance of the marine environment. Therefore any action or policy that has a risk of causing significant damage to the environment can be revoked. It is therefore important that every design feature of the harvester and offshore related activity adheres to these guidelines.

2 Problem Statement

The Clarion-Clipperton Zone consists of very soft high plasticity clay on the top layer for most of the region. This type of clay has been proven to be problematic in a multitude of offshore projects due to its tendency to stick or "adhere" onto the sub-sea equipment based on projects in the region. Royal IHC has also developed a concept design for a harvester with a rotary mechanical cutter-wheel as part of the Blue Nodules project. Blue nodules is a research and innovation project to develop a deep sea mining system. Reports from the trial tests are summarized by Boosma and De Jonge, the manager of marine mining: "The idea behind the mechanical collector was to see if you could harvest selectively on the seabed, because you want to avoid picking up a lot of sediments. However, this turned out to be very tricky, especially because the nodules have different sizes and are embedded in clay, which is sticky." Boomsma adds: "We started with a kind of comb with the idea that the clay would then fall through it, but the deep sea sediments turned out to be too sticky. You'd end up with a kind of bulldozer and pick up as much sediment as with the hydraulic one." "Because you also have a lot more moving parts than with a hydraulic one, the clay would stick to everything with consequences for operation, wear and tear and maintenance," De Jonge points out (Jong, n.d.).

As this indicates, the use of a mechanical harvester is expected to face very sticky situations. The adherence of clay causes a contribution to unwanted resistances, abrasion of the soil engaging tool, and most importantly clogging of hydraulic flow paths if too much sediment is picked up. At the Clarion-Clipperton fracture zone, the harvester will have to be lowered approximately 5 kilometers below the ocean surface, so stopping and retrieving the harvester will be significantly expensive and time consuming. Therefore, potential geotechnical issues need to be addressed and solved before deployment in 2021. In this study, the mechanisms of adhesion, the properties of extremely soft to soft, high plasticity clay under strain, and potential solutions of adhesion to the harvester will be investigated.

The adhesion effect to the trafficability was found to be beneficial to the overall traction force except when the grousers are fully plugged, so the main concerns regarding adhesion is in the collection and processing scopes. Collecting the nodules from the seabed will inevitably contain a good deal of seabed material. The maximum cutting depth to collect the nodules is estimated to be around 18 centimeters, although this could potentially be more due to dynamic sinkage. In the processing unit, the nodules and clay material are usually separated through the use of screens and high turbulence by eductors and jets. The problem of adherence in the processing unit will only be problematic if a sufficient concentration ratio of clay to water to surpassed. To ensure the operational efficiency of the harvester during its mining life, the issue of adherence will have to be directed to the first engagement with the seabed; the cutter wheel. An optimal cutting wheel would supply the inner unit of the harvester with a large abundance of nodules with a minimum amount of sediment in order to prevent potential disruptions and/or accumulation in the flow ducts. For this, we will need an in depth analysis of cutting cohesive seabed material and a thorough understanding of clay behaviour and adhesive tendencies. If soil plugging is to occur between the cutter teeth, a bulldozer-like mechanism will be enabled picking up much more sediment than is manageable.

The proposed research question is therefore as follows:

"What are the main influencing factors of adhesion onto the cutterwheel and how can this be expressed?"

The research question is a rather general question which entails many aspects of clay properties under different stresses, strains and boundary conditions. This imposes various underlying sub-questions. The coupling of hydromechanical and geotechnical information is necessary to implement a feasible solution for this issue. In this dissertation, the issue from a geotechnical perspective is of concern. Therefore, the research question can be scaled down into the following sub questions:

1. Can adhesion be expressed experimentally and what can it tell us?
2. What influences the effect of adhesion and what does it contribute to cutting forces?
3. What adhesion mitigation measures are most suitable for cutting clay and picking up nodules?

The objective is to ultimately establish a full understanding of the adhesion of soft high plasticity marine clay and its corresponding characteristics. Through the use of past literature, laboratory experiments and practical scaled experiments, different aspects of adhesion can be explored and expressed.

3 Clay Fundamentals

First, a basis of understanding of clays will be underlined. Clay mineralogy and engineering properties are correlated to a degree; depending on the microscopic structure of the clay, clay behaviour can vary significantly.

3.1 Clay Mineralogy

To understand the consequences of adhesive clays on subsea equipment, the issue needs to be extracted from its fundamental microscopic composition, which can then be applied in macroscopic conditions in engineering applications. Clays are fine grained layered secondary silicates of colloidal size ($< 2mm$). They are formed from the breakdown and modification of phyllosilicates (micas) and of other silicates (mainly feldspar). Primary silicate weathering found in clay fractions usually consists of oxides and hydroxides of Si, Fe, Al, and Mn. Namely, three different types of clay minerals can be distinguished based on the layering type:

1. 1:1 Layering Type: This layering type has one Si-O tetrahedral sheet and one Al-OH octahedral sheet connected by strong hydrogen (OH-O) bonds. Figure **??** shows the most common clay mineral, Kaolinite, for this type of layering configuration. The 1:1 layered structure of kaolinite is formed by chemical weathering and disintegration of aluminium rich feldspar and mica particles or other acidic igneous rocks, followed by precipitation from $Al[OH]_3$ and $Si[OH]_4$ in pore solution. (Cherian, Chinchu, Arenapalli, & Naidu, 2015). The interlayer space is rather small, and ions are adsorbed only on the outside on cleavage surfaces and broken edges. When stacked on When the layers are stacked one above the other, O2-of the silica sheet and OH- of the alumina sheet forms very strong hydrogen bond; and hence, these minerals are characterized by insignificant expansive nature.
2. The 2 : 1 layering type consists of two Si-O tetrahedral sheets covalently bonded to one $Al - OH$ octahedral sheet that is sandwiched in between. These type of clays are formed by chemical weathering/hydrothermal alteration of extrusive basaltic rocks such as tuffs, volcanic ash, etc.

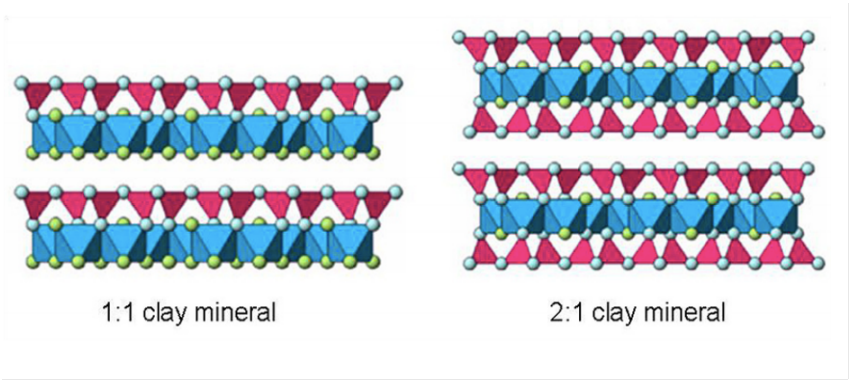

Figure 3.1: 1:1 2:1 Clay Layering Types (Krenz, Lee, & Owens, 2006)

Adjacent sheets of this type of clay have only weak van der Waals between O^{2-} ions and so are easily broken exposing a highly reactive surface. Composition of clay minerals varies frequently due to the substitution of ions within the mineral structure. The process of replacing one structural cation for another of similar size is referred to as isomorphic substitution. Isomorphic substitution is very common for this layering type producing a net negative charge which can further be neutralised by cations in between clay layers. Common minerals with this configuration include Illites and Smectites. Illites have their structural charge com-

pensated by non-hydrated K+ cations, while Smectites have their charge compensated by hydrated cations which leads to a high swelling capacity.

3. The last clay type to be distinguished is the 3:1 layered type which is essentially the same configuration of the 2:1 clay but with an additional sheet of $Al-OH$, $Fe-OH$, or $Mg-OH$ octahedral. The additional octahedral sheet neutralizes the excess negative charge of 2:1 layers producing a net charge close to zero. The hydroxide ions form strong inter-layer bonds with the 0^{2-} in the silica sheet. This produces a relatively stable clay mineral that is resistant to inter-layer swelling and adsorption of cations. Chlorite is an example of a common clay type of this layering type.

In geotechnics, it is often important to find the type of minerals present in the clay to understand the mechanical behaviour. Clays are affected at the first degree by the physico-chemical composition and the microstructre present. The substitution of ions on the clay surface with different valencies cause a net negative charge. For example, aluminium Al^{3+} may be replaced by iron Fe^{2+} or magnesium Mg^{2+} leading to a net negative charge. Separation of the hydroxyl ions from the clay surface leads to an electrical imbalance which attracts anions to adsorb on the the crystal surface. This causes an extreme affinity to water and cations when the clay is submerged under an electrolyte. When suspended in an electrolyte, clay particles are surrounded by a hydrosphere of adsorbed water that contains a thin layer of adsorbed cations (Mojid, 2011). This configuration of adsorbed water molecules and sea of cations form what is known as the *diffuse double layer*.

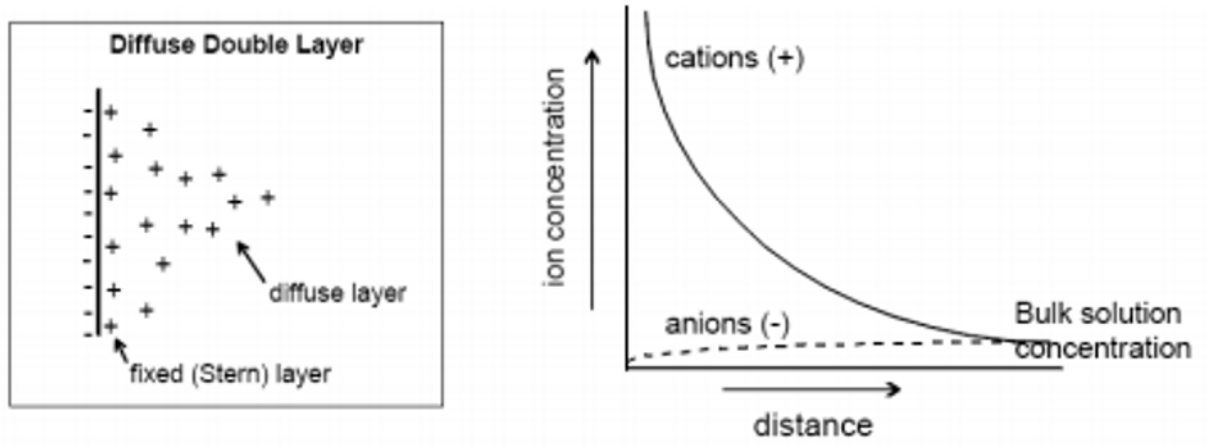

Figure 3.2: Diffuse Double Layer (*Diffuse Double Layer*, 2013)

The innermost layer of the double layer in which water is very strongly bonded to the clay surface is known as the stern layer. Cation exchange capacity is a measure of isomorph displacement capacity within the clay microstructure. There is an established relationship between cation exchange capacity (CEC) and plasticity characteristics. In general, a larger cation exchange capacity such as in smectites leads to more plastic behaviour. This is due to the greater specific surface area that is attributed to 2:1 clays over other types of crystals. The specific surface area is a property which is defined as the total surface area of a material per unit mass. This can be schematically seen in Figure 3.3 which shows a montmorillonite crystal size in comparison with a a kaolinite crystal with layers of adsorbed water.

Montmorillonite crystals are much more likely to adsorb water and hence cations than kaolinite crystals due to the much larger specific surface area. Common techniques for the determination of

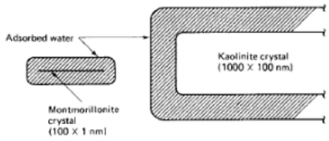

CLAY MINERAL	SPECIFIC SURFACE (m^2/g)	VOL. OF ADSORBED H_2O IN DBL LAYER (% PORE VOLUME)
Kaolinite	20	2
Illite	100	9
Montmorillonite	800	70

Figure 3.3: Montmorillonite and sodium Kaolinite crystals with adsorbed water layers (*Diffuse Double Layer*, 2013)

micro-structural properties are the X-ray diffractometer (XRD) and scanning electron microscope (SEM) that can magnify up to 1 million times depending on the specifications. Chemical aspects such as the pH of the soil also influence mechanical aspects of the clay. The pH value indicates the degree of H^+ and OH^- ions present in the measured solution. A low pH indicates flocculation, and high pH indicates dispersion (Ural, 2018). Seawater conditions usually exhibit a slightly high ph of around 7-8 which may help to prevent clay accumulations as compared to fresh water sources.

3.2 Clay Engineering Properties

With grasping the microscopic attributes of cohesive soils, the engineering properties of clay are more understood. Cohesive soils in offshore applications are characterized by compressibility, internal cohesion, and adhesion to other material surfaces. The first data requirement concerns the shear strength, which largely dictates the method of cutting, the required power, and the rate of production which can be achieved [INA, 2000, p.10]. As we are of concern of cutting clay to scoop the nodules, compressibility is not a main criteria. It is sufficient to identify the consolidation state the soil is in as this has a significant impact on the measured shear strengths. Normally consolidated soils are generally less stiff, but can exhibit highly ductile consistencies as what is generally found in the CCZ region. Therefore, the consistency or plasticity of the clay is a vital concern in order to identify potential problems relating to adhesion.

3.2.1 Internal (shear) Strength

One of the most important engineering properties associated with clay is its shear strength. The term 'shear' is associated with a stress development that leads to a higher deviatoric stress. Unlike compression, soils can lead to a state of failure under shear. The shear strength of a clay is not a fixed value, and it usually increases with an increasing confinement pressure. The shear strength of a soil is usually given by the Mohr Coulomb Criterion:

$$\tau_f = c' + \sigma' * tan(\theta')$$

Undrained conditions occur if the rate of shearing is sufficiently fast that the time for any significant drainage is longer than the time for load application. If a clay is sheared undrained, i.e. without volume change, then the maximum shear stress that a clay can withstand depends only on the initial void ratio. Under undrained conditions, the total stress approach is often applied which assume the effective friction angle θ' to be equal to zero and the undrained shear strength is assumed equal to the cohesion intercept c_u of the Mohr-Colomb Criterion.

$$\tau_f = c_u$$

For these assumptions the undrained strength of a saturated clay is not affected by changes in confining stress so long as the water content does not change (A. Skempton, 1948).

The undrained shear strength of a saturated clay is heavily influenced by the consolidation history of the deposit. Normally consolidated or lightly overconsolidated clays tend to decrease in strength with an increasing shear load due to the generation of positive pore water pressures to compensate for the no volume change condition. Typically in normally consolidated clays, the drained shear strength is larger than the undrained. If the clay sample is overconsolidated, meaning the preconsolidation stress is larger than the current stress state, an increase in shear loading will induce negative pore water pressures thus increasing the undrained shear strength. It is typical of OC-clays that the undrained shear strength is larger than the drained for this very reason.

There are various methods to determine the undrained shear strength of offshore clays whether it is in a laboratory or in-situ measurements. For a given clay, differences in strengths occur among these measurements since each method imposes different loading conditions, boundary conditions, initial stress states, and strain rates (Mayne, 1985). The most common laboratory tests to measure the undrained shear strength include undrained triaxial tests or direct shear tests. The preconsolidation history of the clay deposit effects the undrained shear strength significantly. This can be understood by analysing typical stress paths in s-t space for a normally consolidated and overconsolidated clays under triaxial loading.

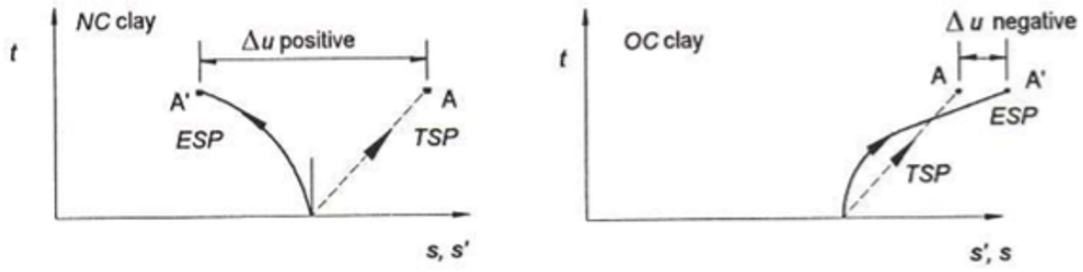

Figure 3.4: Typical stress paths for NC and OC clays

The restriction of volumetric change gives rise to excess pore pressure developments. In normally consolidated clays, the clay particle configuration are in a relatively looser state than OC clays which gives rise to a positive pore pressure contribution, hence lowering the effective stress. For overconsolidated case, the dense configuration of clay particles gives rise to 'tensile' pore pressures which contributes to the overall strength of the clay under isotropic loading. Due to the importance of consolidation history, The undrained shear strength "s_u" from laboratory tests normalized with effective overburden stress "σ_{vo}" or maximum past pressure σ_{vmax} is an important index in evaluating the shear strength and stress history of in-situ clay(Ratananikom, Yimsiri, & Likitlersuang, 2015).

Shear tests are not suited for measuring undrained shear strength due to the issues controlling drainage. It can give an estimate for a fully saturated sample, but there is bound to be some drainage during shear. However, the obtained shear strength obtained in a DSS is important as it gives an intermediate value between triaxial compression and triaxial extension tests. This value is usually taken to be the average mobilized strength. Direct shear tests are often sought out due to the simplicity of the procedure and quick consolidation times due to the relatively small thicknesses of the specimens. Furthermore, residual and peak strengths of the specimens as well as the shear strength to consolidation ratio can be found which can contribute to any correlations that can be inferred. There are a number of empirical relations to obtain the undrained shear test from shear testing but are not very frequently used. It is much more common to directly determine the undrained shear strength through in-situ testing.

In-situ testing results are frequently used in engineering calculations for different operations. There are various site investigation techniques used nowadays but the focus will be on shallow penetration

testing. The two most widely used shallow penetration testing techniques in offshore environments are the vane shear test and cone penetration tests. Due to the lack of site investigation data, vane tests will only be discussed. Vane tests are usually done on-board the site investigation vessel and are often used for its versatility and a good primary approximation of the shear strength of homogeneous clay samples. A vane consists of vertical blades that are pushed into the soil sample. A rotary force is then applied to the blades with a rotation speed of about 0.1 degrees/sec. The torque required to rotate the vane is a function of the angular deformation. The maximum torque, T_m, is recorded and the undrained shear strength is approximated by equation 1:

$$s_u = \frac{6 * T_m}{7 * \pi * D^3} \tag{1}$$

It is important to note that undrained shear strength is not an inherent property of a clay soil, but is dependent on the consolidation state, loading conditions, boundary conditions, and drainage paths. It is therefore not valid to define a clay soil based on this property. It however is useful for short term loading in comparison to the consolidation time.

3.2.2 Atterberg Limits

Atterberg limits or otherwise known as consistency limits, define the relationship between ground particles and water and the state of the soil relative to varying water contents. Atterberg limits provide the basis for a very simple but effective classification system for unconsolidated sediments (Keller & Bennett, 1973). Consistency is a term used to indicate the degree of firmness of cohesive soils. Depending on the water content, the clay material can exist in different states: solid, semi-solid, plastic and liquid states and the boundaries set between the states are the shrinkage limit (SL), Plastic limit (PL), and Liquid limit respectively as shown on Figure 3.5

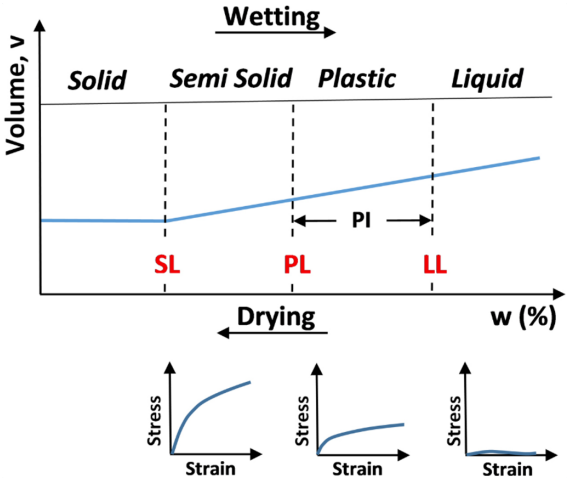

Figure 3.5: Atterberg limits (above) and general stress behaviour (below) (*Atterberg Limits*, n.d.)

The plasticity index is the difference between the liquid limit and the plastic limit, and is very important to classify soil types and has a substantial effect on adhesion properties. It gives the range of water contents over which the material remains in a plastic state. The plasticity index (PI) is given by equation 2.

$$PI = LL - PL \tag{2}$$

In any particular clay stratum, the ratio of the plasticity index to the clay fraction content is approximately constant, and may be defined as the "activity" of the clay (eq. 3).

$$a_c = \frac{PI}{\%\, by\, weight\, finer\, than\, 2\,\mu\, m} \tag{3}$$

Plasticity index tends to increase linearly as the clay content increases. Field data is presented which indicates that the difficulties of taking satisfactory undisturbed samples in deep beds of sensitive clay are restricted to those clays with an activity of less than 0.75 (A. W. Skempton, 1973). Clays are defined as sensitive if the behaviour varies significantly in comparison to in-situ conditions.

The liquidity index (LI) scales the natural water content of the soil to the limits given by eq. 4

$$LI = \frac{w - PL}{LL - PL} \tag{4}$$

Similarly to the liquidity index, the consistency index (CI) indicates the firmness or the hardness of soil. It is defined as the ratio between the difference of the liquid limit and natural water content and the plasticity index as shown in eq. 5.

$$CI = \frac{LL - w}{LL - PL} \tag{5}$$

Both LI and CI are both useful to categorize the firmness of the soil. The denominators are the plasticity index which is a constant for a given soil, so it is the numerator difference that gives the deciding value. For example, if the soil has a natural moisture content equal to the liquid limit, LI would be 1 while CI would be zero. For soils like sensitive clay, the natural moisture content may be greater than the liquid limit causing LI to be greater than 1 while CI will be negative.

Water contents can be found experimentally by various ways such as oven drying, pycnometers, or sand bath. The liquid limit is often found via a percussion method known as the Cassegrande method or a falling cone test. The Cassegrande device consists of a brass cup with a hard rubber base of which the soil is placed inside. A groove cut is done in the soil sample of about 13 mm or 1/2" by ASTM D-4318 standards. The cup is then dropped 10 mm for a number of blows by a revolutionary device at a speed of 2 rev/s until the groove cut closes a distance of 12 mm. The liquid limit of a soil is defined as the water content at which the soil groove closes 12 mm in 25 number of blows. Practically it is difficult to obtain exactly 25 blows, so a number of clay samples have to be prepared with varying water contents in order to obtain a relation between the number of blows (usually on a logarithmic scale) and water content of which the water content for 25 blows can be graphically determined. The Cassagrande Method presents a high dispersion of the results due to the influence of the operator and the conditions of the apparatus used to conduct the analysis (Crevelin & Bicalho, 2019). Furthermore, limitations such as the difficultly of making a groove in sandy clay soils and ensuring flow failure cause some engineers to turn to other methods. An attractive alternative to the Casagrande method is the falling cone test method. The apparatus consists of a 30° tip cone that is allowed to fall into a prepared clay sample for 5 seconds. The reading of the penetration distance is taken to the nearest milimeter.

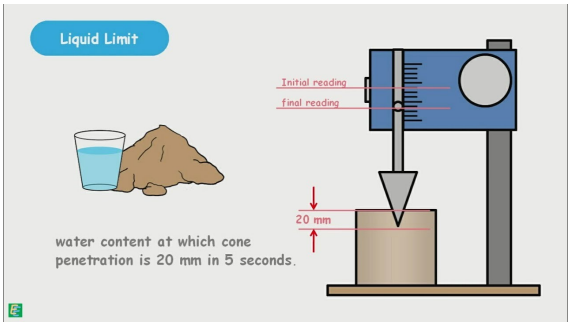

Figure 3.6: Falling Cone Test

The liquid limit is taken as the water content corresponding to the the penetration of a certain length, which varies depending on the countries standards (in Figure 3.6, it is taken as 20 mm). As with the Casagrande method, the procedure is repeated with samples with varying water contents and the penetration value (in a log scale) to obtain a relation.

Depending on the type of clay, the consistency limits will vary significantly. Atterburg limits are conclusively useful for the following (Orabi, 2016):

- To obtain general information about a soil such as shear strength - consistency relation, compressibility and permeability properties
- Soil classification
- Empirical correlations for some engineering properties

4 Adhesion

(Myers, 1991) defines adhesion to be "the state in which two bodies are held together by intimate interfacial contact in such a way that mechanical force or work can be applied across the interface without causing the bodies to separate". It is important to distinguish adherence from cohesion. Adherence is the tendency of different molecules or surfaces to cling to each other, whereas cohesion is the property of like molecules (of the same substance) to stick to each other due to mutual attraction. Adhesion can provide resistance to tensile forces and shear forces.

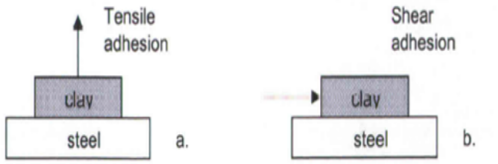

Figure 4.1: Tensile (a) and shear (b) adhesion (Zimnik, van Baalen, Verhoef, & Ngan-Tillard, 2000)

In this chapter, the nature of adhesion will be explored by reviewing previous literature research on the phenomenon.

4.1 Occurrence of Adhesion in Clay

There are multiple identified sources of adhesion. It is impossible to say what exactly each source of adhesion contributes quantitatively to the overall adhesive force due to the complexity of the system, but it could be differentiated relative to other types and can provide valuable insight on the mechanisms behind the force. To narrow it down, adhesion can be described by being either "true adhesion" or "apparent adhesion". True adhesion arises from the thermodynamic and chemical interactions while apparent adhesion arises from the mechanical and physical interactions at the soil-component interface. The categorical subdivision of adhesion force is shown on Figure 4.2.

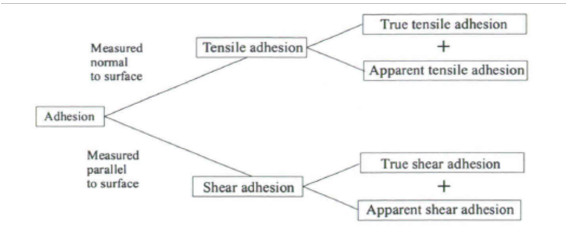

Figure 4.2: Adhesion Origin Subdivision (Panday, 2003)

True adhesion in clays is the adhesion arising from thermodynamic properties and chemical properties. Thermodynamically, adhesion can be a result of molecular attractions such as van der Waals forces and electrostatic forces. This is rather weak, and is not the dominant source of adhesion in most cases. Chemical interactions at the clay-equipment interface can occur such as crystallization of salts or through the use of artificial adhesives. Apparent adhesion is the adhesion caused by mechanical and physical interactions. Mechanical adhesion is caused by the interlocking of two phases at irregularities in the interface. Physical adhesion arises from the capillary stresses due to differential pore pressures in saturated soil. Furthermore, the viscous resistance of water contributes to physical adhesion. This can be showed by placing two non-contacting discs submerged underwater. The time 't' required to increase the separation from distance of 'h1' to 'h2' under tensile force 'F' is given by equation 6.

$$t = [\frac{3\pi\eta R_d^2}{4F}][\frac{1}{h_1^2} - \frac{1}{h_2^2}] \tag{6}$$

This shows that if the two solids are separated in a short time, a very large force would be required. It also shows the proportionality between viscosity η and the required tensile force 'F'. The adhesion increases with liquid viscosity.

The total adhesive force can be generalized by adding up all the aforementioned contributions to adhesion:

$$P = p_m + p_e + p_c + p_v + p_w + p_g \tag{7}$$

P = Soil adhesive force
p_m = sum of the molecular forces of soil molecules contact with other bodies
p_e = sum of the forces of electro-static attraction between contact surfaces
p_c = sum of the capillary forces produced by surface of meniscus formed by soil liquid with contact surface
p_v = viscous resistance of soil liquid
p_w = wedged pressure produced by potential chemical non equilibrium between liquid film of area of contact and void liquid
p_g = negative air pressure produced by closing of soil pores of the area of contact of soil and other surfaces

Research by Thewes (1999) showed that physical adherence prevailed in saturated conditions due to the mitigation of van der Waals forces and interlocking effects at irregularities. In case of marine clays with degrees of saturation around 100%, capillary forces will be the main cause of tensile adhesion. Thewes (1999) explained this as follows: at high degrees of saturation and with the occurrence of water at the clay-steel interface, capillary forces develop. This capillary "under-pressure" has to be overcome when applying tensile stresses on the clay. In general, multiple research studies including (Fountaine, 1954), (Thewes, 1954), (Burbaum, 2009) described the significant adhesive physical force to be boundary layer effect between the clay and the soil engaging tool arising from the capillary forces of the interfacial fluid film. The strength of the capillary forces depend on the thickness of the interfacial fluid film and has shown to generally increase with decreasing thickness of the fluid film. In fully saturated conditions in the ocean, the question arises of how the capillary stresses are developed if water saturated clays, by definition, have no pore water tension. The answer lies when assessing the dynamic behaviour of the disturbance to the clay soil. When disturbing a clay soil such as cutting or shearing, pore fluid is first transported out of the interface into the soil matrix and then re-transported back in the interface when separating forces are applied (Burbaum & Sass, 2016). Hence one could say that at a particular instance of time, the water film between the tool and the clay is at its minimum thickness which corresponds to the optimal adhesion point.

4.2 Factors Effecting Adhesion

With the adhesive mechanism being a function of the interfacial water film at a particular instance of time, there are many factors effecting thickness of this water film. The factors affecting adhesion is summarized in Figure 4.3.

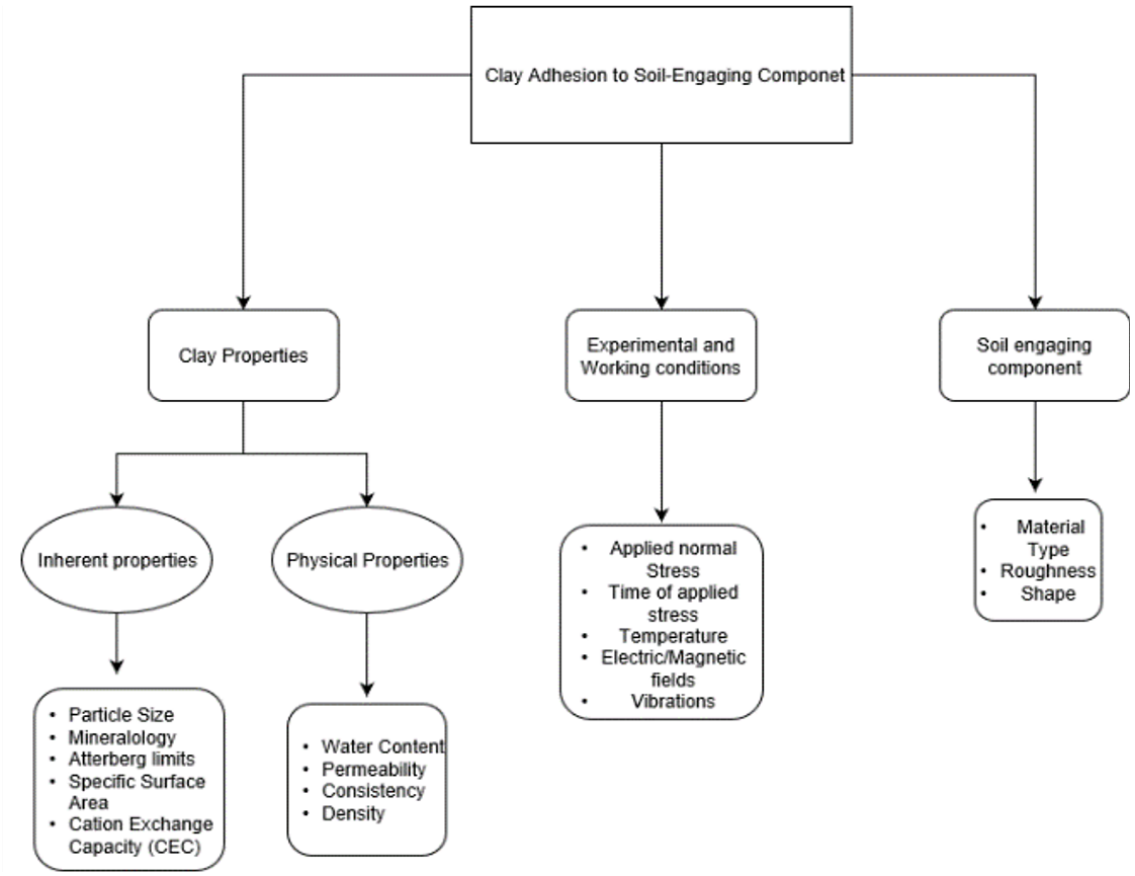

Figure 4.3: Factors Affecting Adhesion

4.2.1 Clay Properties

It is well known that the type of clay mineral plays an important role in the stickiness of clays. As previously discussed in Section 3, a mineral with a high cation exchange capacity such as those in 2:1 structured clays generally exhibit higher plasticity's. Although no quantitative relation is available between plasticity and CEC, it was found in many tests by using the ammonium acetate (NH4OAc) method and subsequent regression analysis that there was a high coefficient of correlation (R=0.97) (Carroll, 1970). This correlation can be understood as both are a function of the surface area and activity of the soil particles. For example, the low particle diameter to thickness ratio of kaolin explain its low CEC and PI values. The higher the CEC values, the more statically unstable the basal sheet of the clay surface becomes, the more intermolecular bonds can be formed with H_2O particles in the double layer, which leads to more water retention capacities. This explains why swelling clays such as smectites are more likely to develop strong adhesive forces than kaolinite.

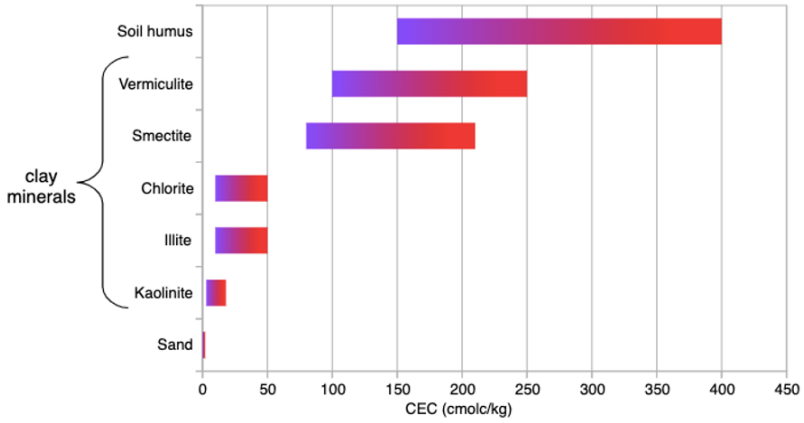

Figure 4.4: Cation Exchange Capacities of different soil types

The net negative charge on the stern layer found in many clay types are neutralized by the surrounding cations in the double layer. With the exception of hydrogen, ions with a higher valence and greater atomic weight are preferred to be exchanged at the clay surface. The order of preference of the different cations to be adsorbed on the basal surface of the clay crystal may generally be predicted from the Hofmeister series: H^+, Al^{3+}, Ba^{++}, Sr^{++}, Ca^{++}, Mg^{++}, NH_4^+, K^+, Na^+, Li^+ (Schwieger, 1965). The availability of potential ion interactions raises the potential for bonds to be formed between a clay surface and soil-engaging tool.

Besides the mineralogical content, the adhesive stress can also be a function of the matrix composition. A large amount of clay particles in a soil will more likely attract a water film on the stern layer leading to adhesion potential. However, the soil must have a minimum permeability to allow water to flow from the interface into the soil. Extremely low permeability of some clays could explain why clayey soil with high matrix potential do not develop high adherence stresses.

From a physical perspective, the water content of the soil vastly alters the adhesive strength measured. Depending on the mineralogical content, clays can exhibit high water retention properties leading to high plasticity clays. Clay minerals such as smectites with high water retention properties will tend to absorb water from the clay surface into the soil matrix, reducing the interfacial water film and thus increasing adhesive stresses. High plasticity clays will also tend to morph and cover more surface area when a normal force is applied over a solid surface. This increased contact area leads to a larger amount of adhesive contact forces at the soil-tool interface. The largest amount of adhesion forces was found to be present when the clay soil is between the plastic limit and the liquid limit. (Thewes, 1954) found an empirical relationship of adherence potential to consistency index as a function of plasticity index shown in Figure 4.5.

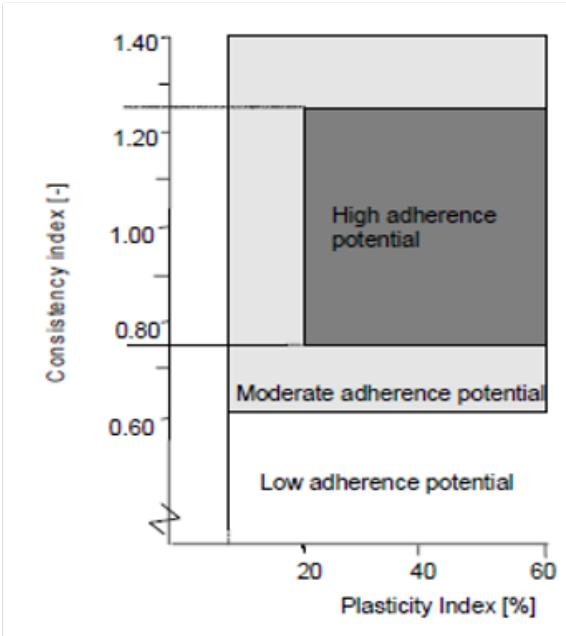

Figure 4.5: Adhesion relation to Atterburg limits (Thewes, 1954)

4.2.2 Working environment

Clay particles are sheet-like platelets that become increasingly more parallel with an increased amount of normal stress applied to it. The mechanism leads to a non-linear parabolic shear stress - normal stress adhesive friction envelope shown on Figure 4.6.

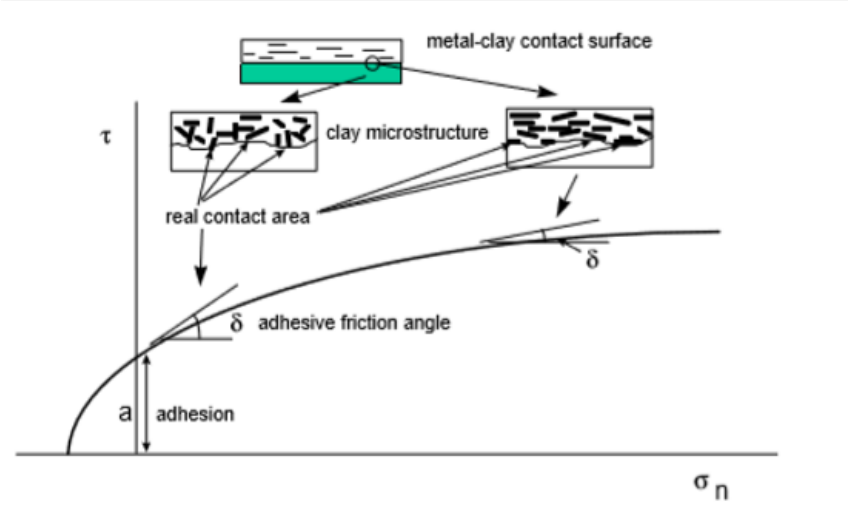

Figure 4.6: Adhesion relation to Atterburg limits (Kooistra, Verhoef, Broere, Ngan-Tillard, & Tol, 1998)

Studying the adhesion phenomenon can become very complex due to the multiple factors that can affect it. Depending on the application, adhesive forces can vary profusely for the same kind of soil. This is mainly due to kind of force imposed on the soil and how long the force is to be applied. In offshore pile installations, depending on the overconsolidation ratio, adhesion has been shown

to contribute to the overall bearing capacity over time due to the consolidation of the clay around the pile shaft. TBM cutterwheels have to optimize the speed when cutting through soft clay to reduce the speed effect on adhesion. Although no founded evidence shows a direct relationship between adhesion and cutting speed, it was found by (Stafford & Tanner, 1983) that the cutting forces generally increased with increase of speed of the model cutterwheel tested. This is mainly due to the increase in shear strength of clay due to the limited time for pore pressure development rather than an issue with adhesion itself. The issue with adhesion should not be based on the speed of disturbance but rather the time the soil engaging component is in contact with the soil. A longer contact time between the adhesive soil and the soil engaging tool leads to stronger bonds being formed as the clay settles on and around the component.

4.2.3 Soil Engaging Component

The last factor to be discussed is the effect of the properties of soil-engaging component surface. Surfaces can be described as having a certain "surface energy". Surfaces of any solid or liquid tend to minimise its energy by adsorbing a material with lower energy onto its surface. High energy surfaces therefore have a larger probability of clays to adhere to its surface. High surface energy materials include metals, metallic compounds and inorganic compounds (i.e. oxides, nitrides, silica and diamond) and low surface energy materials include organic compounds and organic polymers. The contact angle of the water on the surface influences the hydrophilicity (Lu-Quan, Tong, Li, & Chen, 2001). Metallic materials, metallic compounds and inorganic compounds display low contact angles and therefore are more hydrophilic than organic materials. Different surface roughness's or perturbing areas can influence the adhesion potential. The idea is minimize the contact area between the clay and the tool surface by breaking the continuous water film by varying surface morphology's.

4.3 Adhesion and Clogging

An often overlooked aspect when assessing clogging potential of a tube or container is the soil aggregate dynamics within the flow after the detachment from the soil matrix. For this, the coupling of hydromechanics and geomechanics for the colloid mixture needs to be hypothesized. For this hypothesis, the understanding of colloids in suspension, flocculation, and accumulation processes is evident. The feasibility of the formed hypothesis will depend on the model and conditions established.

The clogging potential of a clay formation (clay soils or clay rich rocks) was defined as the interaction of four single effect mechanisms by Thewes and Burger (Thewes & Burger, 2004) as: adhesion of clay particles on a component surface, bridging of clay particles over openings in the path of the spoil transport, cohesion of clay particles, sticking to each other and the low tendency of a clay towards dissolving in water as shown in Figure 4.7.

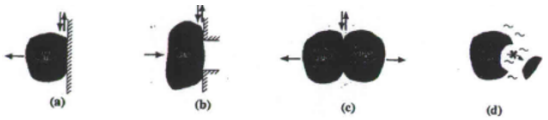

Figure 4.7: Clogging mechanism: (a) adhesion onto surface (b) bridging (c) sticking to each other (d) dissolution (Thewes & Burger, 2004)

Clay particles alone are very small in size and so will not clog if suspended in sufficient fluid volumes. However, depending on the application, particles can be deposited in stagnant zones such as corners and will likely accumulate over time. Inside the harvester, clay sediment and nodules are to be pumped through screens in preparation for the VTS. If there are any blockages due to stagnant zones or nodules that have settled on a screen, clay accumulation and eventual blockage is likely.

4.4 Adhesion Reduction Techniques

Previous research on clay adhesion mitigation measures are limited, but still provide valuable insight on what measures proved to work and what hasn't. Adhesion reduction tests were mainly carried in the context of agriculture and tunneling. Clay adhesion to a ploughs were quickly realised to vastly reduce ploughing efficiency in the fields due to the reduction of space on the plough itself and the resistive force that comes along with it. Similarly, in the tunneling industry, researchers have been keen on finding an optimal solution to adhesion of soft soils on the TBM cutter-wheel. The use of chemical additives and hydrophillic polymer solutions were mainly investigated to alter the consistency of the excavated material, as this was the most logistically sound technique. Unfortunately, the use of additives in deep sea mining will severe the the environmental constraints for such projects. Regardless of the application, clay adhesion mitigation measures from previous conducted research can be utilized to find an applicable solution to a deep sea mining harvester. The chart in Figure summarizes the most recent techniques found to reduce adhesion:

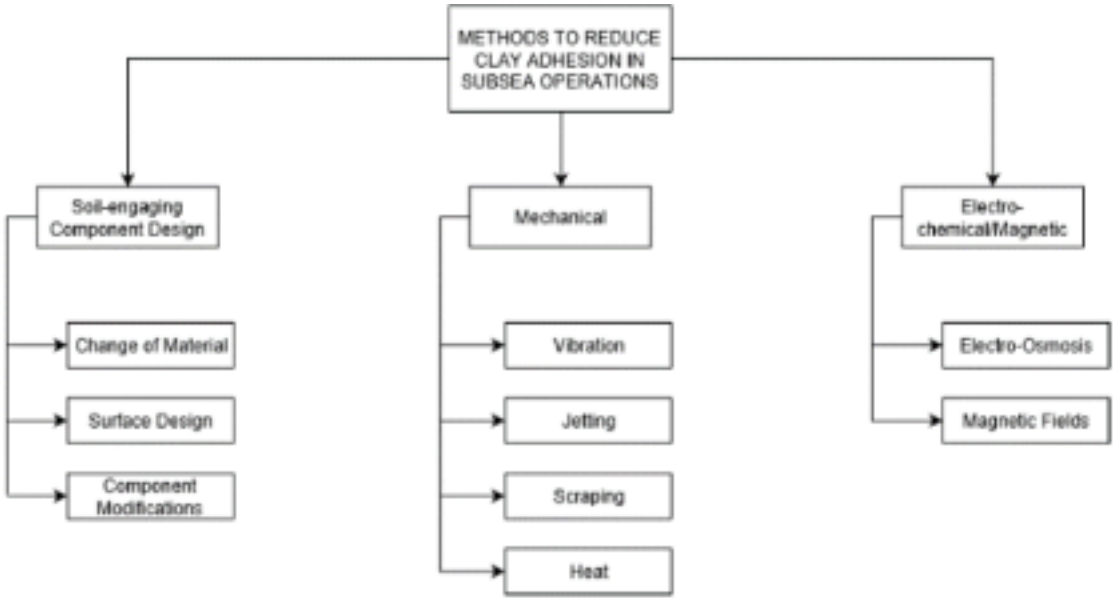

Figure 4.8: Adhesion Reduction Techniques

4.4.1 Surface Modifications

Alterations and modifications to the surfaces of soil-engaging components can help significantly reduce soil adhesion to the component surfaces. By having discontinuities in the surface the real contact area is decreased and the continuous interfacial water film between the soil and solid surface is broken resulting in reduced adhesion. For example, ridges or grooves on the side of a plough keel can help reduce interfacial friction and adhesive resistances leading to lower necessary pulling forces. The non-smooth shape can form a cavities when contacting with the soil resulting in a higher normal adhesion than tangential adhesion, destroying the adhesion interface and reducing resistance. Ploughs with irregular hole patterns have been proven to reduce the total plough resistive force. A study in Surface and Coatings Technology showed that an increase in surface area of roughness regions on a 45 steel mold fabricated by lasers led to an increase of the apparent contact angle from 76.9° to 97.5° of water to the mold ("Biomimetic$_C hen''$, n.d.-a). This decrease in wettability leads to a decrease in clay adhesion potential. A change in a components material can help the tendency of soil sticking. The key is to increase the contact angle of interfacial liquid by using materials with low surface energy. Low surface energy materials are much more hydrophobic that will hence resist any sticking potential of materials. Multiple studies have tested

the adhesion of soil types to certain surfaces (Fox & Backhup, 1965; Salokhe & Gee-Clough, 1989; Tong et al., 1998; Lu et al., 1996 and many more), where they have concluded that surface materials do significantly change the adhesive potential of surfaces. Low surface energy materials such as polymeric materials can be used, but are however limited due to their poor abrasion resistance. A solution is to use polymer composite coatings on steel equipment. Enamel coating offers good corrosion protection for steel surfaces while also reducing surface energy of that surface. However, enamel coating has limited practical use due the spalling nature under abrasive conditions (Tong, Chen, A.R., & Chen, 1994). Cast white iron is one of the most commonly used tillage materials. It was found that when including more phosphorous and silicon, it improved anti-adhesive properties (Tong, Ren, & Chen, 1994b). However, this is limited to soil engaging components due the brittle nature of white iron with an abundance of phosphorous. Polymers were found to reduce both normal adhesion and sliding resistance, whereas, enamel coating or iron based alloy coatings can reduce the sliding resistance to some extent (Tong, Ren, & Chen, 1994a). A study at the University of Mohaghegh Ardabili, Iran, showed through experimental means, how the external friction factor (adhesion) alters with a change in material (Yousef, Hasankhani-Ghavam, S., Vali, & Mohamadreza, 2018). In order to achieve this, a system comprising of a soil box that was moved on two parallel rails by an electric motor. A piece of material used as a slider was in tangential contact with the soil located inside the soil box during movement. The material of the slider was changed between steel, cast iron, rubber and Teflon. An S-shaped load cell was used to measure the required friction force and was subsequently loaded in a computer. The adhesion tendencies was found to decrease in the following order:

Steel – Cast iron – Rubber – Teflon

Tong (1990) prepared an alumina particle reinforced Teflon composite material. When the alumina content was less than 20% by weight, the abrasive wear resistance was increased considerably and soil adhesion was affected a little. Jia (1995) prepared an alumina particle reinforced PA1010, epoxy EP, Polyurethane (PU) matrix coatings and the steel-T9 coating impregnated with polysiloxane to a smooth and non-smooth bulldozing blade and tested the resistance in a soil cutting. The soil used was clay with a moisture content of 33%. The cutting speed was 0.04 m/s and the depth of the cut was 20 mm at 45°. In the comparison with an uncoated smooth blade, the reductions in cutting resistance were 38%, 23% and 27% for the smooth bulldozing blades coated with PA1010, EP and steel-T8 coatings, respectively, and 58% and 20% for the non-smooth bulldozing blades coated with PA1010 and PU composite coatings, respectively.

It is clear from many studies that composite polymer materials mitigate adhesion potential more than other materials. It is also evident that the combination of hydrophobic materials and geometrically non-smooth surfaces was an optimal method for reducing adhesion and interfacial friction. However, challenges for the use of composite polymers can vary depending on the technical, cultural, financial and logistical aspects involved. Steel is used more frequently as it is much more readily available and in general a more economically viable solution. Therefore, in order to benefit from both material properties, polymer coatings on steel structures are a common practice in offshore applications. Surface engineering research is being more readily carried out to produce a coating that has good anti-adhesion properties while maintain high hardness and wear resistance. There are many surface coatings available in market such as those previously mentioned of which hard composite coatings such as UHMWPE are favourable. Coatings consisting of diamond-like carbon (DLC) and chromium nitride layers are also great examples of such coatings. Elements such as fluorine and silicon significantly reduce surface energy while nitrogen, boron and oxygen cause the opposite effect. One such newly modified surface coating is the so called "Magna-Coat" which is a fluro-polymer which offers good adhesion and wear resistance. It would be interesting to test such a coating for adhesion reduction effectiveness.

4.4.2 Mechanical Methods

Mechanical interactions help separate clay from the component surface by physically breaking bonds and/or thickening the interfacial water film between the clay and equipment surface. Developments in mechanical innovation include automating mechanical scrapers or brushes on equipment to reduce soil build- up. For example, (Yin, Cheng, & Chen, 1990) designed an automated tongue scraper mechanism for a loader bucket to remove soil accretion in the bucket. Agricultural tests have shown that vibrations perpendicular to the contact area between the soil engaging tool were especially effective in the frequency range between 60 and 100 Hz (Wang, Ito, & Kito, 1996). Last of all, raising the temperature of the equipment surface in contact with the soil has been found to reduce adhesion due to the decrease of viscosity of the water in the vicinity of the tool.

Mechanical solutions to soil adhesion relies on innovative methods when applied to a deep sea mining harvester. Most mechanical methods are not applicable to such conditions; supplying heat so far down in the ocean is energetically unfeasible and applying vibrations to the harvester is not technically and logistically sound. However, depending on the mechanical design, a tongue scraping mechanism or a sort of brush can be utilized to brush off clay accumulations between the cutter teeth. Furthermore, jetting is a common practice in offshore geotechnics (e.g. ploughing) and has been proven to be effective when slicing through cohesive soils. If the jet can be mounted on the harvester to clean out the cutter teeth before depositing the nodules in the inner duct, this can be the most optimal solution. (Keeney, 1987) determined that the best general operating technique included a standoff distance of 1/2 inch to 3 inches with an impingement angle of 40 to 90.

4.4.3 Electro-Chemical/Magnetic Methods

When an electric charge is applied to a soil-engaging component, water can be transported through the clay by electro-osmosis to the interface between the clay and the component creating a thicker film of water. This process is known as electro-osmosis. When a current is applied parallel to the clay surface, cations begin to migrate from the anode towards the cathode. Figure 28 shows the development of the electro-osmotic flow.

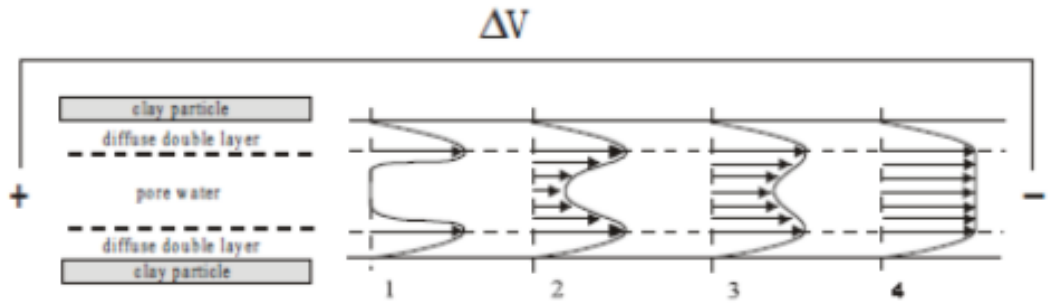

Figure 4.9: Development of the electro-osmotic flow between two clay particles, with arrows representing flow velocities.1) Switching on of electric field, 2)-3) development of electro-osmotic flow, 4) steady-state flow

This description of electro-osmotic flow is best described by ("Electro-Osmosis", n.d.-b):

"As the cations migrate towards the cathode, a drag force is created between the hydrated water molecules around the cations and the surrounding unhydrated (free) water molecules of the pore water. This drag causes the free water molecules to move (see Figure 6.5) and thus creates an additional transport of water. The macroscopic effect of electro-osmosis is then seen as a flow of water through the clay mass."

This phenomenon has been researched thoroughly in applications of TBMs. However, most TBM contractors are still hesitant about using such an application because of the worry about stray currents in the TBM excavation chamber. Effects of electro-osmosis has been utilized in past projects such as decomissioning pipelines sunken at the sea bottom or to clean sives from diamond mining in soils rich in smectites, so in application to deep sea mining, it is not entirely unreasonable to supply electrical currents to the harvester if the effects are evident.

5 Cutting Clay

In this section, a brief overview of what to expect when cutting clay will be established. It is evident that a theoretical framework for cutting clay should be validated against the experimental analysis. The velocity of the cutting, or the shear rate, is of vital importance to test for optimal cutting. Strain rate is the rate of change of the strain with respect to time defined by the velocity divided by the characteristic length. Clay can be seen to exhibit elastic behaviour until a certain yield stress, beyond which, plastic strains begin to develop. Plasticity is characterized by permanent deformations which is what typically occurs during clay cutting. Moreover, plasticity is defined as not only a yield stress, but by a yield function. This yield function is not only a function of stress, but also of a state-parameter "$\kappa(k)$". The evolution of the state parameter itself is a function of plastic strain, thereby introducing the concept of hardening or softening. It is generally believed that shearing a clay soil results in hardening which in turn results in an increase of shear strength. However, hardening is defined as a reduction of stiffness due to the generation of plastic strains but does not necessarily result in an increase in strength. From a global perspective, when slicing through clay, the soil undergoes hardening until the peak strength is reached and is subsequently followed by softening. Softening is typically associated with failure. Semantics aside, clay generally exhibits strengthening until a peak shear stress, followed by large strains (softening). To deal with the hardening effect clay exhibits when sheared past a certain yield stress, a strengthening factor λ was utilized. In dredging, it is found that clay undergoes more strengthening when the shearing rate increases. During cutting of clay, strain and deformation rates are so large that the internal and external friction angles can be considered to be zero, known as the phi=0 concept. Clay has a very low permeability so when sheared at a high rate in undrained conditions, the water in the pores cannot dissipate in time and therefore bear the imposed pressure. Therefore, there is no more relation between normal and shear stresses during cutting, so it makes sense that that the internal friction is zero ($\phi = 0$). Therefore, during harvesting on a clay seabed, the only forces that play a dominant role are the adhesive and cohesive forces.

To estimate the cutting forces through clay, a theoretical framework will be utilized, namely, "The Delft Sand, Clay and Rock Cutting Model" developed by (Miedema, 2019). The horizontal cutting forces as well as the energy required can be reasonably estimated with such a model. It is worth noting that the model considers a two dimensional cutting process under the assumption that the cutting edge of a unit element of the blade is perpendicular to the direction of the velocity of that particular element. This is rarely the case in actual cutting experiments, but this assumption still proves to be quite effective in predicting the minimum force to be expected in practice. (Miedema, 2019) uses cutting depth, cutting angle, cutting speed and soil properties as an input which yields cutting forces and power as outputs. The cutting of clay is solely dependent on the cohesion and adhesion properties, namely the adhesion coefficient ($r = a/c$). Figure 5.3 shows the parameters needed for energy and power calculations for cutting clay in general (Miedema, 2019):

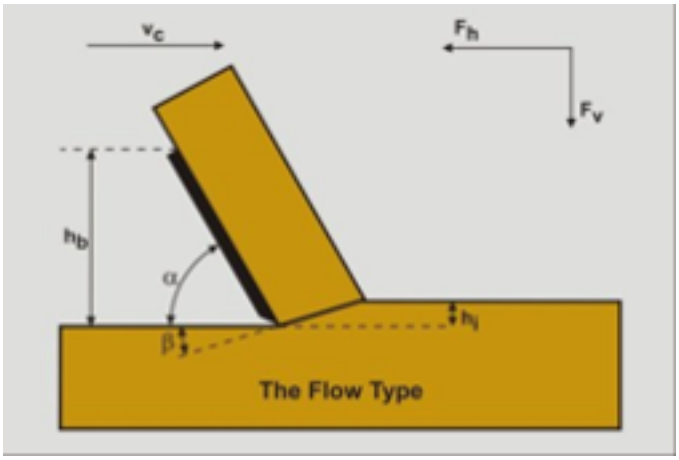

Figure 5.1: Generic cutting theory

The derivation is made under the assumption that the stresses on the shear plane and the blade are constant and equal to the average stresses acting on the surfaces. Since the vertical force is perpendicular to the cutting velocity, the vertical force does not contribute to the cutting power. The power required to cut the clay is simply:

$$P_c = F_h * v_c \tag{8}$$

In practice, there are three types of cutting mechanisms that could occur in clay:

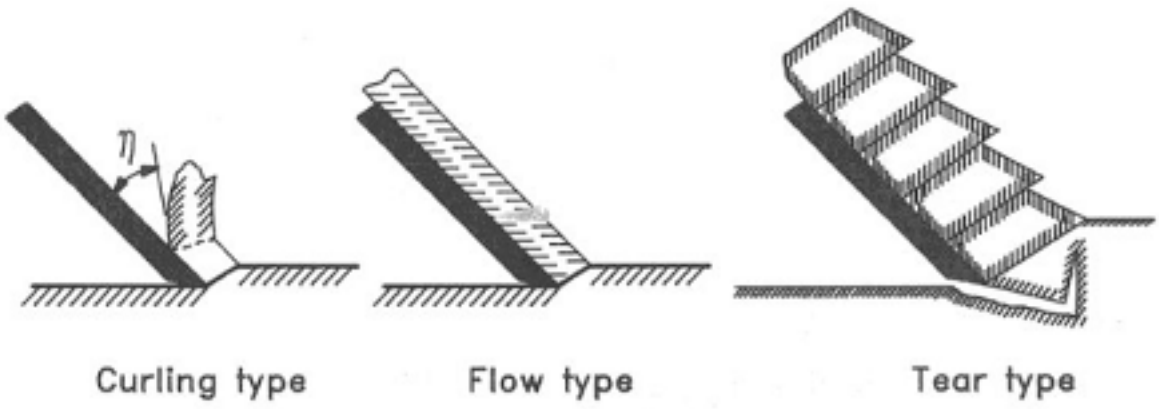

Figure 5.2: Cutting Clay Mechanisms

(Miedema, 2019) states that "Under normal circumstances clay will be cut with the flow mechanism, but under certain circumstances the curling type or tear type may occur. The curling type will occur when the blade height is big with respect to the layer thickness, and/or the adhesion is high compared to the cohesion and the blade angle is relatively big. The tear type will occur when the blade height is small with respect to the layer thickness, the adhesion is small compared to the cohesion and the blade angle is relatively small. "

In the deep-sea mining process, the nodules are located across the surface of the seabed, so the layer thickness will be ominously thinner than the blade height. Furthermore, we are dealing with very soft (2.5 kPa) high plasticity clay, so the adhesion ratio will be quite high. That being said, the tear type will not be of concern for this project due to the unlikely occurrence. It is therefore evident that force and energy calculations should be done on the flow type and curling type mechanisms.

The flow type is the most common cutting mechanism in clay. The forces acting on a cut layer wedge is shown in Figure 5.3. This model assumes that the cohesive stress is the same everywhere. Also, we have a uniform distribution of the normal stress, signifying that the forces act in the middle.

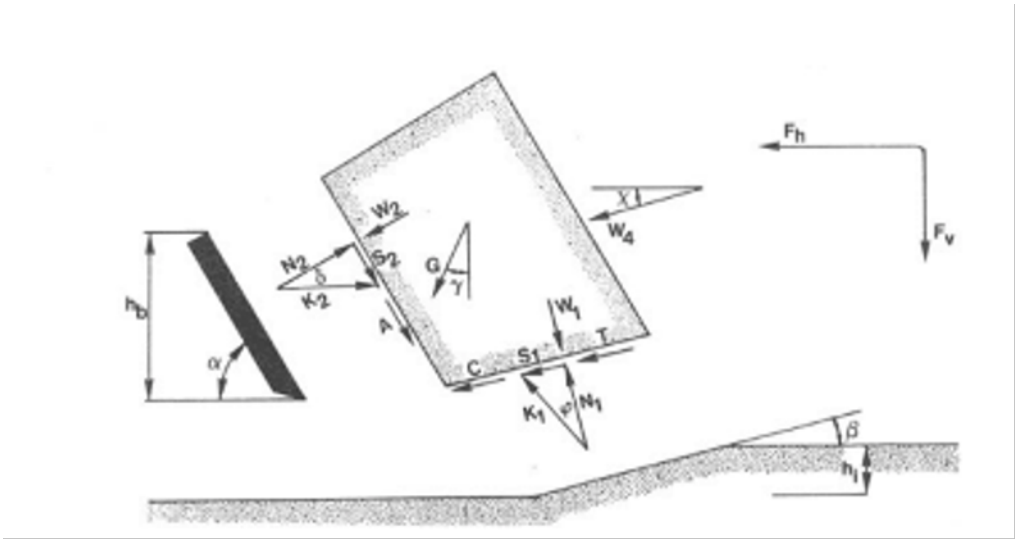

Figure 5.3: Forces on layer cut (Miedema, 2019)

The forces acting on this are:

1. The forces occurring on the blade
2. A normal force acting on the shear surface N_1
3. A shear force S_1 as a result of internal friction $N_1 * tan[\phi]$
4. A force W_1 as a result of water under pressure int the shear zone
5. A shear force C as a result of pure cohesion τ_c. This force can be calculated by multiplying the cohesive shear strength τ_c with the area of the shear plane.
6. A gravity force G as a result of the weight of the layer cut
7. An inertial force I, resulting from acceleration of the soil.

The reactionary normal force acting on the shear surface N1 is computed by:

$$N_1 = \frac{-C * cos(\alpha + \beta) + A}{sin(\alpha + \beta)} \tag{9}$$

The normal force acting on the blade, N_2, resulting from the grain stresses is computed by:

$$N_2 = \frac{C - A * cos(\alpha + \beta)}{sin(\alpha + \beta)} \tag{10}$$

Where

- C = shear force as a result of pure cohesion. This force is found by multiplying the cohesion/cohesive shear strength (τ_c) with the area of the shear plane.
- A = Shear force as a result of pure adhesion between the soil and the blade (τ_a)

As can be seen by equations 9 and 10, an adhesion ratio that is significantly larger than 1 results in the negative normal force on the blade which will correspond to the curling type, and an adhesion ratio that is significantly less than 1 results in a negative normal force on the shear plane. If both normal forces are positive, then the flow type mechanism would occur.

5.1 Flow Type

The most common type of cutting mechanism encountered in practice is the flow type mechanism. It has been established from multiple researchers that adhesion and cohesion of clay increase with an increasing deformation rate. Therefore, a strengthening factor is introduced to account for the strain rate effect on clay. This strengthening factor was derived by an adapted version of the 'rate process theory' that utilizes a Boltzman distribution for the minimum energy needed to shear a cohesive soil. The energy concept was related to shearing cohesive soil and matched up with the Mohr-Coulomb criterion to derive the strain rate for the cohesion and adhesion shown in equations 11 and 12. Note that two different equations are needed to account for the difference in deformation velocity in the shear plane and on the blade.

$$\dot{\epsilon_c} = 1.4 * \frac{v_c}{h_i} * \frac{sin(\alpha)}{sin(\alpha+\beta)} \tag{11}$$

$$\dot{\epsilon_a} = 1.4 * \frac{v_c}{h_i} * \frac{sin(\beta)}{sin(\alpha+\beta)} \tag{12}$$

By taking into consideration the strengthening property of clay and all relevant parameters, the equations for horizontal and vertical force can be formulated shown in equations 5.1 & 5.1 respectively.

$$F_h = \lambda * c * h_i * w * \frac{sin^2(\alpha) + r * sin^2(\beta)}{sin(\alpha+\beta) * sin(\beta) * sin(\alpha)} = \lambda * c * h_i * w * \lambda_(HF)$$

(13)

And:

$$F_v = \lambda_s * c * h_i * w * \frac{sin(\alpha) * cos(\alpha) - r * sin(\beta) * cos(\beta)}{sin(\alpha+\beta) * sin(\beta) * sin(\alpha)} = \lambda_s * c * h_i * w * \lambda_(VF)$$

(14)

With $r = \frac{\alpha * h_b}{c * h_i}$

The strengthening factor λ is a multiplication factor that uses the derived strain rates found in equations 11 and 12. Here (Miedema, 2019) associates multiplication factor λ_a and λ_c for the

strain rates $\dot{\epsilon_a}$ and $\dot{\epsilon_c}$ respectively. Both multiplication factors, however, are almost identical so an average value λ_s has been taken, where:

$$\lambda_s = (1 + \frac{\tau_0}{\tau_y} * ln(1 + \frac{1.4 * \frac{v_c}{h_i} * \frac{sin(\alpha)}{sin(\alpha+\beta)}}{\dot{\epsilon_0}})) \tag{15}$$

Where $\frac{\tau_0}{\tau_y} = 0.1428$ and $\dot{\epsilon_0} = 0.03$ for typical dredging velocities of 1 m/s.

This strengthening factor can be used to find relations for the cohesive force and adhesive force on the blade:

$$C = \frac{\lambda_s * c * h_i * w}{sin(\beta)} \tag{16}$$

$$A = \frac{\lambda_s * a * h_b * w}{sin(\alpha)} \tag{17}$$

Where 'a' and 'c' can be determined experimentally as the adhesive and cohesive shear strength.

5.2 Curling Type

The second mechanism of concern for this application is the curling type mechanism. The curling type mechanism occurs when the layer thickness becomes sufficiently small. This can lead to the normal force (N_2) on the blade to become negative, i.e. a force of the clay adhering to the blade (10).

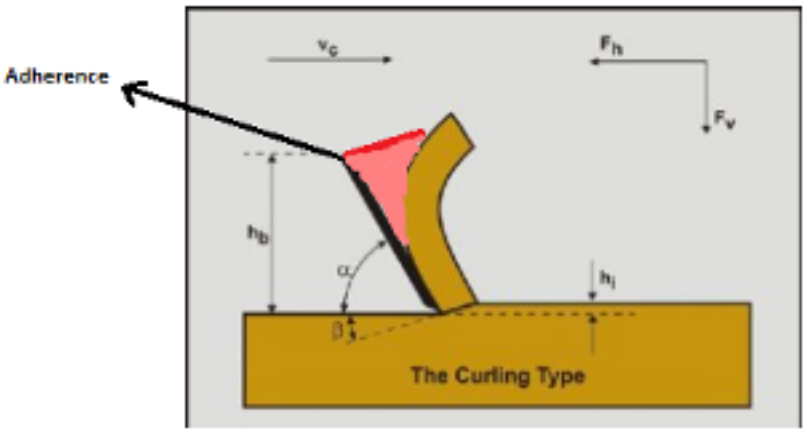

Figure 5.4: Curling Type Mechanism (Miedema, 2019)

This occurs under small cutting angles. Due to the adhesion of clay on part of the blade, the blade height h_b will be defined by the mobilised blade height h_bm. This represents the part of the blade that is in direct contact with the soil. This gives a different meaning to the horizontal force calculation due to the inclusion of the mobilized blade height. (Miedema, 2019) states that the equilibrium of moments about the blade tip must be fulfilled where the normal forces on the blade and clay cut are equated and redistributed. The obtained equation for horizontal and vertical forces are shown in equations 18 & 5.2:

$$F_h = \lambda * c * h_i * w * \frac{sin^2(\alpha) + r_m * sin^2(\beta)}{sin(\alpha + \beta) * sin(\beta) * sin(\alpha)} = \lambda * c * h_i * w * \lambda_(CF) \tag{18}$$

And:

$$F_v = \lambda_s * c * h_i * w * \frac{sin(\alpha) * cos(\alpha) - r_m * sin(\beta) * cos(\beta)}{sin(\alpha + \beta) * sin(\beta) * sin(\alpha)} = \lambda_s * c * h_i * w * \lambda_(VC)$$

(19)

With:

$$r_m = \frac{a * h_b, m}{c * h_i} \tag{20}$$

6 Direction of Approach

Now that the underlying mechanism of adhesion and clay properties have been established, the underlying theoretical points can be wrapped together and quantified by experimental means. Firstly, as discussed previously, the adhesive force of the clay depends largely on the application. A typical cutterwheel consists of a rotary core where racks of cutterblades assembled in a rake-like configuration are mounted for collection. Each rack of teeth follow one another in a circular motion along the sea bed as shown schematically in Figure 6.1.

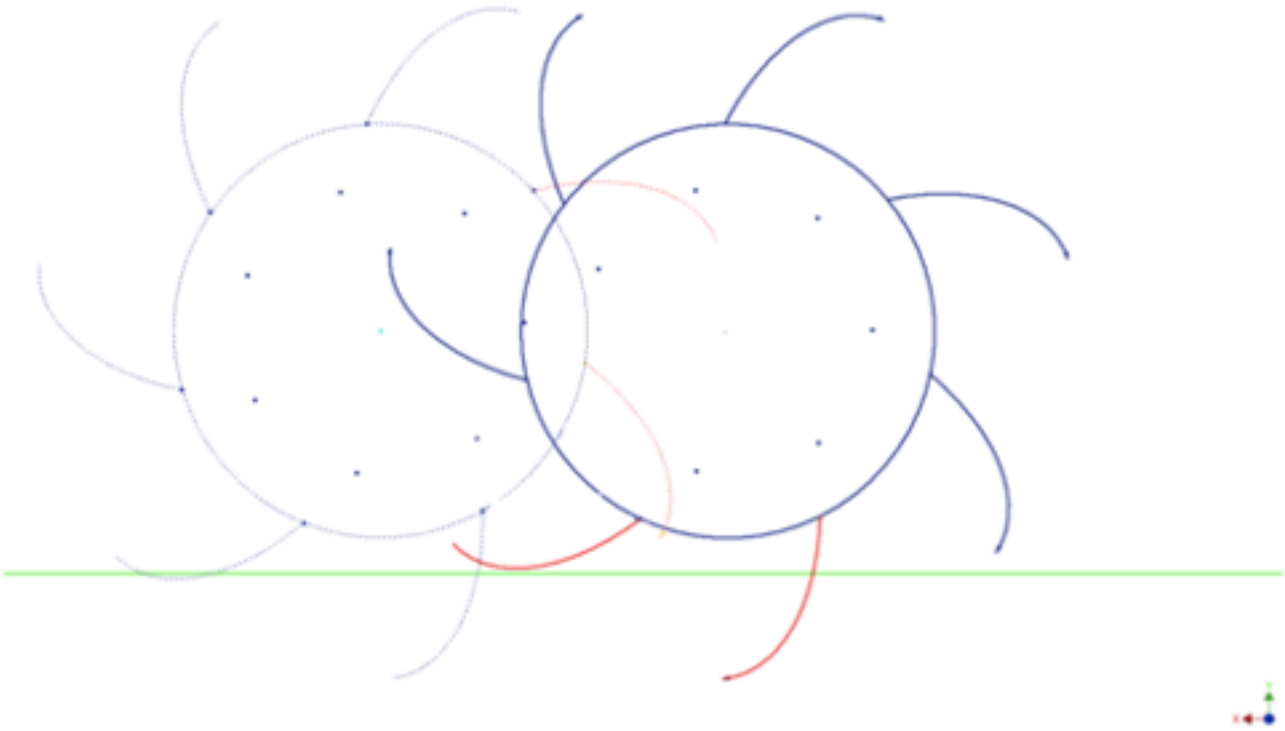

Figure 6.1: Simulation of rotation of cutterwheel around blue circle

To narrow down the scope of the analysis, the focus will be on what force is experienced on each rack of cutter teeth. The rack approaches the soil at a certain angle, penetrates to a certain embedment depth, and finally pulls out of the soil. This process can be divided into two stages:

- Stage 1: Shearing Stage
- Stage 2: Pull out Stage

Both stages will occur at the same trailing velocity (v_c) and rotational velocity (v_r). In Stage 1, the shear strength and shear adhesion prevails, while in Stage 2, the tensile cohesive strength and tensile adhesion prevails. It is important to note that the cohesive strength of the clay depends on the application of loading. Under compressive shear loading, the inter-particle contact increases, the void ratio decreases, and the soil densifies. The opposite occurs under tensile loading, where the void ratio increases and the soil loosens. This is conventionally understood in a triaxial test, where σ_1 refers to the normal larger component of loading while σ_3 is the lateral lower point of stress in which both are related by a horizontal earth coefficient K_0.

6.1 Shearing Stage

The shearing stage is defined when the cutter blade penetrates through the clay. Here, the blade will need to overcome the cohesion of the soil and the resistive adhesive forces on the blade area shown schematically in 2D on Figure 6.3,

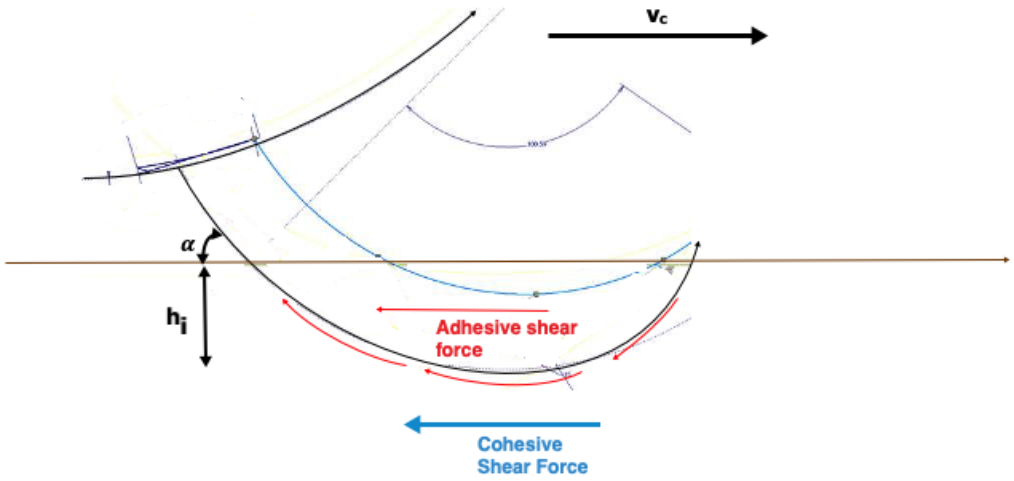

Figure 6.2: Shear Stage of Cutterwheel process

The soil can be seen to shear over a specified shear plane and along the metal-clay interface. Fortunately, the effect of both cohesion and adhesion can be quantitatively measured using a direct shear apparatus. The direct shear test was selected due to the ability to force shear plane in the clay. This is ideal as it mimics the horizontal shear component in practice when slicing through the soil. Moreover, interface tests can be performed by simply replacing or filling up the lower half of the shear box with the test material. A typical shear test set up is shown in Figure 6.3.

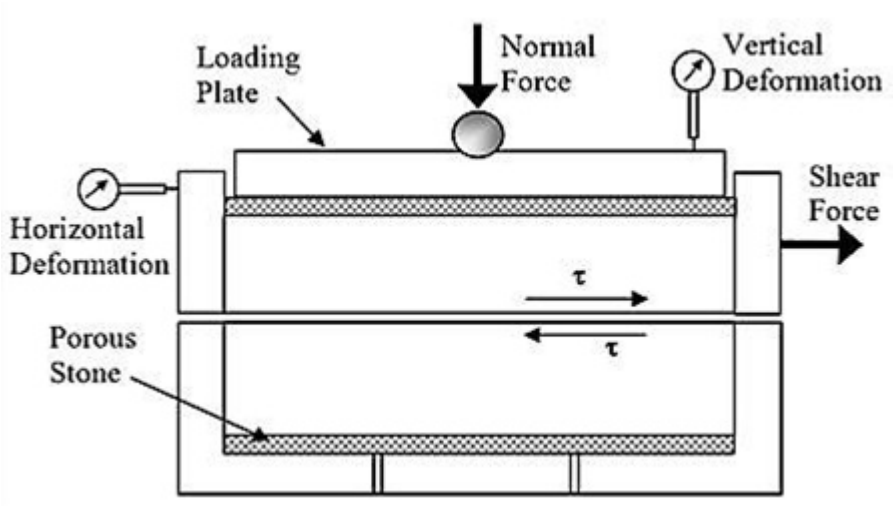

Figure 6.3: Typical Direct Shear Test Set-up

The overall shear resistance on the blade is the summation of the adhesive force on the blade and the cohesive force of the shear plane. Both the internal tangential resistance and the external tangential resistance follow a linear Coulomb type expression where the cohesion and adhesion can be found by shearing over a range of normal stresses.

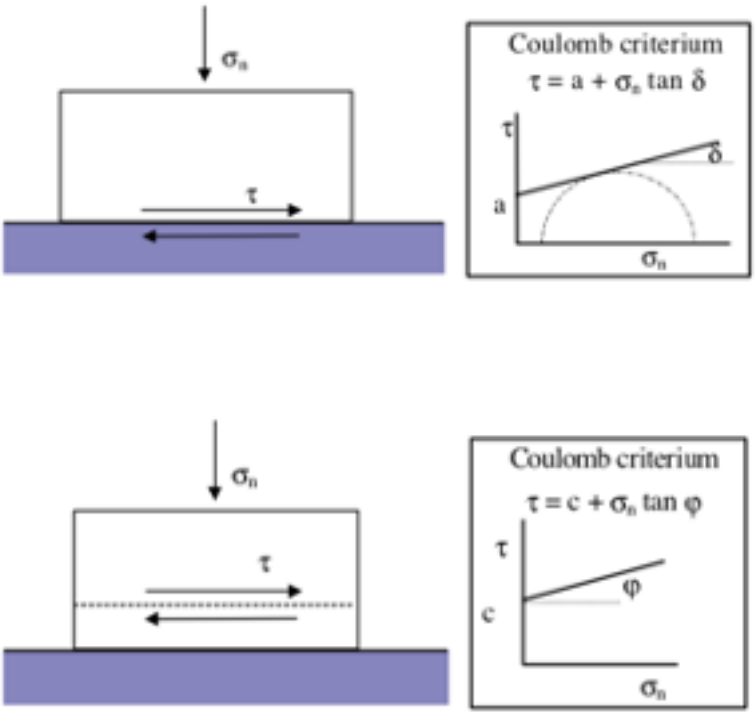

Figure 6.4: Internal and External Tangential Resistances (Verhoef, Ngan-Tillard, Broere, & van Tol F., 1998)

It can be seen that both Coulomb criterion's express the shear strength with a soil property component and a frictional component. The soil sample is said to slide along the clay-steel interface when the adhesive shear strength (τ_a) is less than both the applied shear stress and the cohesive shear strength (τ_c). On the contrary, the sample slides along the clay-clay interface when the internal shear strength is less than the applied shear stress and adhesive shear strength (τ_a). Similarly to cohesion c, the adhesion (a) is described as the resistance at zero normal stress. The second contribution to the shear stress are the internal (ϕ) and external (δ) friction components.

6.2 Pull out Stage

The pull out stage can be defined as when the cutter teeth move upward through the soil as the wheel rotates.

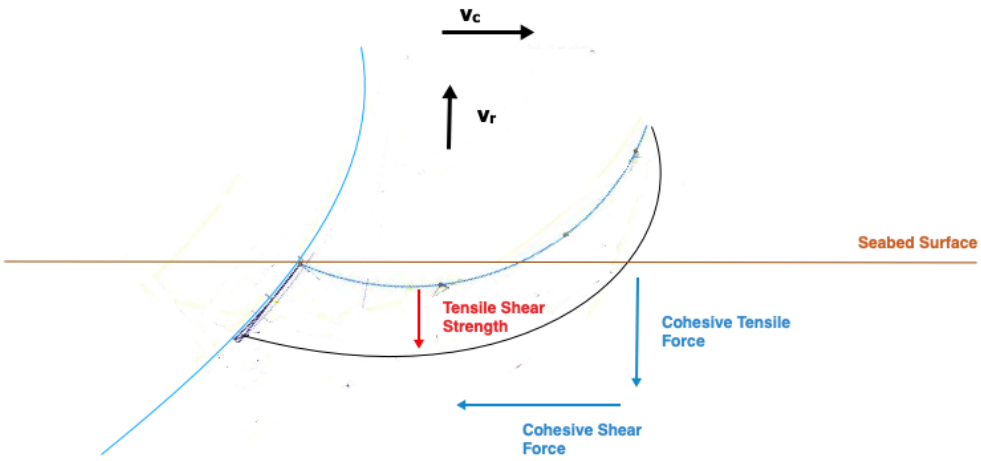

Figure 6.5: Tensile Stage of Cutterwheel process

The upward movement will first have resistances both from slicing through the soil and pulling out from the surface. This pull out force results from the tensile adhesive resistance of the soil. (Zimnik et al., 2000) describes tensile adhesion as shown in equation

$$a_t = \frac{F}{A_s} \tag{21}$$

Where a_t is the adhesive tensile strength, F is the required pulling force, and A_s is the effective contact area. To analyze the pull out resistance endured on the cutterteeth, it would be beneficial to test a similar material using a pull-out apparatus. Pull out tests have been conducted in the past mainly for geosynthetics such as (Mallick, Adanur, & Elton, 1995), (Gorniak et al., 2016) and (Abdi & Arjomandkhah, 2011) to name a few. However, these pull out tests were conducted mainly on reinforced clay (e.g. geogrids) or interbedded sand layers. The tensile pull out interaction between materials and clay have rarely been explored. Fortunately, the tensile adhesion can be easily quantified by simply embedding a test material onto a clay soil and measuring the force required to pull out the material until detachment.

6.3 Total Force Quantification

As shown in section 5, (Miedema, 2019) presents an established method to determine the theoretical cutting force of an underwater excavation for the horizontal and vertical directions using the adhesion coefficient ($r = \frac{a*h_b}{c*h_i}$) which can be utilized for a deep sea mining vehicle. If the adhesion a and cohesion c can be determined experimentally, so can the adhesion coefficient, which can then be implemented in the cutting equations along with all other input parameters. The adhesion parameter a can be found by performing interface tests as seen on Figure 6.4. Similarly, with the acquired adhesion coefficient, a reasonable estimate of the vertical component of the force is found. By performing pull out tests, it would be interesting to see if the obtained adhesive stress (a_t) relates to the vertical force calculated by equation 5.1 or 5.2.

However, the use of the clay cutting equations is for a singular generic straight blade cutting through soil. To be able to apply it to the cutterwheel design, the effect of the design aspects should be considered. To account for the use of multiple blades with a certain spacing in between it is proposed that a scaled model of a cutter rack through clay should be undertaken. This is explored in the next section.

6.4 Selected Adhesion Mitigation Measures

Applying most mitigation measures in section 4.4 are not logistically or energetically sound when in application to deep sea mining. When considering mitigating measures it should fulfill the following requirements:

- Energetically efficient
- Within financial budget
- Easily applicable
- Risk-free
- Environmentally friendly

When considering energetic efficiency, techniques such as raising the temperature are not viable. (Azadegan & Massah, 2012) only realized a significant reduction in adhesion potential when raising the temperature from 5°C to 30°. A 25°C increase to the harvester 5 kilometers down the ocean can prove to be difficult to apply within reasonable energetic constraints. Electro-osmosis does not require as much energy for it to be effective, as typically 100 V to 300 V is enough to create a thick enough water film between the clay and soil engaging component. However, the issue lies on whether there is enough contact time between the blades and soil to allow the water film to develop. It is plausible that mechanical innovations can significantly improve the design of the harvester such as adding a counter-scraper during wheel rotation to remove excess clay or mounting jet nozzles to spray off adhered clay before depositing the nodules in the processing unit. However, this depends on the mechanical aspects of the harvester itself and can not be easily tested for in this thesis.

The focus is shifted to the component surface design. On picking up nodules, the blades can be modified to break the continuous interfacial water film. Adding convex corrugations on the blade is not ideal, as it will falter the sleek penetration design of the blades generating more force to penetrate the soil. The two selected surface design methods are therefore applying surface coatings and adding perforations on the blade. The surface coating should be able to mitigate adhesion while also maintaining its structural integrity during its application. The MagnaCoat, fulfills these requirements and it would be interesting to see the degree of its adhesion reduction potential. Furthermore, having perforations in the blades will break the continuous water film between the clay and the blade which could have potential to reduce the adhesive force and thereby the total horizontal force required to slice through the soil. This concludes that blade surface modifications are most ideal, specifically blade perforations and Magna-coated blades.

7 Materials and Methods

To investigate the influence of adhesion on the cutterwheel it is proposed that both laboratory and scaled tests are to be done for a full experimental analysis. The lab tests to be performed will be done using two apparatuses. The first a standard direct shear test. The direct shear test will be used to find the shear strength of the soil specimen under a certain normal load and strain rate. The same apparatus can be used to measure the adhesive shear strength of the clay, by moving the soil specimen a custom built plate fitted in the bottom half of the shear box. The second apparatus to be used is a tensile pull-out test.

7.1 Test Soils

For both tests, two typical offshore clay soils will be tested to determine the significance of certain parameters on shear strength and adhesion potential.

It is interesting to find out the Atterberg limits of such a soil, so procedures are carried out under ASTM standards to find the plastic limit (PL) and liquid limit (LL). The plastic limit was found by the ASTM standardized procedure of rolling a moistened soil into elongated threads until the threads crumble when it has a diameter greater than 3 mm.An often overlooked parameter, the sticky limit (SL), is defined as the moisture content at which the clay first starts to stick. This is easily found by methodically adding 2 cc's of water and running a nickel-plated or steel spatula over the clay. If sticking is observed, the water content of that sample is the sticky limit. Both methods of finding the plastic and sticky limit have room for personalized error but provides a satisfactory basis due to its simplicity. The liquid limit according to ASTM D-3080 was found by performing the cone penetration tests on three samples at different water contents and linearly interpolating the line on a displacement (mm) vs water content (%) curve to find the water content corresponding to a displacement of 20 mm.

7.1.1 Test Clay 1

The first clay type is a typical offshore clay. The soil is a high plasticity soft soil that is said to contain smectite from XRD test data in nearby sites. However, it is still unknown what the exact proportions of minerals are available. The clay sample is brought in its natural state and was submerged in water for a period of at least 3 days to ensure saturation and allowed to swell.

Figure 7.1: Test Clay 1

First of all, the water content of the saturated clay was determined by oven drying at 110°C and was found to be around 180%. This indicates that swelling minerals are present in the clay. The void ratio can be estimated from the specific gravity and saturation level shown in equation 22:

$$e = \frac{w * G_s}{S_r} \tag{22}$$

The sample is assumed to be fully saturated, $S_r = 1$ with typical values for specific gravity of clay range between 2.70 – 2.80 according to ASTM D 854-092. This yields an estimated void ratio of about 4.95 which indicates the presence of highly expansive minerals. The Atterberg limits found are shown on Table 7.1.1.

Limits:	PL	SL	LL	PI
Water Content:	70%	85%	200%	130%

7.1.2 Test Clay 2

In order to compare data results to another clay type, an artificial clay is to be tested. The artificial clay was chosen in order to imitate typical behaviour of offshore soft clay. The artificial clay available is a mixture of two materials:

1. Sibelco FT-S1 ("Abidichte Ton") consisting of 64% Kaolinite, 10% Illite, 19% Quartz and 7% various other minerals
2. Cebo OMCA Betonite consisting of 17% Kaolinite, 17% Illite and 66% Montmorillonite

The artificial clay is a 2:1 ratio of OCMA and FT-S1. Recorded Atterberg limits are shown in Table 7.1.2

Limits:	PL	SL	LL	PI
Water Content:	60%	75%	260%	200%

This type of clay is purely used as a reference to establish more authentic correlations from having more empirical data. This type of clay shows to have a wider plasticity index indicating the presence of a significant amount of 2:1 type clay minerals.

7.2 Sample Preparation

Directly utilizing the clay from the box core will be quite problematic due to the relative inhomogeneity's and swelling behaviour. Due to the presence of swelling minerals, the clay will tend to absorb a large quantity of water leading to volumetric expansion. Furthermore, for direct shear testing, the sample clay is much too soft and ductile to be handled in a shear testing machine. It is therefore proposed that the samples will first need to be consolidated to sufficiently withstand normal loads imposed during testing. For the clay sample 1, it was found through trial and error that a minimum of 20 kPa is necessary to obtain a manageable sample. By similar trial and error, clay sample 2 needed 100 kPa normal stress. A minimum value normal load was sought out to create a sample with a desired minimum thickness and to keep a degree of plasticity to obtain workable values when measuring adhesion.

Direct shear samples of the clay soils were prepared by drying and crushing the soil to fine particles passed through a 425 micron sieve and mixed thoroughly to a slurry approximately 1.5 times the liquid limit. This process ensures a uniform homogeneous sample suitable for the direct shear test. The clay 1 slurry was consolidated in a piston consolidometer (see Appendix A.2) under 20 kPa of pressure to obtain a manageable sample. Here, weights measuring up to 60 kg where uniformly place on the slurry and left for 24 hours to ensure full consolidation. Resulting samples exhibited water contents near the plastic limit of around 90-120%. This plasticity was enough to maintain its shape when cut with a square-shaped moulder to fit in the shear machine.

For the Clay 2 sample, a larger normal stress of 100 kPa was applied in a Rowe cell in order to obtain a manageable sample (Appendix A.2). The need for a higher consolidation load could be due to the relatively low permeability of the clay which slows the consolidation significantly. The Rowe cell has a porous disk at the bottom and top of the sample which will methodically extract water as the air pressure increases. The advantage of the Rowe Cell is that consolidation times were cut by a factor of four due to the double drainage from the sample. Resulting samples exhibit water contents around 110-145% which was deemed sufficient for use in the direct shear apparatus.

7.3 Shear Testing

The internal and external shear strength or cohesion and adhesion respectively, of the samples are determined by performing direct shear tests over a range of normal stresses. The direct shear test used is an ELE manufactured apparatus that meets the standards for ASTM D-3080 shown in Figure 7.2.

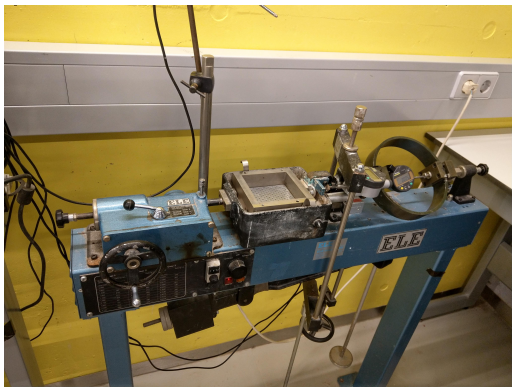

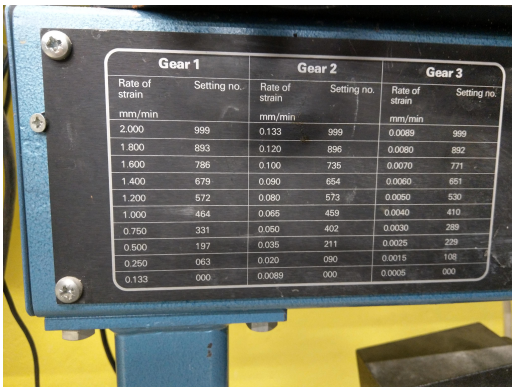

Gear 1		Gear 2		Gear 3	
Rate of strain mm/min	Setting no.	Rate of strain mm/min	Setting no.	Rate of strain mm/min	Setting no.
2.000	999	0.133	999	0.0089	999
1.800	893	0.120	896	0.0080	892
1.600	786	0.100	735	0.0070	771
1.400	679	0.090	654	0.0060	651
1.200	572	0.080	573	0.0050	530
1.000	464	0.065	459	0.0040	410
0.750	331	0.050	402	0.0030	289
0.500	197	0.035	211	0.0025	229
0.250	063	0.020	090	0.0015	108
0.133	000	0.0089	000	0.0005	000

Figure 7.2: ELE Shear Testing Machine - TU Delft

The apparatus is fitted with vertical and lateral needle extensometers to measure the displacements with an accuracy of +/- 0.001 mm. A third extensometer is fitted to measure the radial deformation of the ring that is calibrated to give the shear force in Newtons. The shear box canister is to be filled with distilled water before commencing of shear strains to mimic so called 'undrained' conditions. Undrained conditions in this thesis is to refer to the blockage of flow paths of water during shear testing to a degree. The moisture in the clay sample is not entirely contained, but it is a fair assumption considering the relatively quick shearing rate. Therefore, 'drained' tests will refer to a direct shear test of a sample at 0.1 mm/s with no water in the canister, and 'undrained' tests refer to a direct shear test of a sample at 0.5 mm/s with distilled water in the canister. The square shear box to be used measures 10 x 10 cm with a bottom plate, two drainage plates, and a loading cap shown in Figure 7.3.

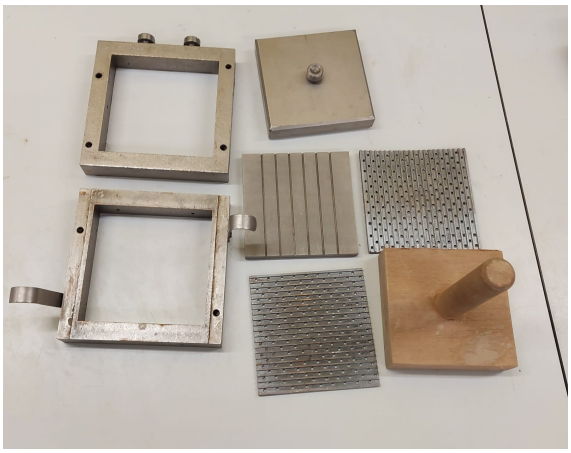

Figure 7.3: Shear box and plates used

7.3.1 Direct Shear Testing Procedure

The procedure for a the consolidated undrained (CU) Direct Shear test is carried out by the following procedure:

1. Consolidate clay in Piston cell or Rowe cell to desired stress level
2. Cut and place clay sample into sample box. Place porous inserts over the clay sample and place the shear box into the apparatus and align it to the load frame.

3. Fill shear box canister with distilled water (if undrained test) and adjust gear to the desired shear speed
4. Connect and adjust the shear force loading system so that there is no load recorded on the load measuring device
5. Position and adjust the shear displacement measurement device. Obtain an initial reading or set the displacement to zero
6. Place the normal force loading yoke into position and adjust it so the loading bar is aligned.
7. Wait until vertical displacement is relatively constant (about 30 seconds) and commence shearing until failure

Sample clay 1 was sheared under normal loads 20, 50 and 100 kPa. The load was applied until there is little to no change in the vertical displacement, then shearing commenced. Both consolidated drained and consolidated undrained tests were performed on the clay sample to interpret the different behaviour. The undrained DS test was performed at a rate of 0.5 mm/s with the resulting stress paths shown in 7.4.

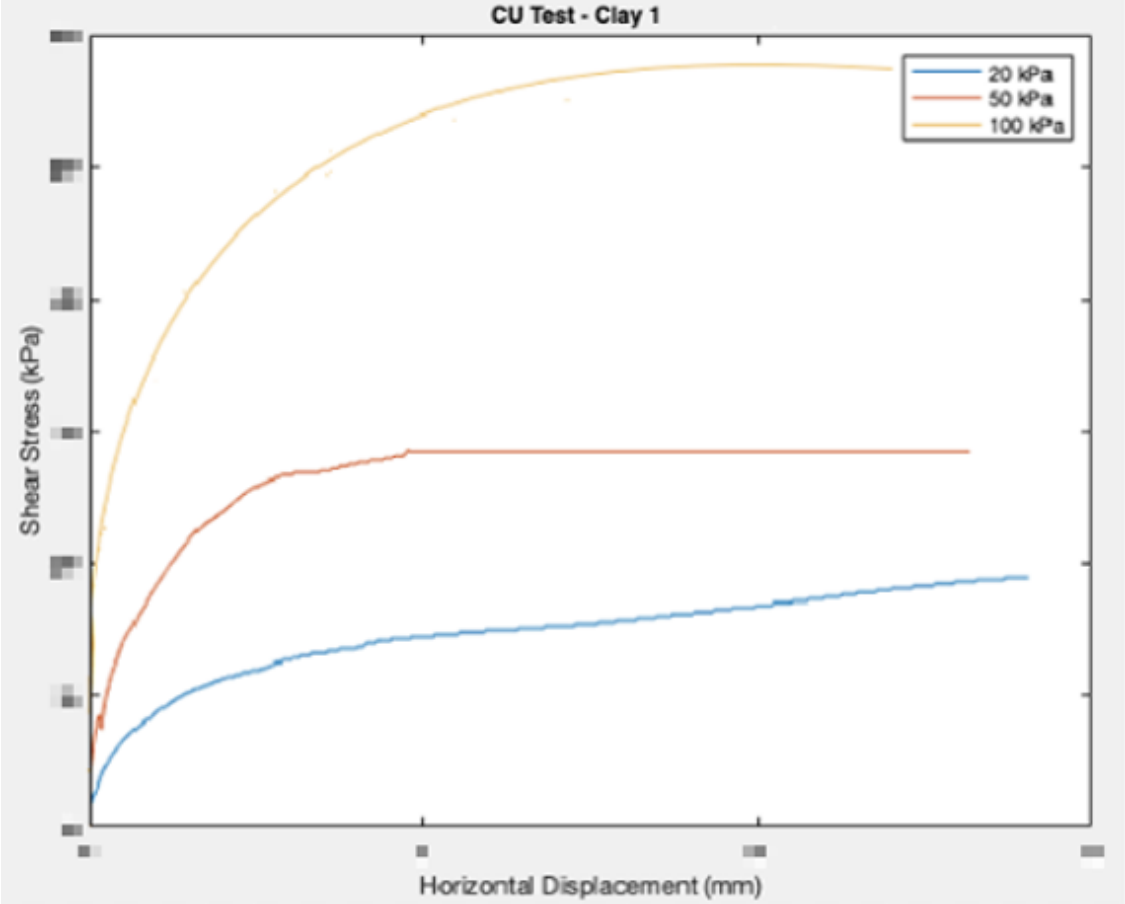

Figure 7.4: Undrained Shear Stress Paths - Clay 1 Sample

Similarly, DS tests were done at a speed of 0.1 mm/s to allow pore pressures to dissipate more evenly during shearing. The failure envelopes of the undrained and drained samples of Clay 1 are compared in Figure 7.5.

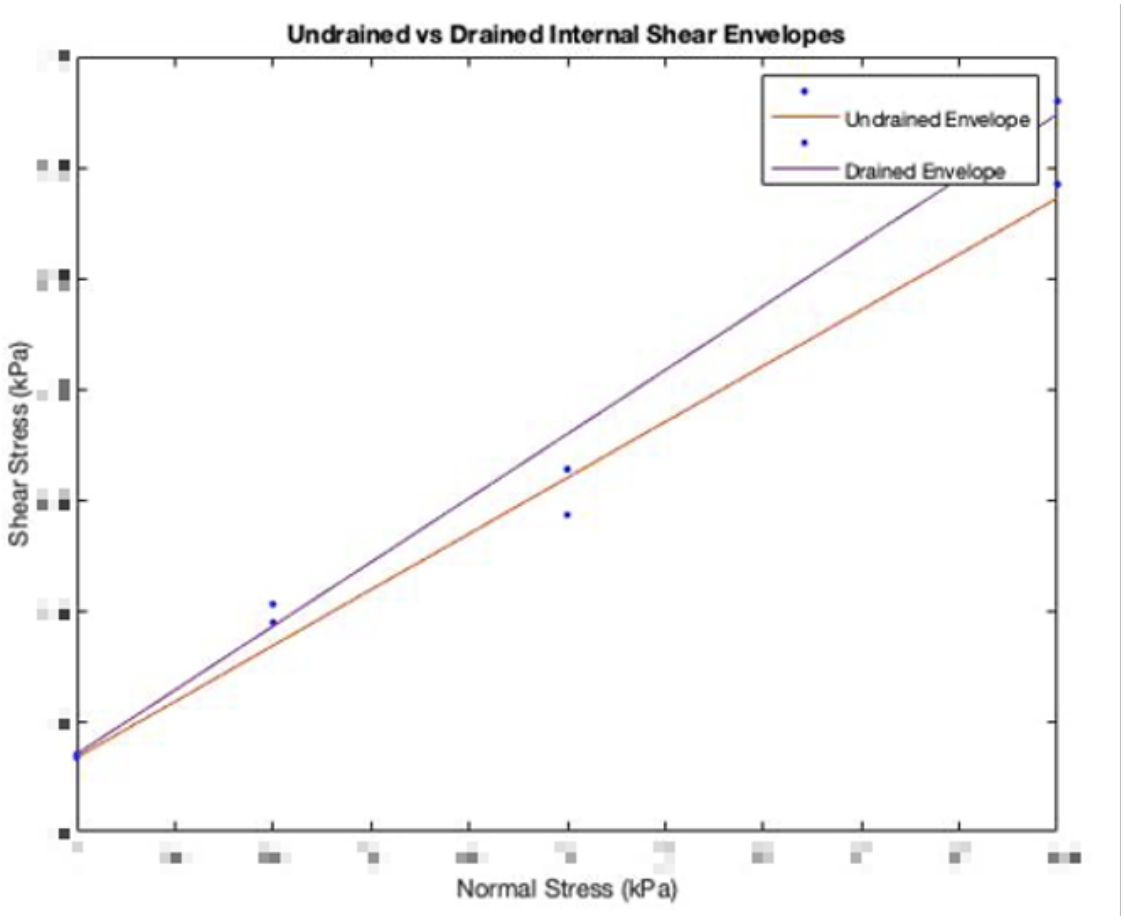

Figure 7.5: Undrained vs Drained Internal Shear Envelopes

It can be expected that the drained stress path shows a steeper gradient than its undrained counterpart. The undrained shear strength shows to be less than the drained shear strength which is a typical property of normally consolidated clay soils. Theoretically, a pure clay shows quite a shallow inclination of the failure envelope in comparison to other soils, so it makes sense that as the inclination becomes more shallow with increasing undrained behaviour. Shearing NC clays exhibit an increase in pore water pressure which negatively influences the effective stress. It shows, that with minimizing drainage, the shear strength will show to reduce.

To overcome the insufficiency's of calculating undrained strength with a direct shear apparatus, a hand held shear vane is tested on all consolidated samples prior to shearing. The vane used is the Gilson pocket shear vane model Hm-504A shown in Appendix A. Following the standard procedure of ASTM-D8121, the blades are embedded into the soil sample and slowly rotated until soil matrix failure occurs. The 47.6 mm attachment is used in which one complete revolution is approximately $0.2186 kg/cm^2$ which is separated in 10 divisions. By multiplying the reading of the vane during failure with the correct multiplier will yield the correct shear stress. The shear strength of a cohesive soil is dependent upon many factors, including rate of loading, progressive failure, orientation of the failure plane, and pore water migration during testing. Although the vane shear test device does not eliminate these variables, it does give repeatable values in a homogeneous clay yielding a relatively good accuracy of shear strength.

7.4 External Shear Strength

The external shear strength can easily be found by shearing the top half of the shear box against the test material. In order to do this, the test material should be cut to perfectly level with the top of the bottom half of the shear box. Similarly to the standard DS test, consolidated undrained samples are prepared as explained in section 7.2.

7.4.1 Interface Materials

The materials to be tested are materials that are found on the harvester. It is also noteworthy to assess the effect of material type on adhesion. Various materials will have a different affinity to the clay due to differences in surface energies. The materials to be tested are synthetic rubber, aluminium, stainless steel (304), and MagnaCoat polymer shown from left to right on Figure 7.6.

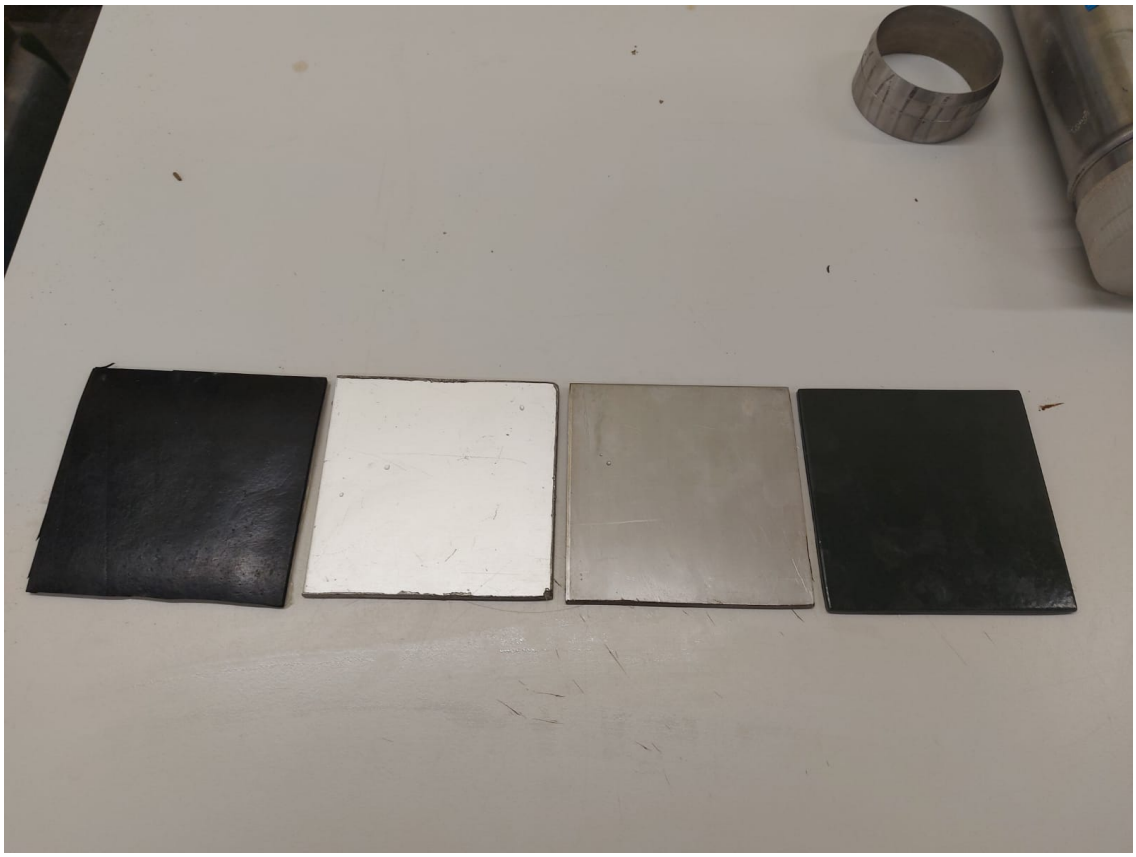

Figure 7.6: Interface Test Materials : *From left to right: Synthetic Rubber, Aluminium, Stainless steel, MagnaCoat*

The experiment is to determine the effect of the material on interface shear resistance, but surface roughness of the material can also significantly influence the obtained readings. The exact materials used along with their corresponding roughness's are presented in table 7.1. The values are average values for the specific type of material according to NEN-EN-ISO standard for surface roughness's:

Material	Average Roughness Ra (μm)
AISI 304 Stainless Steel	0.30 - 0.50
1xx.x Aluminium	0.24 - 0.74
Synthetic Rubber	0.03 - 0.25
MagnaCoat Fluropolymer	0.00 - 0.5

Table 7.1: Plate Materials and average roughness

Porous filler plates are placed in the shear box to occupy the empty space ensuring the test material plate is level with the top surface of the bottom half of the shear box. The test plates are thoroughly cleaned with dish soap and distilled water and dried using acetone solution. The materials were cut by a metal saw and may leave rough edges on the sides. The sides were filed down with an angle grinder to mitigate the side roughness in comparison with the middle.

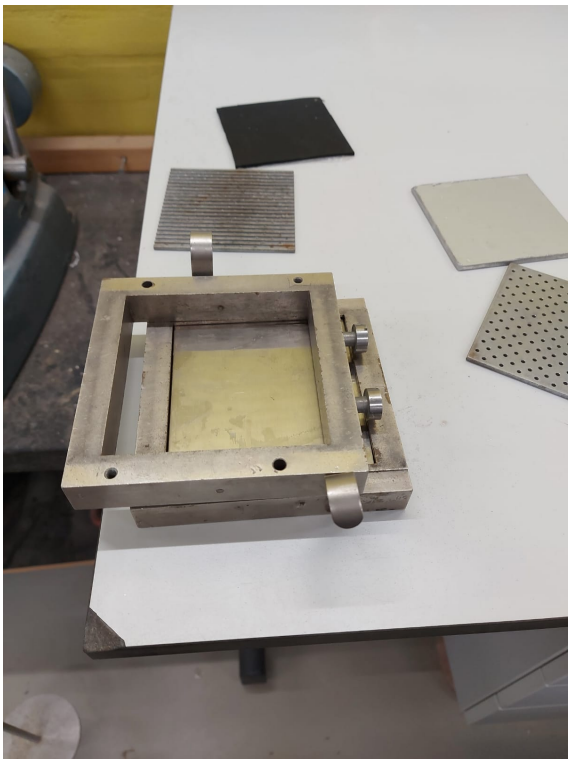

Figure 7.7: Interface Setup with Steel Plate

7.4.2 Interface Shear Test Procedure

The procedure to find the adhesive shear stress can now be underlined. This process is not a standardized procedure, but has been suggested below:

1. Consolidate clay in Piston cell or Rowe cell to desired stress level (as described in section 7.2)
2. Cut a sample of clay into the mold of the upper half of the shear box and place it in the apparatus. Add porous filler plate along with a porous inserts over the clay sample to allow topside drainage and place the shear box into the apparatus and align it to the load frame.
3. Fill shear box canister with distilled water (if undrained test) and adjust gear to the desired shear speed

4. Connect and adjust the shear force loading system so that there is no load recorded on the load measuring device
5. Position and adjust the shear displacement measurement device. Obtain an initial reading or set the displacement to zero
6. Place the normal force loading yoke into position and adjust it so the loading bar is aligned. As soon as the normal load is applied, time 30 seconds which is defined as the 'contact time'.
7. After 30 seconds of contact time begin shearing sample over the material plate.

7.5 DS Test Limitations

Note that a dimensional analysis of small-scale data to predict in-situ results directly is usually not accepted in geotechnical analysis due to the fact that some soil properties and foundation characteristics are not easy to simulate accurately (unless in a centrifuge). Furthermore, an undrained test is generally not possible in a direct shear test, as there is bound to be some drainage during testing. Lastly, the direct shear test has a non-uniform distribution because the failure plane is imposed by the user. However, the direct shear test can still give quite accurate results of the shear strength and how the shear strength varies with different normal load and strain rates. The imposed failure plane can also be somewhat representative of how the soil is to be sheared in practice when slicing through the soil with cutterwheel blades.

7.6 Tensile Pull out Tests

The adhesive resistance of clay can be measured by measuring the force required to pull a test material from a clay surface. Separation tests have been carried out through the use of separation pistons in previous literature: (Thewes, 1954),(Feinendegen, Ziegler, Spagnoli, Fernandez-Steeger, & Stanjek, 2010),(Burbaum, 2009), & (Yalamarty, 2012), where the tensile adhesive force was measured for unsaturated clay samples at various moisture content. Literature have shown that the maximum tensile force was found at a 'peak' moisture content between the plastic limit and liquid limit and decreased with increasing water content past the optimum adhesion point. Furthermore, increased normal loads into the clay sample and increased contact times have shown to increase the pull-out force potential. However, there has been no literature on the pull out forces relating to adhesion on saturated samples. In offshore geotechnics, pull-out force necessary to remove a mudmat or suction caisson, for example, is weighted against the suction force and frictional resistance along the geometry of the object to be removed. Several models such as the IBW PAN and Oxford model can be used to predict the break-out force necessary to remove an object from a soil. The adhesion phenomenon in prediction models and analysis have been disregarded and categorized as 'suction'. This is no surprise, as discussed in section 4, the capillary pressure between the clay seabed and soil-engaging component makes up the majority of the adhesive force. Therefore, the pull-out force or suction can be regarded as the tensile adhesive strength in pull-out testing.

The pull-out test will be performed for completely submerged clay to simulate offshore conditions. When submerged and fully saturated, the clay is expected to exhibit the very soft characteristics observed in practice. Therefore, it is not applicable to test the pull-out forces for varying normal loads, as there will be significant sinkage and the goal of measuring the tensile adhesion will be compromised. If the plate is to sink before pull-out, the force observed is no longer a measure of the interfacial bond between the clay and the plate, but also the cohesive force of the clay. To mitigate this impact, a small load will be placed on the test plates before initiation of the pull force. The load is necessary to ensure there is sufficient contact between the test plate and the test soil. What is typically of concern especially in offshore practices, it the rate of pull-off. It is one of the key factors when predicting the force necessary to remove an object residing on the ocean floor.

7.6.1 Testing Apparatus

To measure the tensile adhesive force of a saturated clay a custom testing apparatus is built called the STICH unit in the GE lab at TU Delft. The STICH unit consists of a manoeuvrable cart that moves along a rail given an electrical input voltage. The test set-up is schematically shown in Figure 7.8.

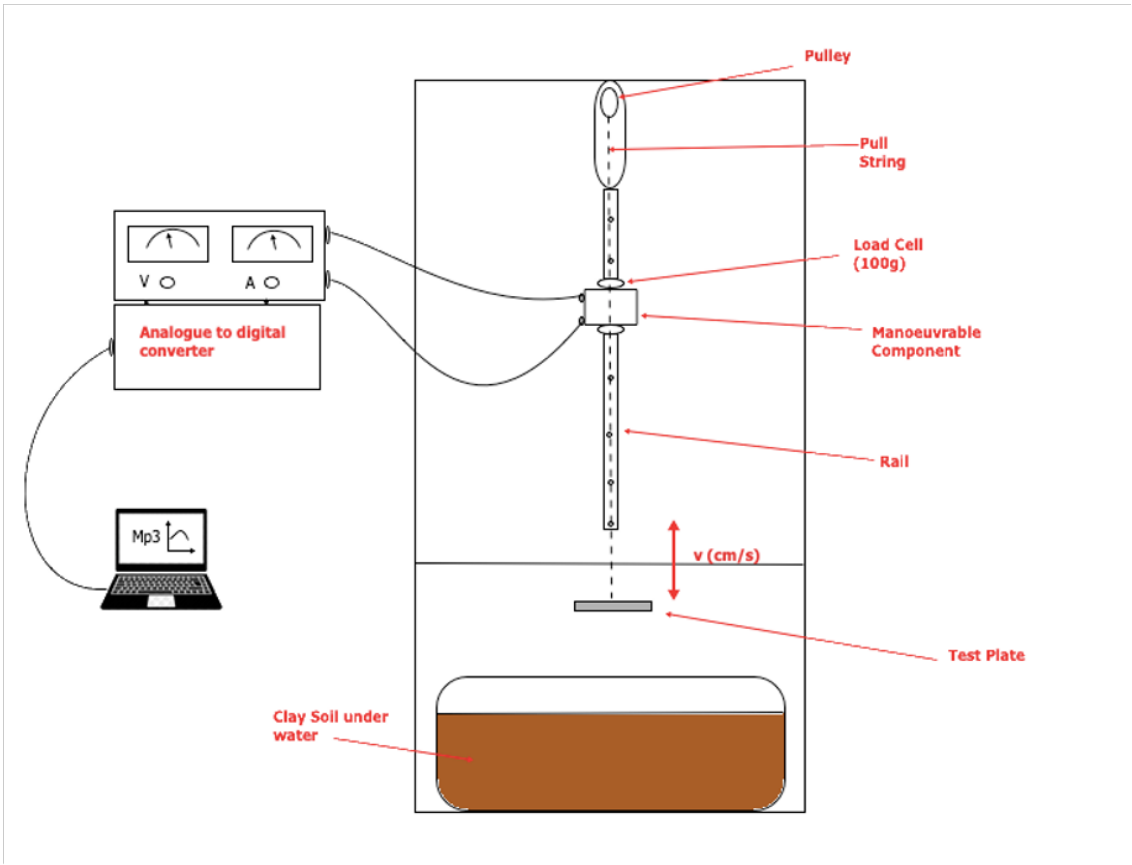

Figure 7.8: STICH unit Schematic

Two sensitive 100g load cells are attached to either side of the manoeuvrable component which in turn are linked to a pull string. The string runs down along the full length of the STITCH unit which is to be connected to the test plates. The testing plates are the same plates used in the interface DS tests measuring 10x10 cm. At the bottom of the STICH unit lies a large container with the test soil. The container needs to be significantly larger than the test plates to mitigate the effects of the boundaries on test readings. Figure A.13 & 7.10 show the actual STICH unit set-up:

Figure 7.9: Front View of STICH Unit

Figure 7.10: Zoom in on Manoeuvrable Electrical Component

The test plates are fitted with wire clips that have been attached to one side of the plates with a super adhesive hot glue as seen on Figure 7.11. This ensures that there is no interference at the testing face. Acetone solution is used to dry the surface before applying the glue. The glue has a much higher adhesive strength then expected from the saturated clay and provides a sufficient method for this test set-up.

Figure 7.11: Wire Clips on Test Plates

The plates are to be suspended on the tow wire in the STICH unit set-up and are attached by tie-wraps. The tie-wraps go through each of the four corners of the test plate to ensure simultaneous detachment of the test plate.

7.6.2 Setup and Calibration

The manoeuvrable component runs on a smaller tow wire system, where the component is pulled by an electrical pulley along the rail which in turn pulls on the string and metal test plate. Given a certain voltage input, the component is moved at a certain rate. The rate at which the plate will be moved can easily be determined by measuring a certain distance along the rail, and recording the time needed for the component to travel that distance. The control unit box has a maximum input of 30 V given a 1.5 amp supply (Figure 7.12). The voltage and rate of pull are recorded and follow a linear trend shown in Figure 7.13.

Figure 7.12: Control Input Unit - Voltage

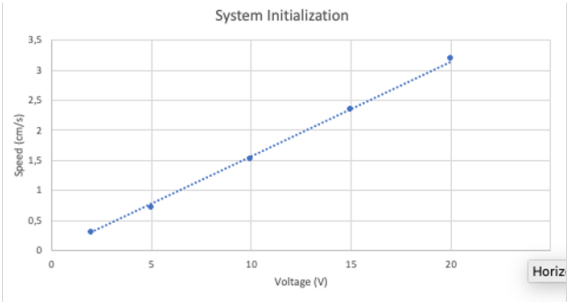

Figure 7.13: Rate of Speed System Initialization

7.6.3 Tensile Testing Procedure

The tensile test is performed in order to see the influence of the pull out rate on the tensile adhesion. Pull off tests are performed as follows:

1. The container is filled with test clay and water is poured to about 5 cm above the soil surface and left to settle.
2. The plate is hooked onto the tow string with tie-wraps and adjusted to ensure the plate is perfectly perpendicular to the clay surface.
3. The tow string is brought down until there is contact between the plate and clay.
4. A 500 g square weight is placed in the center of the test plate to ensure sufficient contact between the clay and the test plate.
5. The desired voltage input is selected and the system software MP3 is initialized.
6. After 30 seconds from placing the weight, the pull-out test starts and the force is recorded on the MP3 software.

It is important that the time the test plate is in contact with the clay are the same for each test. The test 'time' is defined from the moment the 500g weight is placed on the test plate to the moment it is removed before initiation of the pull-out force. The influence of the test time for both test clays can be measured by varying the test times and recording the pull-out force needed for complete detachment. Each test is repeated at least three times to obtain a reliable estimate of the pull-out force. The testing procedure as well as how the results will be interpreted are schematically presented in Figure 7.14:

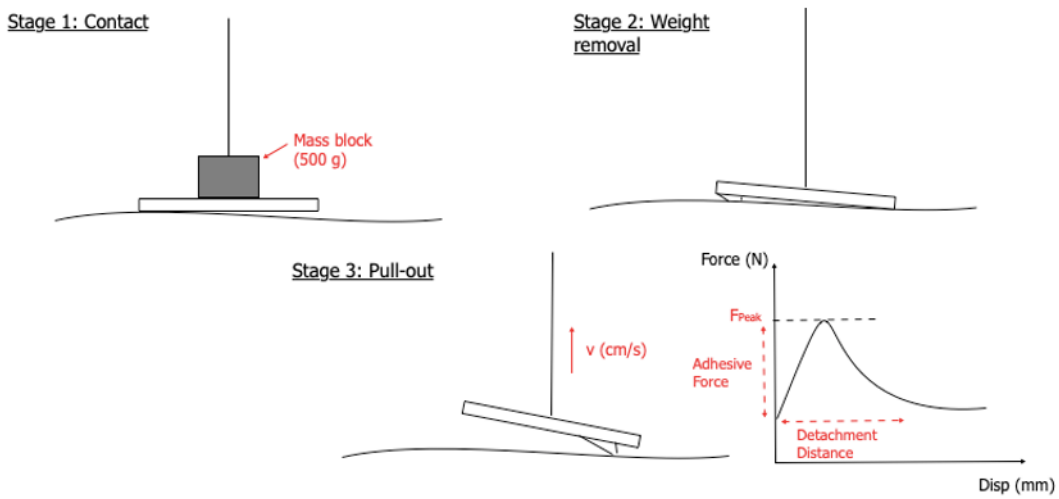

Figure 7.14: Tensile Testing Procedure

7.7 Scaled Cutter Test

In order to apply the acquired knowledge of adhesion in its relation to the cutting force, a scaled model of one cutter rack is suggested. The objective is to measure the horizontal force required to drag the cutter teeth through the test soils and relate the acquired adhesion values from the laboratory tests to the cutting equations of (Miedema, 2019).

7.7.1 Set-up

The soil will be held in a rectangular flume shown in an AutoCAD image in Figure 7.15.

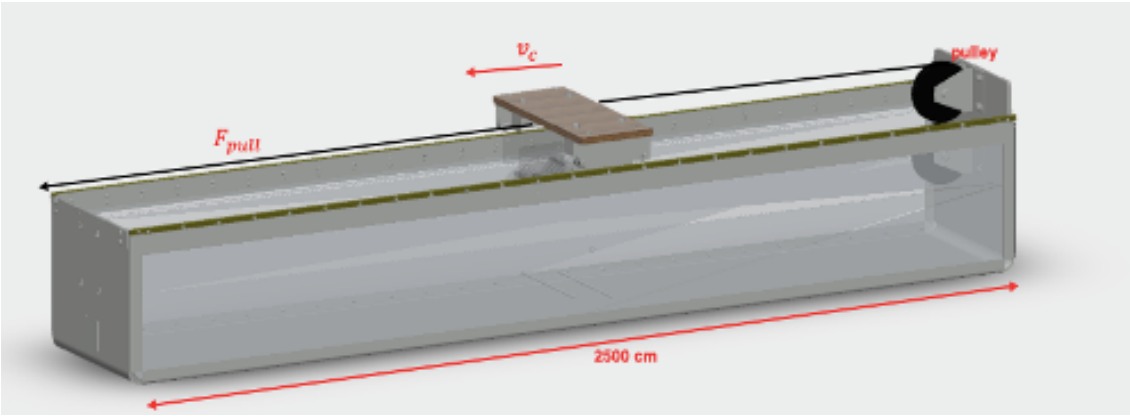

Figure 7.15: Test Flume

The flume measures 2.5 m x 0.4 m x 0.4 m and fitted with a rail on the sides and a pulley at the end. The soil to be tested is filled inside the flume to a layer thickness of 10 cm. A movable cart with wheels can move smoothly along the length of the flume. Mounted onto the cart, are the test blades to be dragged through the soil. A 5 mm thick steel pull wire attaches the pulley to the

cart which is pulled along the length of the flume by an overhead crane at a fixed speed of 0.85 m/min. The pulley and rails are lubricated to reduce frictional effect on the movement.

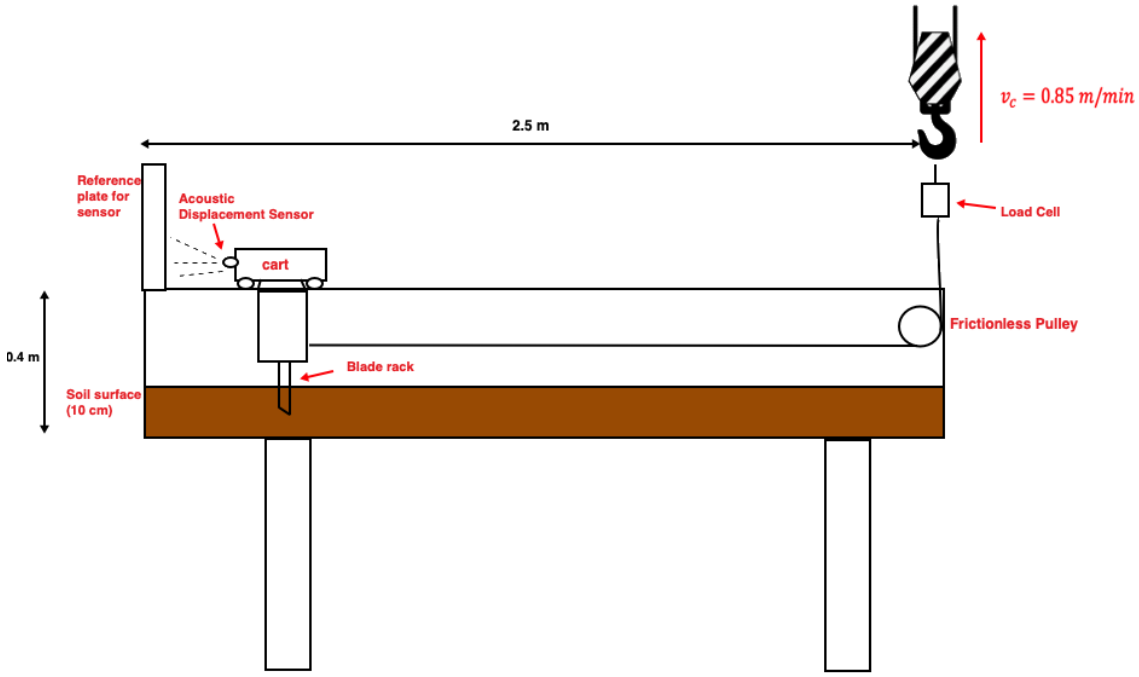

Figure 7.16: Scaled Test Schematic

The stainless steel cutter teeth are mounted on a steel plate attachment to the cart. The steel plate attachment allows for variation in blade angle (α) and embedment depth (h_i). The blades measure 11 cm in length and are bolted onto a threaded rod at a blade spacing (w_i) shown in Figure 7.17.

Figure 7.17: Cutter Rack configuration

To measure the effect of surface design on adhesion potential, a perforated blade and MagnaCoated blade are tested along side the normal stainless steel blade shown side by side in Figure 7.18:

Figure 7.18: Test Blades: Stainless Steel (left), Perforated Stainless Steel (Mid), and MagnaCoated Blade (Right)

It will be interesting to see if the design variations influence the adhesive, and therefore, the overall pulling force. Perforations should break-up the continuous contact surface between the clay and the soil thereby reducing the adhesive force. Coating the blade is expected to reduce the force by having a "smoother" surface and reducing the bond strength of the clay due to its significantly lower surface energy.

The pulling force is measured with a tension/compression load cell weighing up to 500 kg with an accuracy of +/- 0.2-0.5% model 615 by VPGtransducers. The load cell is calibrated by linear fitting the voltage reading against the force by hanging at least two known weights and recording the voltage output from the cell. The calibration line of best fit, shown in Appendix B, is the equation that is inputted into the software. The displacement sensor is an ultrasonic acoustic sensor with a standoff distance of 20 cm. Both sensors are connected through a LabJack controller system which is in turn connected to the computer with the LabJack software. The layout of sensors and measurement devices are summarized in Figure 7.19.

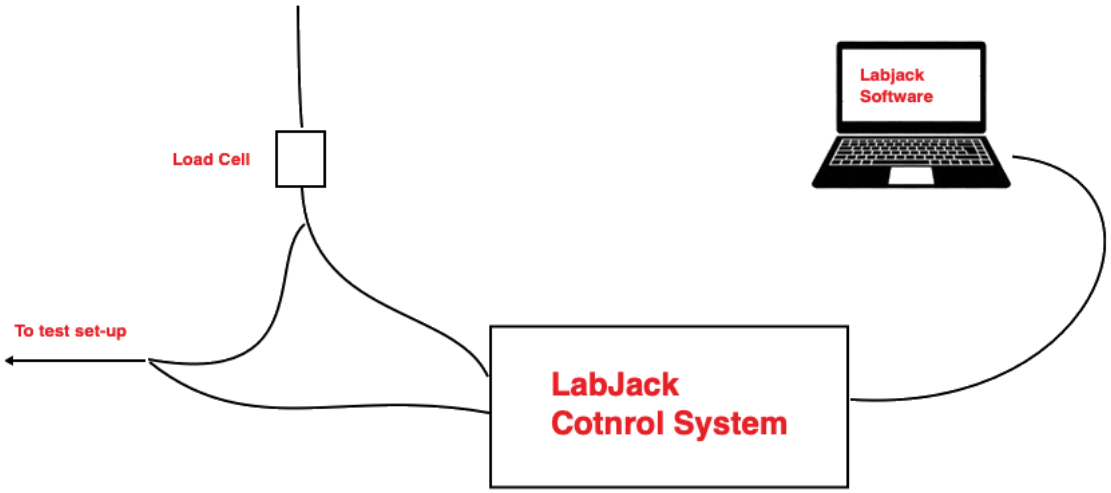

Figure 7.19: Sensor Setup layout

The output from the sensors give the variation of the horizontal pulling load (kg) versus the horizontal displacement (mm). The pulling load recorded will vary according to some design parameters. According to (Miedema, 2019), the pulling force depends on the blade angle, embedment depth and the velocity of cutting. The crane can only operate at a speed of 0.85 m/min, so this is a fixed value. However, the blade angle and embedment depth can be varied to determine the optimal cutting situation. While cutting a cohesive soil, it is not expected that the clay will pass in between neighboring blades, but rather follow the typical flow type mechanism. It is therefore important to asses the influence of blade spacing on the overall cutting force. For in-situ conditions, the clay will be more easily sheared due to the completely saturated conditions, so this test will provide a rather worst-case scenario. Last of all, perforated blades and MagnaCoated blades will be tested to see how much reduction, if any, of adhesion onto the blades. These design parameters to be varied are summarized below:

- Embedment depth (h_i)
- Blade angle (α)
- Blade Spacing (w_i)
- Perforations
- Coated blades

By combining the acquired insight from testing with these parameters, a more vivid picture can be drawn about how the cutterwheel can be optimized when mining nodules off the clay seabed. Different test runs are required in order to compare what parameter contributes more significantly to the cutting force, and the stickiness potential. The total pulling force can then be related to the underlying theory to see how significant the adhesive force on this pulling force. The goals of the scaled cutter test therefore are:

- Determine effect of blade spacing, blade angle, and embedment depth on overall pulling force
- Determine effect of surface alterations (perforated coated) on adhesive force and therefore pulling force
- Establish correlation between lab tests and scaled cutter tests
- Conclude the validity of experimental tests for adhesion

7.7.2 Scaled Testing Limitations

As with all experimental methods, the scaled cutter test does come with limitations. Limitations include:

- *Non-homogeneity & Remoulding*

  As with the Tensile Test, the clay used was straight from the box core sample and left to saturate in the flume tank. Non-homogeneous soils tend to have randomly varying shear strength paths throughout the soil, so it is more difficult to establish a typical behaviour pattern for the clay type. Particularly for the artificial sample, due to its impermeable nature, would form lumps when mixed which would shift aside when the cutter teeth moved through. This issue was resolved by remoulding the soil after every test run to close in any cavities from the previous test, to level out the soil for consistency between tests and to randomize the zonation of shear strength throughout the sample.

- *Test-setup impacts*

  The moveable cart runs along the built-in rails of the cart. The weight of the cart and attachment plates along with the frictional effects between the wheels and the rail, and between the tow wire and pulley will increase the obtained pulling forces. This was compensated for by solely determining the force to pull the cart along the rails and deducting this from the cutter rack test runs. Although this deduction helps in reducing the margin of error, there is still room for fluctuations in the frictional forces.

8 Results & Discussion

In this section, the results of the aforementioned methodology is assessed. First of all, both the shear and tensile adhesion resistances are experimentally determined by interface and pull out tests respectively. Afterwards, scaled testing is performed to determine the required forces to cut through clay with different configurations. Lastly, the measured forces are compared to the theoretically determined forces according to Miedema's model for verification. A purely experimental analysis of adhesion comes with underlying limitations and errors, which will be discussed in the next section.

8.1 Interface Shear Test Results

Results from the interface shear test of consolidated undrained samples are presented in this section. It can be assumed that the specimens are sheared under undrained conditions because of the relatively rapid strain rate as compared to the clay's low permeability. Figure 8.1 shows the total stress versus displacement of the clay sample over the test plates.

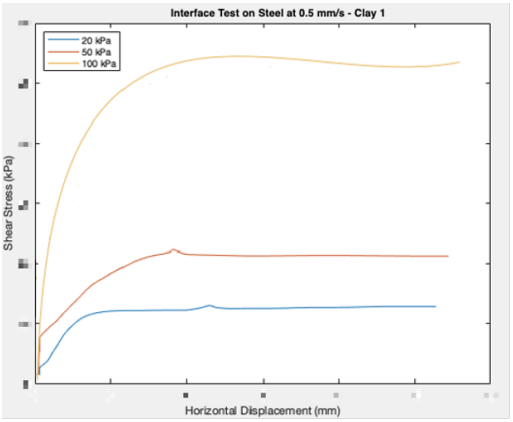

(a) Interface Shear results for Clay 1 on Stainless Steel

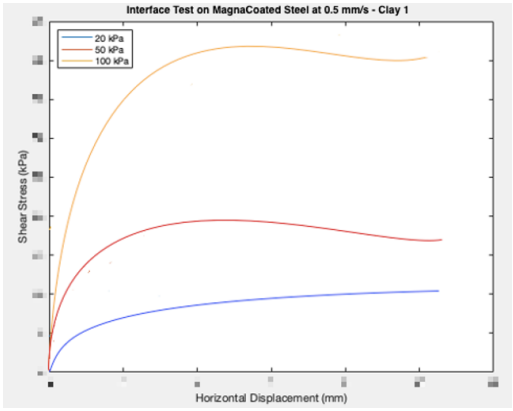

(b) Interface Shear results for Clay 1 on MagnaCoated Steel

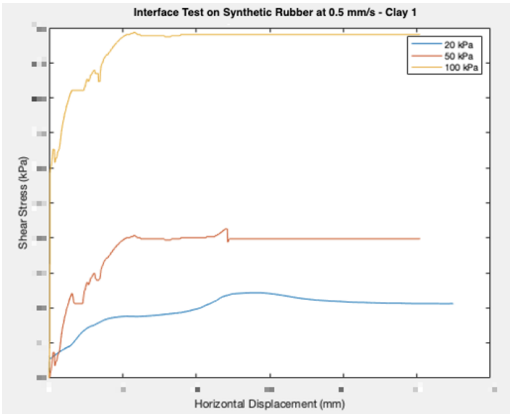

(c) Interface Shear results for Clay 1 on Rubber

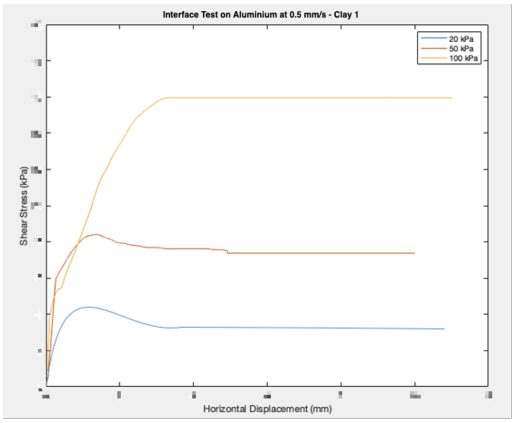

(d) Interface Shear results for Clay 1 on Aluminium

Figure 8.1: Shear Stress Paths for Interface Tests on Test Materials

It can be seen that the stress reaches a peak value and remains a relatively constant value at further strains. With an exception of the coated plate, the interface shear results generally exhibit more distinct peak stresses with narrower transition zones to the constant value relative to a clay

to clay shear plane. This suggests that interface tests have a shorter failure time where the clay slides over the test plate.

The average steady-state value when the maximum stress has been reached is taken as the stress where the clay fails along clay-plate boundary. This sliding stress along with the corresponding normal stress are plotted in a Mohr-Coulomb plot where a linear regression is established:

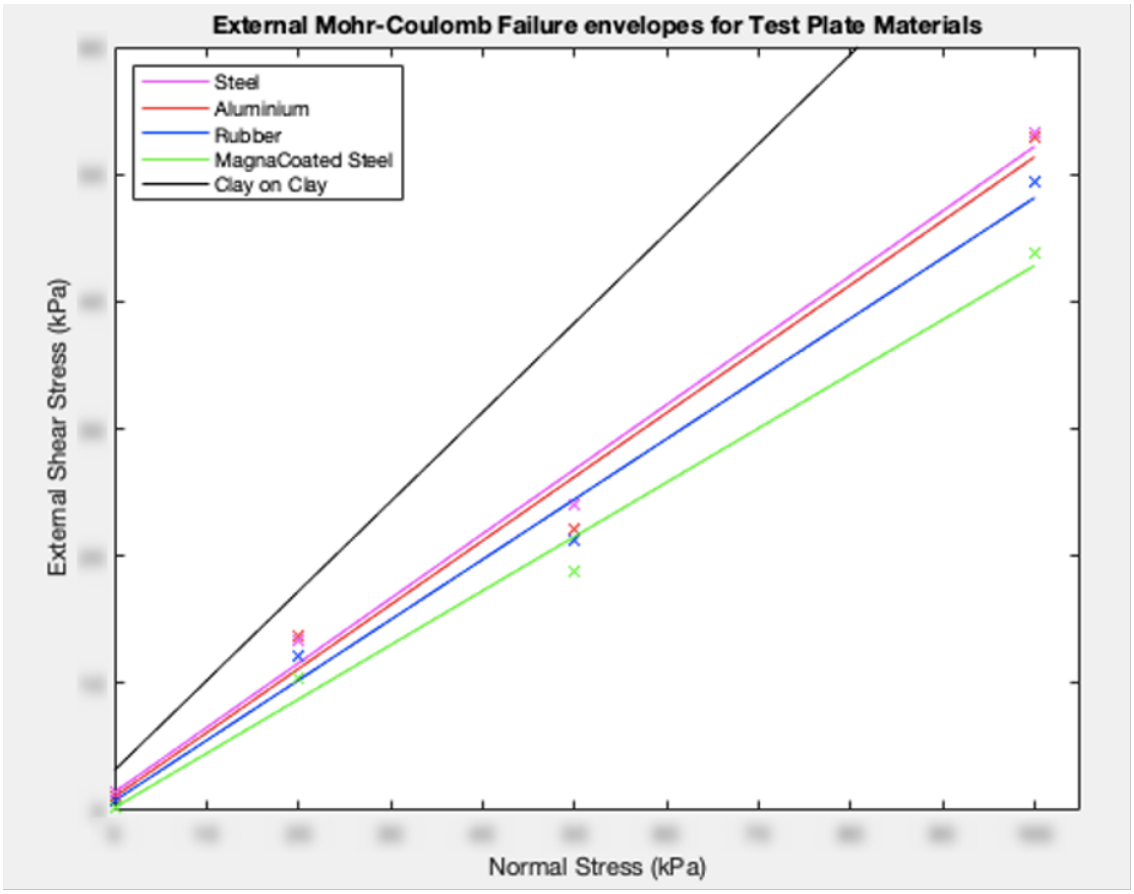

Figure 8.2: Comparison of Mohr-Coulomb Failure Envelopes for CU Interface Tests for Clay 1 on Different Test Materials

The envelopes are extrapolated to zero normal stress to obtain the 'natural adhesion' of the clay to each material. It can be seen envelope varies depending on the test material with the clay being most attracted to Steel, Aluminium, Rubber and finally least attracted to the fluropolymer coating.On Figure 8.2, the cohesive failure envelope is plotted on the same graph indicated in black. The results show that the clay to clay shear plane has more resistance as opposed to other test plate materials. The natural cohesion is shown to be much higher than the measured natural adhesion which inherently points to the fact that this type of clay will be more likely to fail along the soil engaging component surface rather than through the clay itself with applied stresses. However, adherence of clay to soil engaging tools is significantly altered depending on the direction and magnitude of the stress in a specific application. It is also noteworthy to mention to variation of the apparent friction angles. The external friction angles seem to increase as the adherence of clay increases. This increase can be attributed to the increasing attraction of the clay to more hydrophillic material surfaces and increasing roughness of the plate. Roughness is defined as the average deviation of the direction of the normal vector of a surface from its real form. The roughness of the plate has been shown in previous literature ((Zimnik et al., 2000)

(Taha & Fall, 2014)) to influence the shear behaviour in interface tests by generally increasing the interfacial shear resistance with increasing roughness in non-cohesive soils. This increase is also generally seen in cohesive soils due to the increasing contribution of cohesive stresses as the perturbation penetrates more into the sample. What can be interpreted from this is that increasing roughness attributed to the different material could contribute to the convergence of the value of the external friction angle to the value of the internal friction angle. This would be expected because an increase in perturbing in the surface layer will cause the shear plane to be localized within the clay rather then along the clay-surface boundary. The results from the interface shear tests seem to be in agreement to these findings although further research in varying roughness of different materials will need to be done for further validation.

Similarly, interface shear tests were performed with the comparative Clay 2 sample on Steel and MagnaCoated test plates:

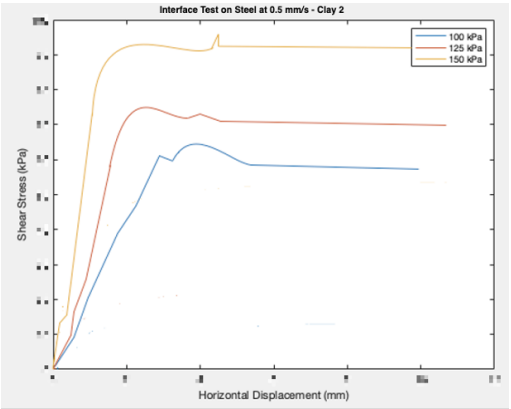

(a) Interface Shear results for Clay 2 on Stainless Steel

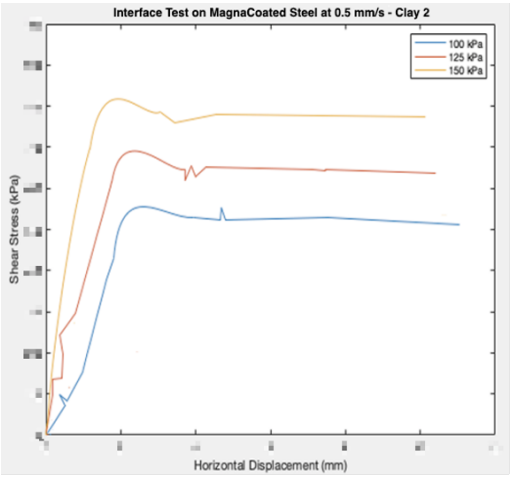

(b) Interface Shear results for Clay 2 on MagnaCoated Steel

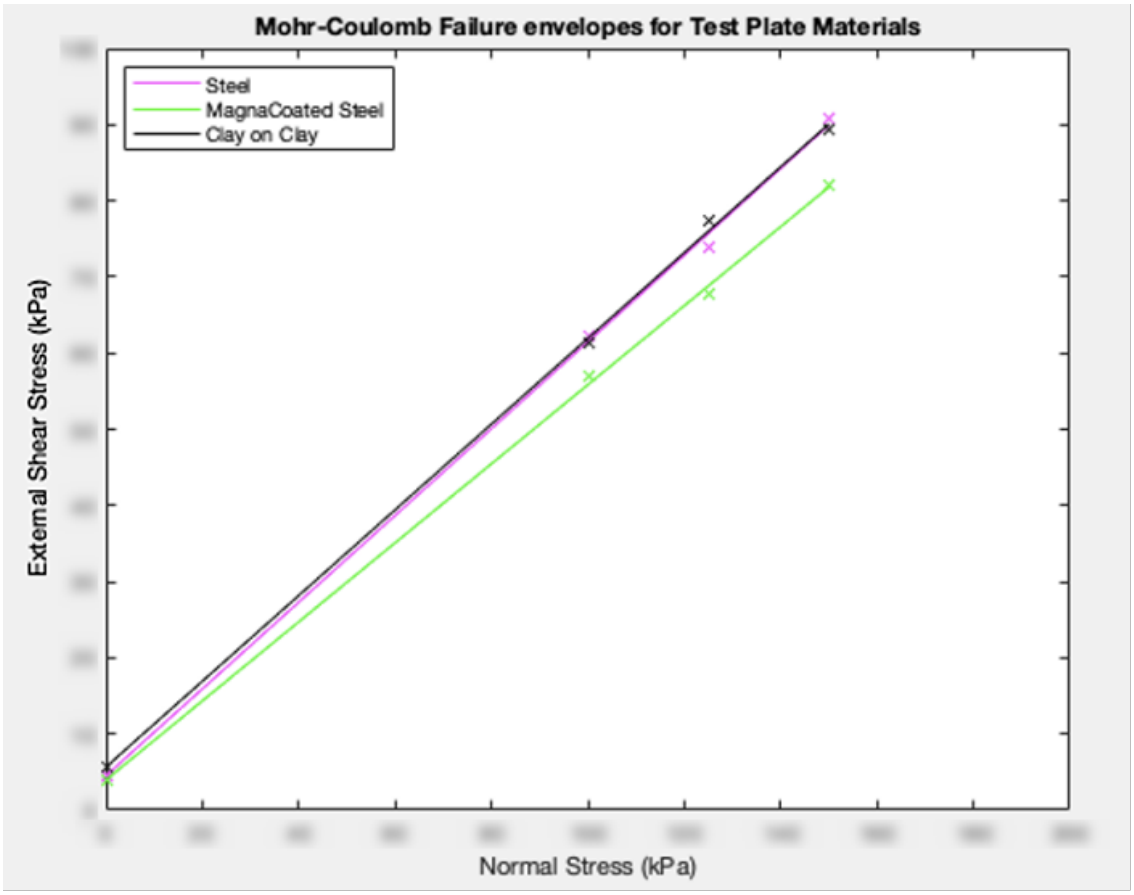

Figure 8.4: Mohr-Coulomb Shear Envelopes for Clay 2 on Test Plates

Figure 8.4 shows the interfacial external shear envelopes between of stainless steel and Magna-Coated steel with Clay 2. For comparative purposes, the internal shear envelope was plotted alongside the external shear envelopes. The artificial clay exhibits softer behaviour with less cohesive resistance but significantly more adhesive resistance in comparison to Clay 1. This provides an adequate comparison between the two test clays to observe the influence of the magnitude of adhesion. For Clay 2, the adhesion to steel is almost as prevalent as the cohesion measured, which leads to an adhesive failure envelope that almost coincides with the cohesive failure envelope. This behaviour shows that significant adhesive forces between the clay and steel causes the shear failure to take place within the clay rather than on the clay-steel boundary. This hypothesis can be confirmed by the converging external friction angle to the internal friction angle of the test clay. MagnaCoating the steel plate again had a reduction in the natural adhesion measured although this reduction is significantly less than what was observed with the Clay 1 sample. This could indicate that there was less sliding action taking place between the clay sample and interface plate due to significant adherence of the clay onto the plate.

8.2 Tensile Pull-off Tests

Tensile pull out tests were performed at a rate of 0.3 cm/s for the four test plates following the methodology scheme shown previously in Figure 7.14. The weights of the test plates themselves are accounted for to obtain the stresses purely from the steel to soil contact:

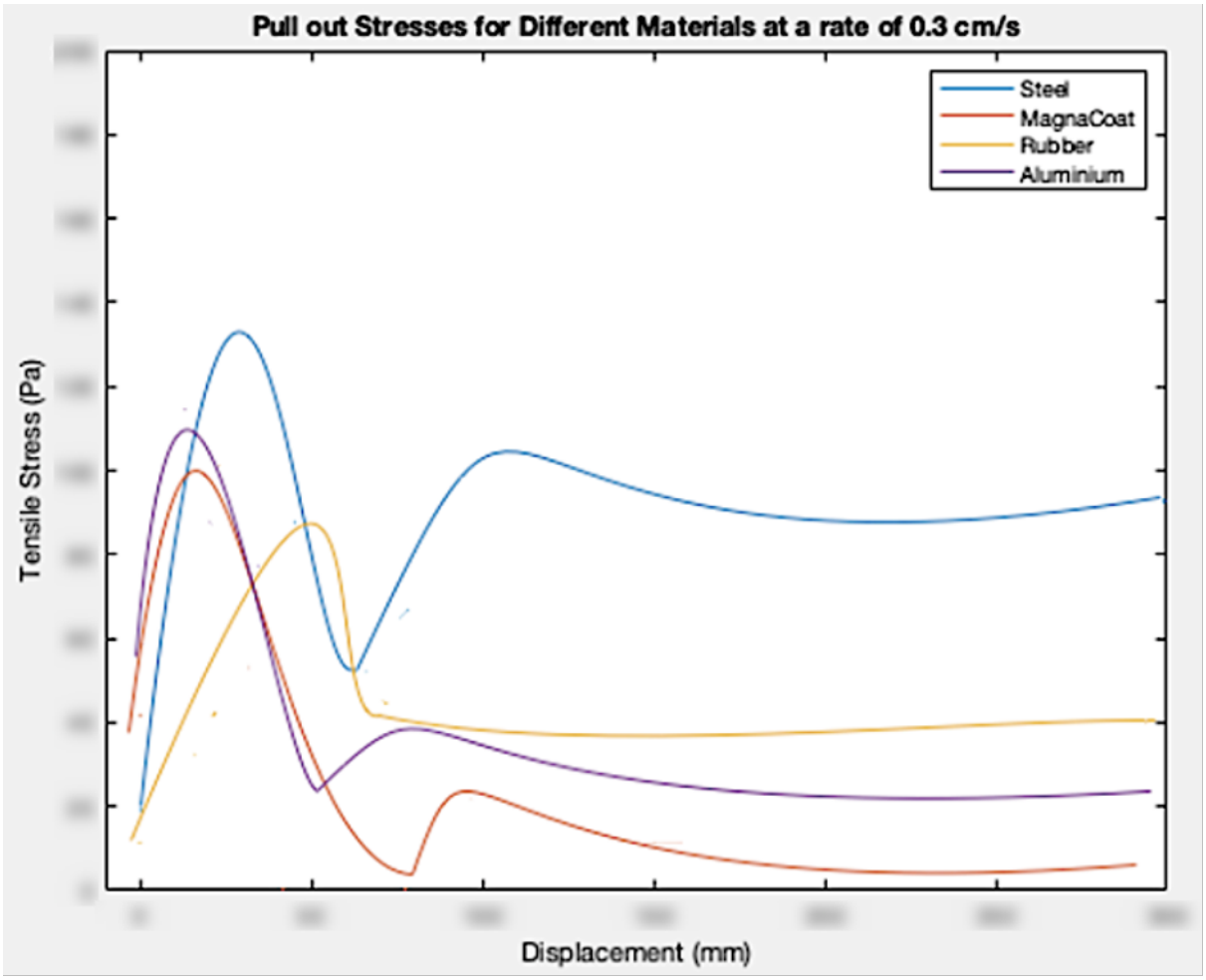

Figure 8.5: Tensile Test Results for Different Materials in Clay 1

Each plot in Figure 8.5 are averages taken from three tests at the same rate. All the plots exhibit a clear maximum peak stress followed by a secondary peak before leveling off. The secondary rise in tensile stress is a result from two factors during testing:

1. Testing procedure was not laterally constrained. Complete detachment of the plate was not achieved in one instance, therefore inducing a second uptick of stress needed for complete detachment.
2. Adhered clay along with some slurry water are picked up with plate that pour off when the plate is suspended in air.

The pull out tests nevertheless give relatively consistent results that can provide some valuable insight on the expected tensile stresses for each material. The test further simulates in-situ conditions by having an irregular non-uniform saturated clay. Contrary to the direct shear test,the synthetic rubber showed to have less adherence to the clay relative to the MagnaCoated plate.

This may indicate that MagnaCoating may improve the sliding resistance more-so in comparison to pull out resistances.

Each defined rate of pull out presented in section 7.6 were tested at least three times to obtain an average tensile force needed for complete detachment of the plate and clay. The rate effect was tested on the steel plate where average values are plotted in a scatter. Linear regression lines with R^2 values of at least 0.9 were fitted through for both Clay 1 and Clay 2 shown on Figure 8.6.

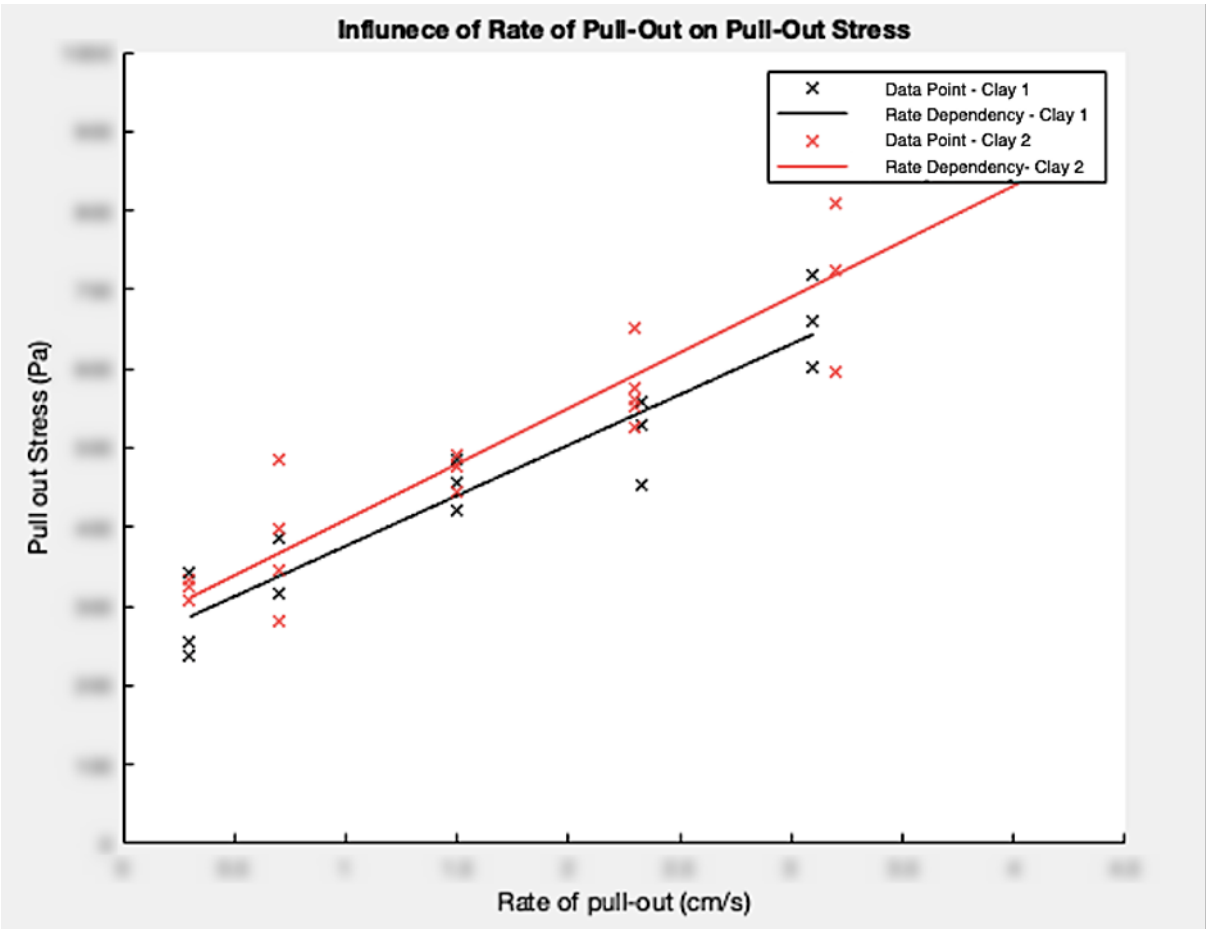

Figure 8.6: Pull Out Stress (Pa) vs Pull out Rate (cm/s) for Steel

Figure 8.6 suggests that increasing the pull-out rate leads to a linear increase in the stress required. This phenomenon is attributed to the viscous effects of the adsorbed water surrounding the active clay minerals. It is expected that this phenomenon is only seen in cohesive soils containing active minerals, where more clay content will lead to even larger suction forces. Slow pull out rates allow more time for water fluxes to intercept the boundary between the clay and test plate which thickens the interfacial water film. Adhesion of clay to the surfaces is therefore also a function of contact time. With time, more bonds between clay minerals and the soil-engaging component commence. To investigate the influence of contact time, pull out forces were recorded for varying contact times between 0 and 30 minutes. A stopwatch starts recording the instant the 500g mass block was placed on the test plate and stops before test initiation.

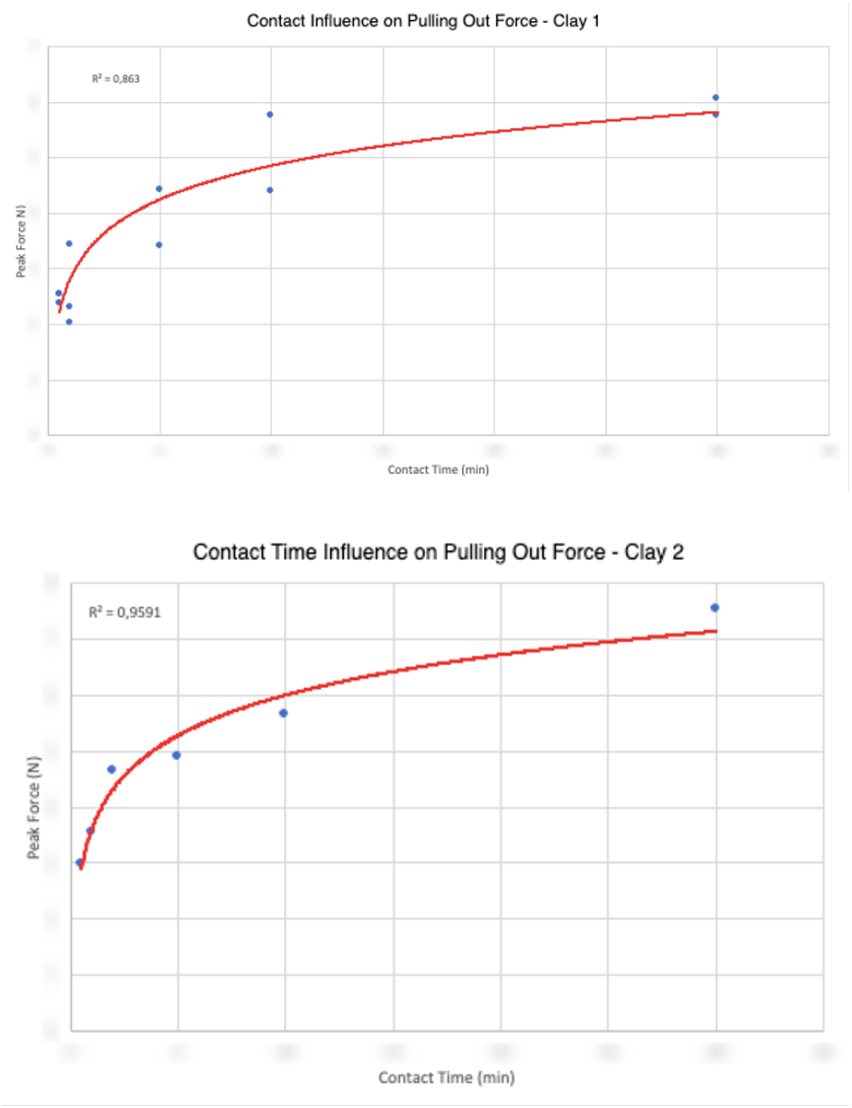

Figure 8.7: Contact Time Influence on Pull Out Force for Clay 1 (top) & Clay 2 (bottom)

The figure shows that with time there is a significant increase in the pulling force. This increase is more evident below the 10 minute mark and seems to become more gradual afterwards. As the contact time increases, the active 2:1 clay minerals have more time to adsorb H_20 molecules in the diffuse double layer which leads to higher water retention capacities in the clay therefore leads to larger suction forces. Inter-molecular bonds and static bonds develop over time as well, although these type of bonds forces are less significant.

8.2.1 Tensile Testing Limitations

The STICH unit can provide pull out force quantification with consistent pull out rates given a voltage input. However, possibilities of error can arise throughout the testing procedure which can provide misleading results. Significant outliers were experienced in some tests that could have been caused by the following limitations:

- *No lateral constraint of plate*: Having no lateral support during pull out provides inconsistent

failure modes for detachment. The test plate mostly did not detach in one instance which can deviate from the true tensile stress experienced.

- *Plate sinkage*: Although no significant normal loads were applied during testing, the soil surface is meant to resemble in-situ conditions by having a non-uniform topography and exhibiting non-homogeneity to a certain extent. Therefore, when placing the mass of 500 g on the test plate, the plate could sink on one end. This was a test error that was best overcome by placing the block precisely in the middle of the test plate at one instance.
- *Stress Distribution Under plate*: Although small in area, the test plate's rigidity in comparison to the underlying soil can cause stress fluctuations along the dimensions of the plate. It is in question if the peak stress calculated is a result from the entire area of the plate.
- *Effect of Remoulding*: It is well known that cohesive soils tend to lose part of its strength when remoulded. After a pull-out test, the soil directly underneath becomes a zone of weakness, which could significantly change the slip surface during breakout. It is of concern that this remoulding affects the adhesion phenomenon as it does its shear strength as the two are directly related. As a precautionary step, after remoulding, the soil is left to sit for about 15 minutes before initiation of the next test.

8.3 Scaled Testing Results

A total of 37 runs of the cutter rack through the test soils were done to realize the influence of the test parameters mentioned in Section 7.7.1 on the obtained cutting forces. The rack consists of cutter teeth bolted on a threaded rod in which the blade angle, embedment depth and blade spacing can be easily adjusted. With the exception of a drained test run, all test runs were carried out on the test clay under submerged saturated conditions. Under these conditions, the clay will more closely resemble in-situ conditions with a reduction in internal and external shear strength. The extent of this reduction was observed by carrying out an unsaturated test in comparison to a saturated test with the same operational parameters. The test showed to reduced the average force as expected (Refer to Figure A.22).

The sampling frequency was around 20 Hz meaning that two data points were recorded every second. The flume was filled with Clay 1 Soil and alternatively Clay 2 to form about a 10 cm thick layer. Half the height of the flume was then filled with water making sure to completely submerge the soil. The soil was left for at least 24 hours to ensure saturation before every testing day. After a test run, the water was drained out, soil was remoulded, and then submerged again before test initiation. Vane tests were taken along the length of the flume to ensure that the shear strength remained fairly consistent to previous tests.

8.3.1 Data Acquisition and Preparation

The result required from this scaled test is the average pulling force necessary to maneuver the cart and cutter rack through the soil. The data points recorded therefore needs to be processed to predict the most accurate pulling force required. Errors in raw data result from testing conditions, sensor errors, and boundary conditions. To justify the average horizontal pulling force, all these conditions must be resolved for each test run.

The boundaries on each side of the flume significantly effect the initial and final data points recorded by the sensors. For starters, the acoustic displacement sensor requires a standoff zone of at least 20 cm to record valid readings, otherwise transmitted and return signals superimpose to large degree. A metal bar has been installed in the flume to mark this standoff distance where readings cannot be recorded. The soil in the flume towards the other end has been inclined to allow drainage of water after a test has been performed. Therefore, the final readings on the load cell will show an upward trend that does not justify the average horizontal force through the desired embedment depth. The boundary effects from both ends of the flume are not taken into consideration as shown in Figure 8.8.

A 50 kg load cell was used to measure an average of 1-5 kg loads which causes fluctuations in the data. Although relatively consistent, some data points are scattered outside the general trend. Outliers significantly effect the mean value and must be removed prior to further analysis. These "outliers" are widely defined as points which are 1.5 times the interquartile ranges (IQRs) below the first quartile and 1.5 interquartile ranges above the third quartile where:

- 1st Quartile: Lowest 25% of the data
- 3rd Quartile: Lowest 75% of the data
- IQR: 3rd Quartile - 1st Quartile

Theses data processing steps are displayed for a particular test run in Figure 8.8:

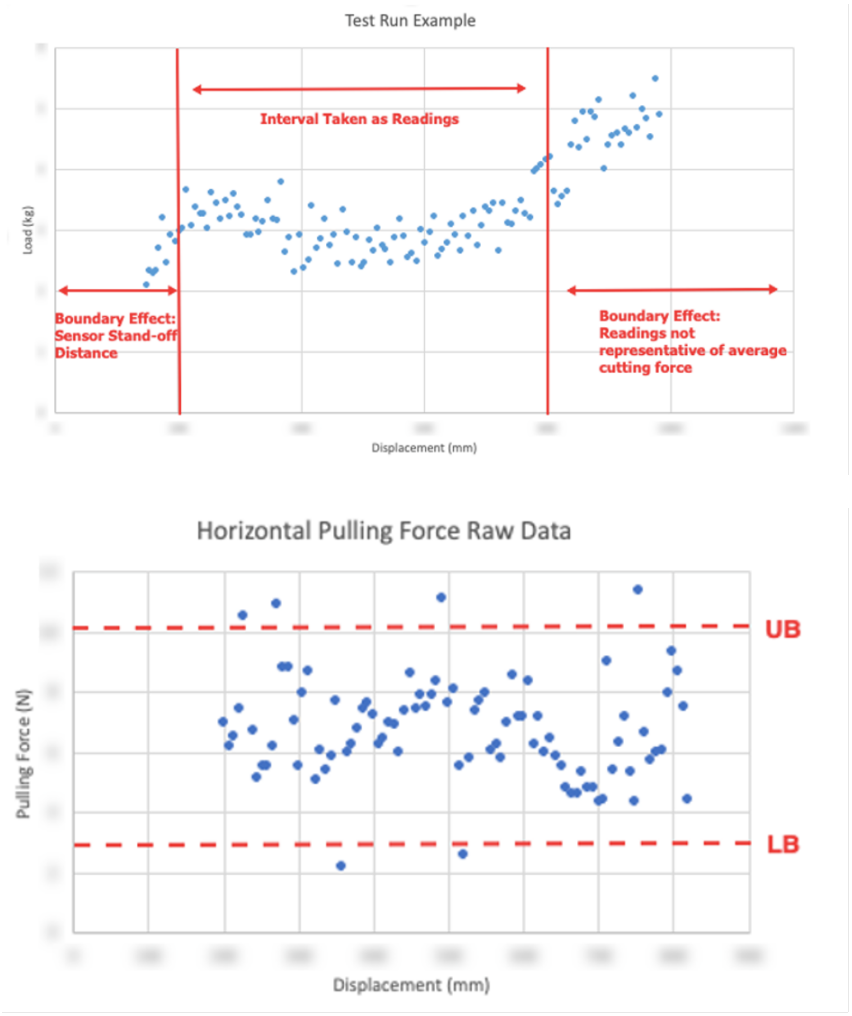

Figure 8.8: Data Selection and Processing Steps: Boundary effects (top) and outlier removal (bottom)

8.3.2 Parameter Variation Results

Accounting for the data processing stage, the cutter rack is to move an interval of about 80 cm lengthwise at a 6.5 cm embedment depth. The number of blades and spacing between each blade were varied in order to determine the influence on the cutter rack structure. The spacing was

measured by separating and moving blades to the desired spacing. Distance between the blades measured were 8 cm, 4 cm, 2 cm, and 1 cm. Cutter racks width spacing variations are shown in Figure 8.9:

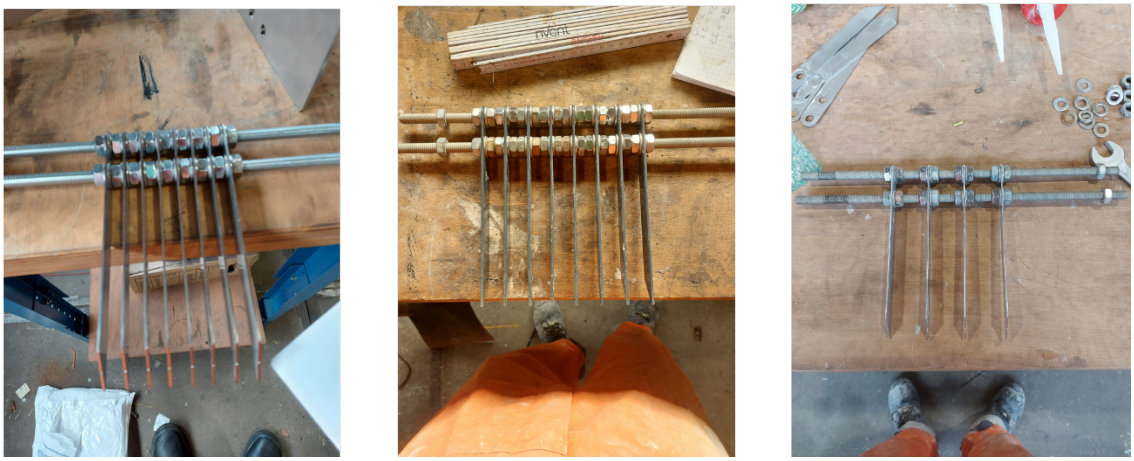

(a) 1 cm (b) 2 cm (c) 4 cm

Figure 8.9: CutterRack Spacing Variations

The effect of the blade itself is accounted for by deducting the average stress induced by it. This was found by carrying out tests with one blade and averaging the resulting forces. The spacing influence was tested for 8 cm spacing, 4 cm spacing, 2 cm spacing, and 1 cm spacing for each blade type which totals to 12 tests. The effect of spacing is presented in Figure 8.10:

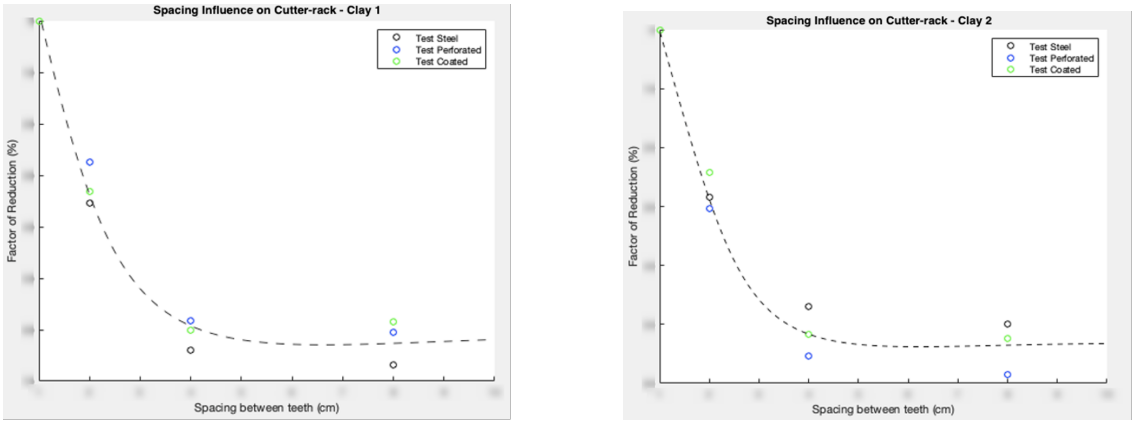

(a) Spacing Influence in Clay 1 Soil (b) Spacing Influence in Clay 2 Soil

Figure 8.10: Spacing Influence on Cutter Rack

It can be seen that the spacing has expectantly reduced the force on the cutter rack significantly. Increasing the spacing shows to reduce the total force by a large margin. This occurs due to the allowance of more movement of clay through the cutter blades spacing's. At large spacing's, the clay failure mechanisms are similar where the blades slice cleanly through the clay without prompting significant clay accumulation development. At lower spacing's, the rack induces a shovel

type failure mechanism which continues to accumulate with increasing displacement as shown in Figure 8.11:

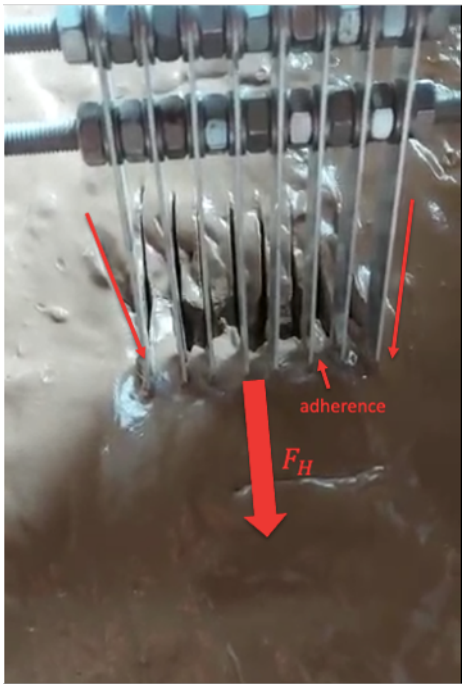

Figure 8.11: Shovel-like Failure Mechanism for 8 blades

It is this adherence and accumulation that causes the initial steep increase in force reduction percentage in Figure 8.10.

The effect of the blade type was also tested given the same conditions and operating parameters. Perforated and Coated blades were tested against the steel blade tests at a 75° angle and 6.5 cm embedment depth for 8 blades, 4 blades and one blade. The reason for the variation in the number of blades is to assess the influence of blade type with blade configuration. The obtained scatter plots for both Clay 1 and Clay 2 are shown on Figures 8.12 and 8.13 respectively where red marks for steel, blue for perforated and green for MagnaCoated blades:

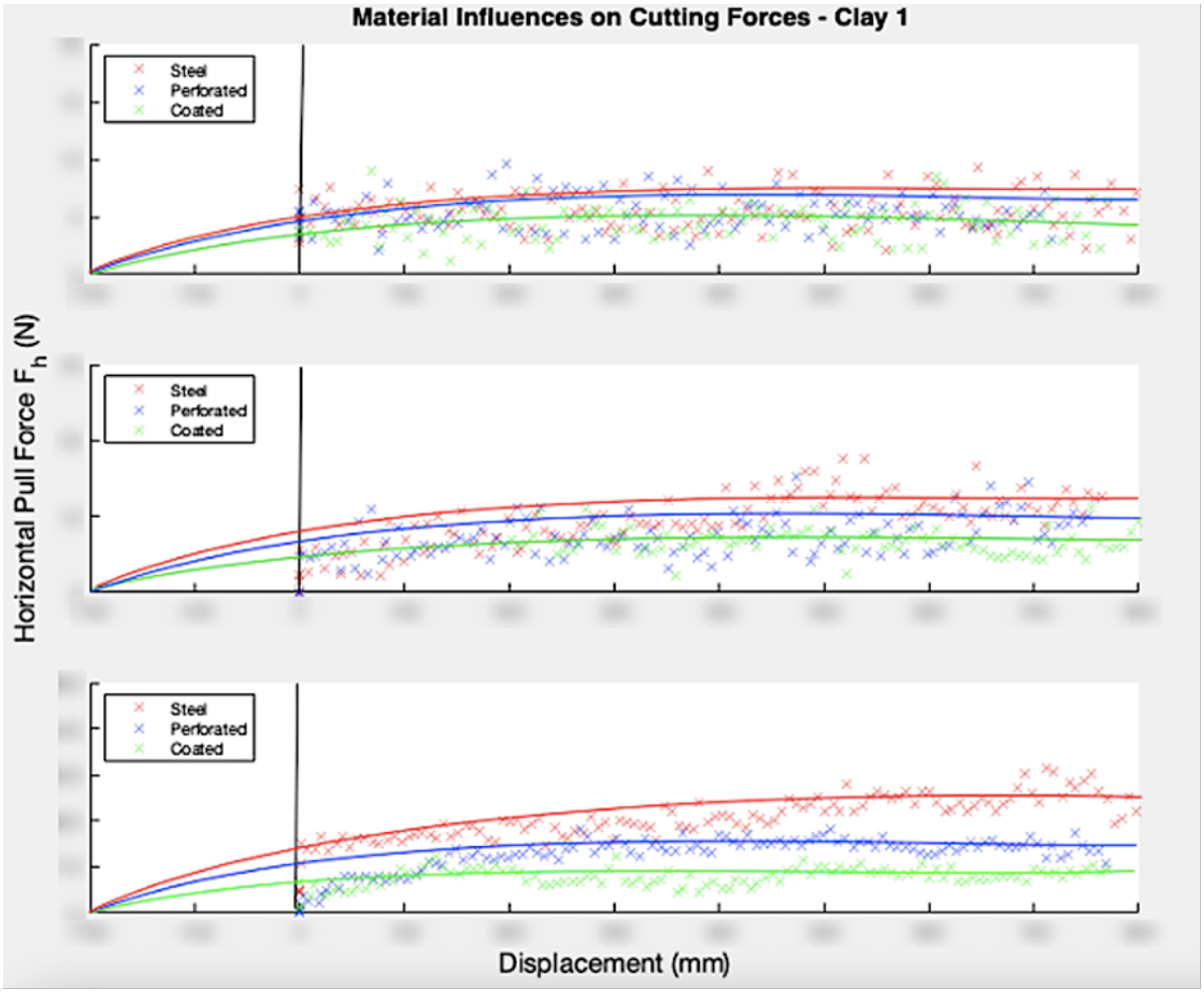

Figure 8.12: Cutting forces for 1 Blade (top), 4 Blades (middle) and 8 Blades (bottom) in Clay 1 Soil

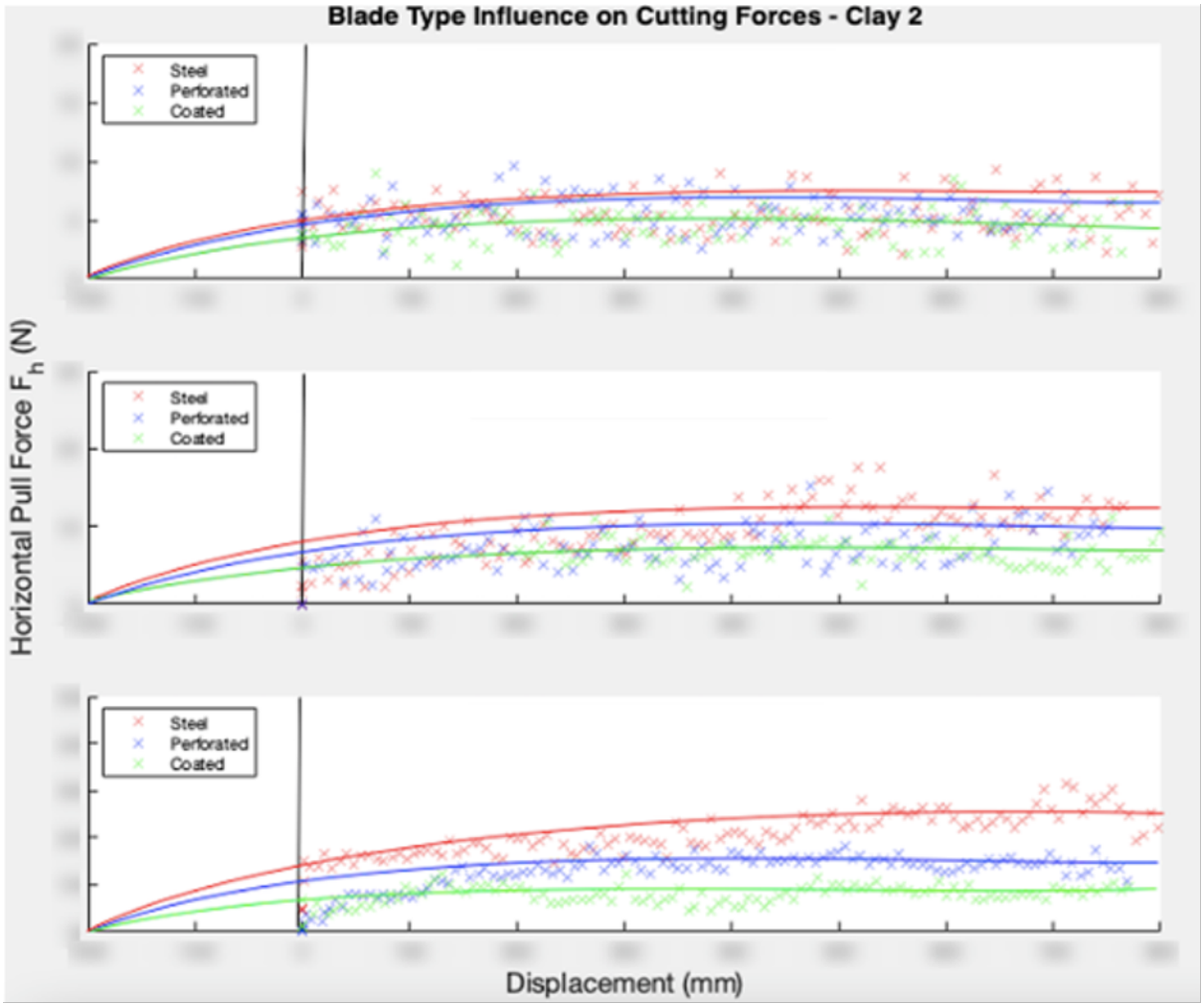

Figure 8.13: Cutting forces for 1 Blade (top), 4 Blades (middle) and 8 Blades (bottom) in Clay 2 Soil

The data is better represented in a bar chart with error bars. The error bars on Figure 8.14 shows the maximum and minimum values obtained during that specific test.

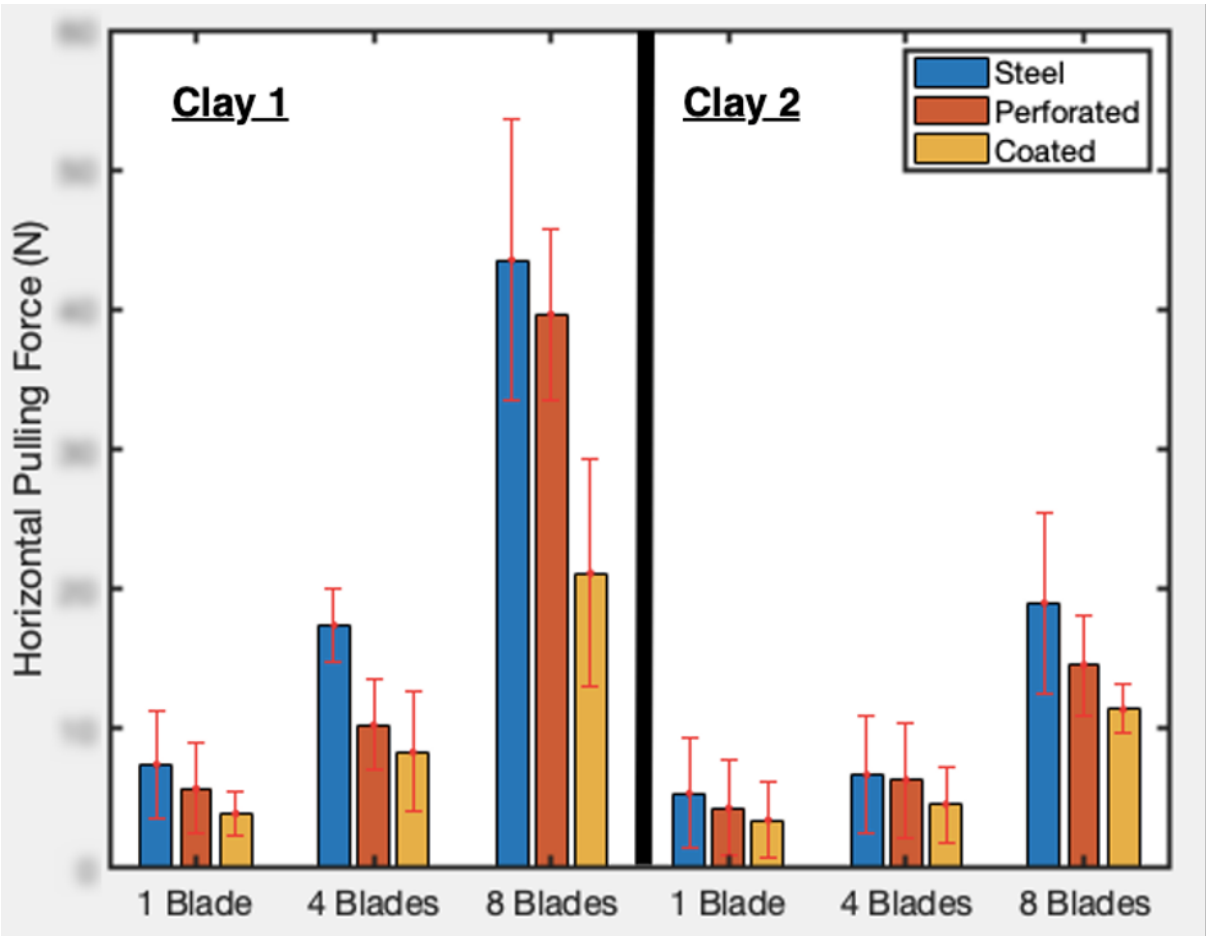

Figure 8.14: Average Cutting Forces Bar Chart with Error Margins

Perforations have shown to alleviate this pressure difference by exposing some of the soil engaging component to the surrounding water. Adhesion forces has been proven to increase with increasing roughness until a critical roughness, where the clay will begin to shear internally. Lastly, Clay 2 exhibited an overall less average pulling force than testing through Clay 1. This reduction in force with clay types can be mainly attributed to the weaker cohesive strength of Clay 2 as seen from the direct shear tests. Furthermore, a portion of the decrease could also be attributed to the high degree of non-homogeneity shown in the artificial Clay 2 soil due to the impermeable nature of this type of clay.

9 Validation of Predicted Cutting Forces by the Miedema Model

In this section, the results are further extrapolated relating practical results to the theoretical interpretation discussed previously. Namely, the Miedema equations in Section 5 are to be validated through the experimental findings of adhesion. Although the model used is a 2D model, it provides a proven basis of horizontal force quantification. Equation 5.1 can be rewritten in terms of the cohesive force "C" in the clay and the Adhesive force "A" on the blade:

$$F_h = \frac{C * sin(\alpha) + A * sin(\beta)}{sin(\alpha + \beta} \tag{23}$$

where:

$$C = \frac{\lambda_s * c * h_i * w}{sin(\beta)} \tag{24}$$

$$A = \frac{\lambda_s * a * h_b * w}{sin(\alpha)} \tag{25}$$

By comparing the horizontal force (F_h) obtained in practice with the theoretical force given certain input parameters, an adequate validation scheme can be initiated. Input parameters with corresponding explanations in equations 23, 24, and 25 are presented below:

- Adhesion value a: the apparent adhesion at zero normal stress found by interface testing
- Cohesion value c: the apparent cohesion at zero normal stress found by Direct Shear Testing
- Blade Embedment Depth h_i: defined as 6.5 cm
- Blade Angle α: tests done at 35°, 55° and 75°
- Width in 3rd dimension w (thickness) taken as 0.0016 m
- Velocity v_c: Taken as the pull rate of the crane which is 0.015 m/s

With the given input parameters, the cohesive and adhesive theoretical force in variation with blade angle can be graphed:

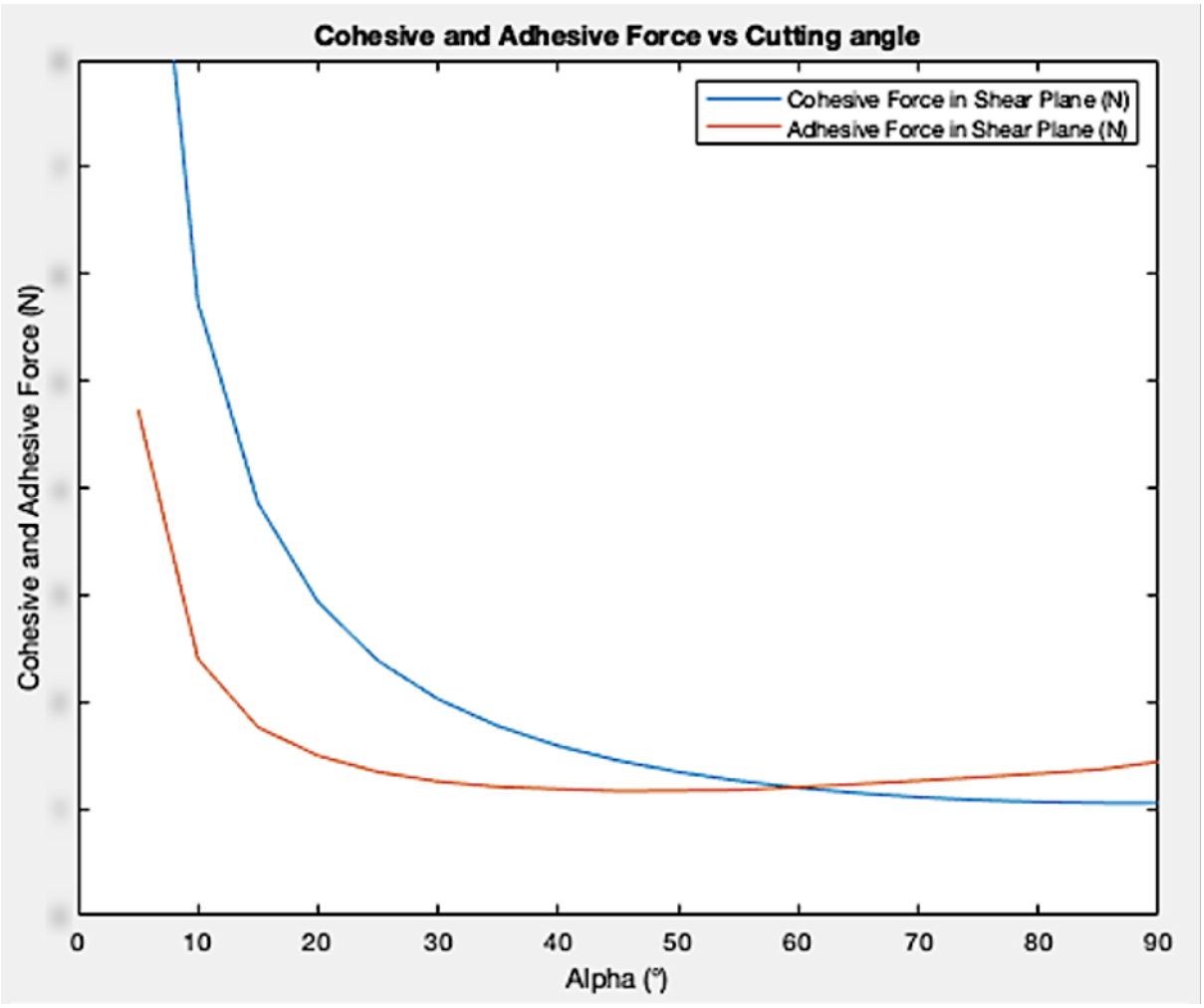

Figure 9.1: Cohesive and Adhesive Force for defined Test Parameters for Clay 1

It can be seen that the adhesive force is significant at low angles and becomes the most prevalent force at angles greater than 60°. Testing clays with different cohesive and adhesive strengths will subsequently change the shape of the graphs. To determine whether the experimental tests presented in this thesis to quantify adhesion values is suitable for predicting horizontal cutting forces, the theoretical horizontal force variation with respect to the blade cutting angle is compared with steel blade tests done at angles 35°, 55° and 75° in Clay 1 is shown in Figure 9.2:

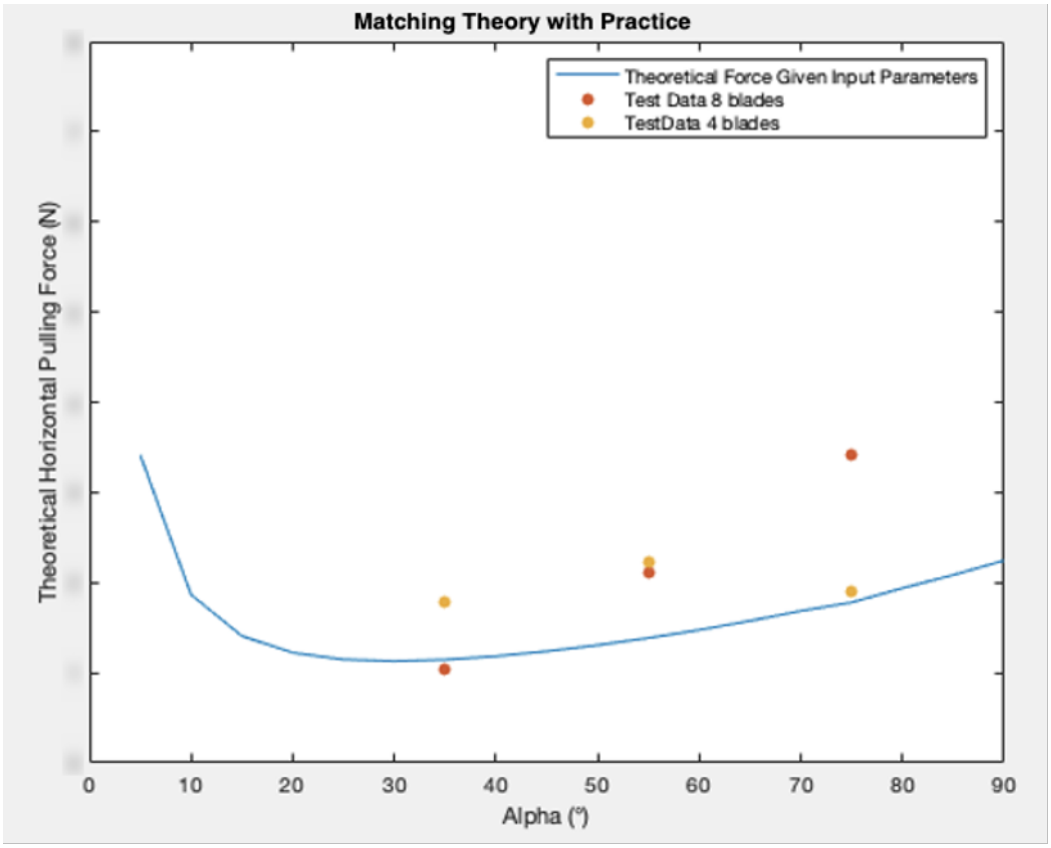

Figure 9.2: Theoretical Horizontal Force vs Obtained Practical Forces

The test data shown as scatter points reside close to the vicinity of the theoretical line. However, the mobilization of the blade length was not taken into consideration for this plot (Curling Type Mechanism). From the scaled tests, a significant amount of clay build-up occurred for narrow blade spacing's in which it can be assumed that full blade mobilization took place. The clay adhered to the blade reduces the contact region between the clay and the blade where the new blade length h_b can be defined under the conditions:

- h_b is used if $h_b > h_i$
- h_i is used if $h_b < h_i$

Figure 9.3: Clay Accumulation during 8 Blade Test in Clay 1

In the scaled tests, the embedment depth is defined to be 6.5 cm for the full 11 cm blade. By considering different mobilization lengths, one can see what clay mobilization length mostly coincides with the practical test data. Mobilization trends of blade heights are plotted along side the scaled test results with their corresponding error bars in Clay 1 and Clay 2 shown in Figures 9.4 & 9.5 respectively.

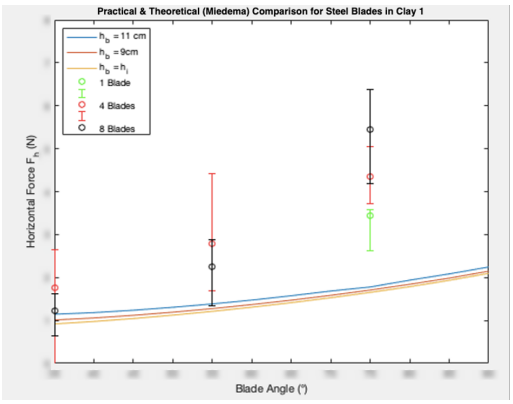

(a) Steel Blades Results

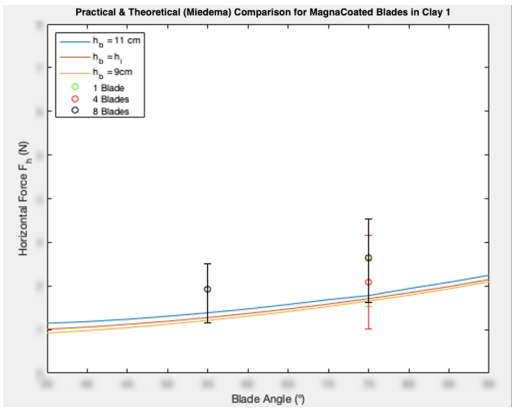

(b) Coated Blades Results

Figure 9.4: Theoretical vs Practical Results in Clay 1

Similarly for Clay 2:

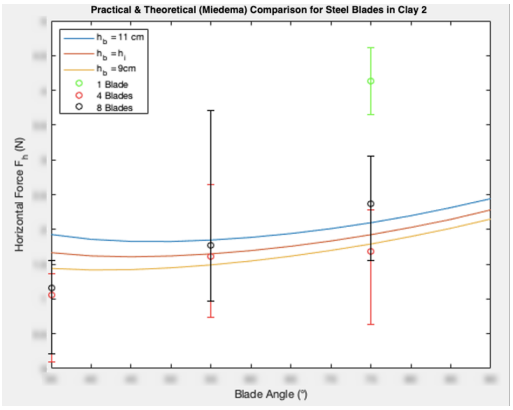

(a) Steel Blades Results

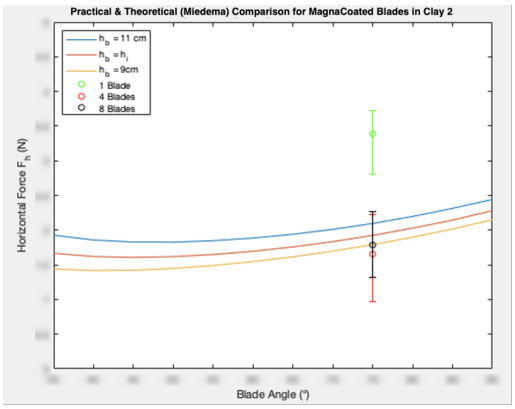

(b) Coated Blades Results

Figure 9.5: Theoretical vs Practical Results in Clay 2

Due to the small size of the test blades, the mobilization of the cut clay on the blade does not vary as much. Most test data seem to over predict the theoretical forces as a result from two aspects:

- *Considering 3D effects*: The clay cutting model is essentially a 2D model that considers the width of the blade and blade height. The model fails to capture adherence forces from the sides of the blades which could explain the lower theoretical cutting forces.
- *Failure mechanism & Accumulation*: For narrow spacing's the cutter rack induces a shovel like mechanism in which a large chunk of clay is displaced from the soil body. As the test proceeds, clay accumulates adding more weight to the recorded loads.

The first point can be further proven by analyzing the difference between steel and coated blades. The coated blades seem to produce a force that more likely coincides with the theoretical cutting trend. As shown previously, coating reduces the total horizontal force by mitigating the adhesive force on the sides of the blades.

In this small scale set-up, the clay showed to significantly accumulate on the blades. The build up sometimes was so significant, that it would accumulate up to the level of the rod as shown previously in Figure 9.3. The accumulation leads to the fact that when the clay is mobilized across the full length of the blade, the theoretical force line agrees more with the obtained practical data.

10 Conclusion & Recommendations

Adhesion of clays to soil engaging components were quantified by experimental methods and showed to be reliable to a certain degree when validated with the theoretical clay cutting equations (Miedema, 2019). In this thesis, shear adhesion was measured by a modified Direct Shear Test and Tensile adhesion of saturated clay was quantified by a Pull-out Test. The testing methods can also be utilized in onshore conditions where adhesion becomes more of a function of water saturation.

10.1 Conclusions

In general, conclusive remarks about clay adhesion on offshore soil engaging components are as follows:

- Interface tests showed that as the adhesive strength approaches the cohesive strength of the clay, the shear plane will tend to reside within the clay itself. This was proven by the coinciding external shear envelopes to the internal shear envelope.
- Adhesion varies depending on the material of the soil engaging component.
- Pull out stresses show a reduction depending on the material but are less significant to that of adhesive shear stresses. This difference is attributed to different testing conditions.
- Pull out stresses show a linear increase with the pull out rate.
- Pull out stress between the test plate and soil has been shown to increase with contact time. Contact times were tested up to 30 minutes. It is predicted beyond 30 minutes that the stresses will increase more and more gradually until a relatively consistent value.
- Obtained apparent adhesion stress values were validated with the clay cutting equations from Delft Sand, Clay & Rock Cutting model. The obtained horizontal cutting forces seemed to agree with the theorized forces relatively well.

The exploration of the adhesion phenomena is yet at its early stages, where if better understood, could help mediate engineering projects in soft cohesive soils significantly. Findings from this dissertation can be extrapolated beyond the scope of Deep-sea mining harvesters to a variety of engineering applications.

10.2 Recommendations for Further Research

The experiments presented in this dissertation are viable options for quantifying adhesion. However, it is suggested that further research on these testing procedures should commence in the near future. A large influence on obtained adhesion stresses are the testing conditions, boundaries and forces implemented on the test sample. The validity of an experimental analysis on soil adhesion can be refined by overcoming limitations mentioned in section 7.

The standard direct shear test has been proven to be effective in predicting the adhesive shear stress of the test sample to a particular material and roughness. However, the DS Test fails to capture residual shear values due to the limitation of the displacement that can be achieved in such a test. (Chen, Van Den Broecke, Liu, Hong, & Miedema, 2019) investigated shear adhesion by a blade pull out test. A steel blade with a certain roughness was placed in a horizontal cut in the test clay and slowly pulled out at a certain rate to obtain the shear adhesion and residual values. This type of testing can give more insight on adhesion behaviour for a complete shearing failure mechanism of a clay soil. (Chen et al., 2019) has also concluded that through the use of adhesive and cohesive shear testing, the missing r parameter in the (Miedema, 2019) equations can be found, and subsequent horizontal forces for a particular application can be reasonably predicted. It is recommended that the approach presented in the thesis should be repeated for many clay types to establish a reliable empirical model. This testing procedure can also be extrapolated to

undrained scenarios. It is however recommended to develop another cutting clay model as the (Miedema, 2019) model is only for submerged saturated conditions.

Pull-out tests were found to be an adequate testing approach for tensile adhesion measurements. However, to overcome to limitation of lateral movements during the proposed test in this thesis, it is recommended to constrain the pull-out stamp by clamps or a hydraulic piston. (Feinendegen et al., 2010) utilized a hydraulic cone with sensitive load cells to accurately measure any slight variations in stress. Using a cone instead of a flat plate also has the advantage of maintaining a consistent stress distribution when penetrating soil.

References

(n.d.-a).

(n.d.-b).

Abdi, M. R., & Arjomandkhah, M. R. (2011, 12). Pullout tests conducted on clay reinforced with geogrid encapsulated in thin layers of sand. *Geotextiles and Geomembranes*, *29*, 588-595. doi: 10.1016/j.geotexmem.2011.04.004

Al-Bared, M., & Marto, A. (2017, 12). A review on the geotechnical and engineering characteristics of marine clay and the modern methods of improvements. *Malaysian Journal of Fundamental and Applied Sciences*, *13*, 825-831. doi: 10.11113/mjfas.v13n4.921

Arrobas, D., Hund, K., Mccormick, M., Ningthoujam, J., & Drexhage, J. (2017). The growing role of minerals and metals for a low carbon future. *World Bank Group*.

Atterberg limits. (n.d.). `https://www.geoengineer.org/education/laboratory-testing/atterberg-limits/`. ((Accessed on 04/02/2020))

Azadegan, B., & Massah, J. (2012). Effect of temperature on adhesion of clay soil to steel. *Cercetari Agronomice in Moldova*, *45*, 588-595.

Barckhausen, U., Bagge, M., & Wilson, D. (2013). Seafloor spreading anomalies and crustal ages of the clarion-clipperton zone. *Mar Geophys Res 34*, 79-88. doi: https://doi.org/10.1007/s11001-013-9184-6

Burbaum, U. (2009). Adhasion bindiger boden an werkstof- foberfla chen von tunnelvortriebsmaschinenden.

Burbaum, U., & Sass, I. (2016, 04). Physics of adhesion of soils to solid surfaces. *Bulletin of Engineering Geology and the Environment*, *76*. doi: 10.1007/s10064-016-0875-5

Carroll, D. (1970). *Clay Minerals: A Guide to Their X-ray Identification.* Geological Society of America. Retrieved from `https://doi.org/10.1130/SPE126` doi: 10.1130/SPE126

Chen, X., Van Den Broecke, J., Liu, G., Hong, G., & Miedema, S. (2019). Experimental analysis of the cohesion-adhesion relation of cohesive soil. In *Proceedings 22nd world dredging congress* (pp. 155–166). Chinese Dredging Association (CHIDA). (22nd World Dredging Congress and Exposition, WODCON 2019 ; Conference date: 22-04-2019 Through 26-04-2019)

Cherian, Chinchu, Arenapalli, & Naidu, D. (2015). A critical appraisal of the role of clay mineralogy in lime stabilization. *International Journal of Geosynthetics and Ground Engineering*. doi: 10.1007/s40891-015-0009-3

Crevelin, L. A.-c. G., & Bicalho, K. A. V. (2019, 00). Comparison of the Casagrande and Fall Cone Methods for Liquid Limit Determinations in Different Clay Soils. *Revista Brasileira de CiÃ̃do Solo*, *43*. Retrieved from `http://www.scielo.br/scielo.php?script=sci_arttext&pid=S0100-06832019000100406&nrm=iso`

Diffuse double layer. (2013, May). `https://pdfs.semanticscholar.org/aa72/ca7aba21b70ec1e2ab5e726b9cd512164c5d.pdf`.

Dreiseitl. (2017). About geotechnical properties of the deep seabed polymetallic nodules. *18th International Conference on Transport and Sedimentation of Solid Particles*, 11-155.

Feinendegen, M., Ziegler, M., Spagnoli, G., Fernandez-Steeger, T., & Stanjek, H. (2010, 06). A new laboratory test to evaluate the problem of clogging in mechanical tunnel driving with epb-shields.

Fountaine, E. (1954). Investigations into the mechanism of soil adhesion. *J Soil Sci*, *5*, 251-263.

Gorniak, J., M.Tankere, Delmas, P., Barral, C., Watn, A., Hyrve, O., & Dahl, A. (2016, 05). Determination of pull-out strength and interface friction of geosynthetic reinforcement embedded in expanded clay lwa..

Hein, J., Mizell, K., Koschinsky, A., & Conrad, T. (2013). Deep-ocean mineral deposits as a source of critical metals for high- and green-technology applications: Comparison with land-based resources. , *15*, 1-14.

ISA. (2010). A geological model of polymetallic nodule deposits in the clarion-clipperton fracture zone. *ISA Technical Study*, *NO.6*, 1-5.

Jong, D. (n.d.). *Electric crawler uses waterjets to pick up nodules from ocean floor — swz—maritime.* `https://www.swzmaritime.nl/news/2020/01/30/electric`

-crawler-uses-waterjets-to-pick-up-nodules-from-ocean-floor/. ((Accessed on 03/13/2020))

Keeney, C. (1987). Procedures and devices for underwater cleaning of civil works structures. *Department of the Navy. Naval civil engineering laboratory*.

Keller, G. H., & Bennett, R. H. (1973). Sediment mass physical properties—panama basin and northeastern equatorial pacific. , 499-512.

Kooistra, A., Verhoef, P., Broere, W., Ngan-Tillard, D., & Tol, F. (1998). Appraisal of stickiness of natural clays from laboratory tests.

Koschinsky, A., Heinrich, L., Boehnke, K., Cohrs, J. C., Markus, T., Shani, M., ... Werner, W. (2018, 06). Deep-sea mining: potential environmental, legal, economic, and societal implications - an interdisciplinary research. *Integrated Environmental Assessment and Management*, *14*. doi: 10.1002/ieam.4071

Krenz, J., Lee, B., & Owens, P. (2006). Swelling clays and septic systems. *Rural Wastewater*.

Lu-Quan, R., Tong, J., Li, J., & Chen, B. (2001). Soil adhesion and biomimetics of soil- engaging components: a review.

Mallick, H., S.B.and Zhai, Adanur, S., & Elton, D. (1995). Testing of geosynthetic reinforcement: State of the art report.

Matthew, N. (2012, September). Clarion clipperton fracture zone technical report ni43-101. *Golder Associates Pty Ltd*.

Mayne, P. (1985, 09). A review of undrained strength in direct simple shear. *SOILS AND FOUNDATIONS*, *25*, 64-72. doi: 10.3208/sandf1972.25.3_64

Mero, J. L. (1965). *Geochemistry and descriptions of manganese nodules and crusts retrieved from the open ocean.* PANGAEA. Retrieved from https://doi.org/10.1594/PANGAEA.864089 (Supplement to: Mero, JL (1965): The Mineral Resources of the Sea. Elsevier Oceanography Series, 1, 312 pp, http://www.sciencedirect.com/science/bookseries/04229894/1/supp/C) doi: 10.1594/PANGAEA.864089

Miedema, S. (2019). *The delft sand, clay rock cutting model* (3rd ed.). TU Delft Open. (Creative Commons license CC BY-NC-SA 4.0 https://creativecommons.org/licenses/by-nc-sa/4.0/) doi: 10.5074/t.2019.001

Mojid, M. A. (2011). Diffuse double layer (ddl). In J. Gliński, J. Horabik, & J. Lipiec (Eds.), *Encyclopedia of agrophysics* (pp. 213–214). Dordrecht: Springer Netherlands. Retrieved from https://doi.org/10.1007/978-90-481-3585-1_41 doi: 10.1007/978-90-481-3585-1_41

Myers, D. (1991). Surfaces, interfaces, and colloids. principles and applications. *VCH Verlagsgesellschaft*.

Orabi, A. (2016, October). *Consistency of soils.* https://www.slideshare.net/DrAbdulmannanOrabi/lecture-3-consistncy-of-soil-67797472/. ((Accessed on 04/02/2020))

Panday, A. (2003). High rate mining tool development. dealing with clay when mining diamonds offshore. *De Beers Marine (Pty) Ltd.*.

Poulos, H. (1988). Marine geotechnics.

Randolph, M. F., & Gourvenec, S. (2011). Offshore geotechnical engineering. , 59-91.

Ratananikom, W., Yimsiri, S., & Likitlersuang, S. (2015, 03). Undrained shear strength of very soft to medium stiff bangkok clay from various laboratory tests. *Geotechnical Engineering*, *46*, 64-75.

Schwieger, K. (1965). *The influence of cation exchange and electrolyte concentrations upon the atterberg limits.* https://scholarsmine.mst.edu/masters_theses/5721. Missouri University of Science and Technology Department of Civil, Architectural and Environmental Engineering. Student Master Thesis 5721.

Shephard, L., & Rutledge, A. (1991). Clay fabric of fine-grained turbidite sequences from the southern nares abyssal plain. *Frontiers in Sedimentary Geology*.

Skempton, A. (1948). The phi = 0 analysis of stability and it's theoretical basis. *Proc. 2nd International Conference on Soil Mechanics and Foundation Engineering*, *1*, 72-78.

Skempton, A. W. (1973). The colloidal activity of clays. university reader in soil mechanics, imperial college. , *3*, 499-512.

Stafford, J., & Tanner, D. (1983). Effect of rate on soil shear strength and soil-metal friction i. shear strength. *Soil and Tillage Research*, *3*(3), 245 - 260. Retrieved from `http://www.sciencedirect.com/science/article/pii/0167198783900260` doi: https://doi.org/10.1016/0167-1987(83)90026-0

Taha, A., & Fall, M. (2014, 12). Shear behavior of sensitive marine clay–steel interfaces. *Acta Geotechnica*, *9*. doi: 10.1007/s11440-014-0321-4

Thewes, M. (1954). Adhasion von tonbo den beim tunnelvortrieb mit fl ssigkeitsschilden. *Berichte aus Grundbau und Boden- mechanik der Bergischen Universita t Gesamthochschule Wuppertal*, *21*.

Thewes, M., & Burger, W. (2004). Clogging risks for tbm drives in clay. *Tunnels Tunneling International*, *6*.

Tilot, V. (2006). Biodiversity and distribution of the megafauna. *Intergovernmental Oceanographic Commission. The Polymetallic nodule ecosystem of the Eastern Equatorial Pacific Ocean*, *1*, 3-6.

Tong, J., Chen, Y., A.R., Q., & Chen, B. (1994). Abrasive properties and mechanism of polytetrafluoroethylene and ultra high molecular weight polyethylene. *Tribology, 14(1)*, 65 - 72.

Tong, J., Ren, L., & Chen, B. (1994a). Characteristics of adhesion between soil and solid surfaces. , *Vol 31*, 93 - 105.

Tong, J., Ren, L., & Chen, B. (1994b). Reducing adhesion of soil by phosphorus white iron on the basis of bionics principles. *In Proceedings of the 10th International Conference of ISTVS*, 57 - 63.

Ural, U. (2018, September). *The importance of clay in geotechnical engineering, current topics in the utilization of clay in industrial and medical applications.* `https://www.intechopen.com/books/current-topics-in-the-utilization-of-clay-in-industrial-and-medical-applications/the-importance-of-clay-in-geotechnical-engineering`. (Accessed on 03/13/2020) doi: 10.5772/intechopen.75817

Verhoef, P. N. W., Ngan-Tillard, D. J. M., Broere, W., & van Tol F. (1998). Appraisal of stickiness of natural clays from laboratory tests.

Wang, X., Ito, N., & Kito, K. (1996). Study on reducing soil adhesion to machines by vibration. *In: Proceedings of the 12th International Conference of ISTVS*, pp 539 - 545.

Yalamarty, P. (2012, 09). Earth handling problems due to stickiness of soils; sticky limit evaluation measurement..

Yin, Y., Cheng, Y., & Chen, B. (1990). A study on cleaning buildup soil in loader shovel on the principle of bionics. *Transactions of the Chinese Society of Agricultural Engineering*, 1-6.

Yousef, A., Hasankhani-Ghavam, F., S., G., Vali, R., & Mohamadreza, A. (2018). Investigation of the effect of soil moisture content, contact surface material and soil texture on soil friction and soil adhesion coefficients. *Acta Technologica Agriculturae*, *21*, 44 - 50. doi: 10.2478/ata-2018-0009

Zawadzki, D., Maciag, L., Abramowski, T., & McCartney, K. (2020, April). Fractionation trends and variability of rare earth elements and selected critical metals in pelagic sediment from abyssal basin of ne pacific (clarion-clipperton fracture zone). *Minerals 2020*, *10*.

Zimnik, A., van Baalen, L., Verhoef, F., & Ngan-Tillard, D. (2000). The adherence of clay to steel surfaces. *International Society for Rock Mechanics and Rock Engineering*.

A Appendices

A.1 Appendix A: Sample Preparation

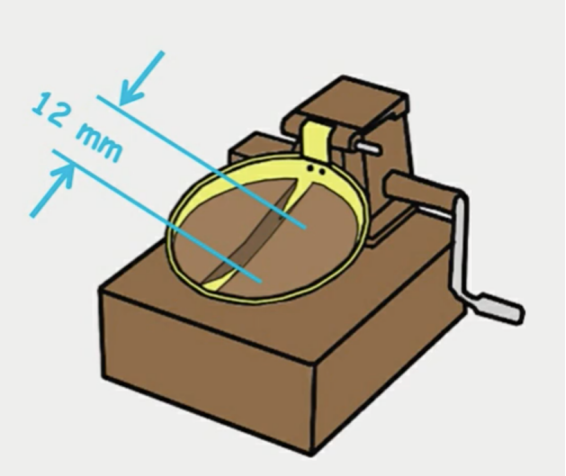

Figure A.1: Cassegrande Apparatus

Figure A.2: Clay Crushing and Sieving (45µm)

Procedure for finding water content:

1. Weigh measuring dish
2. Weigh saturated sample in dish
3. Oven dry sample
4. Record new weight of sample and dish
5. Subtract weight of dish to get weight of solid (Ms)
6. The difference in weight before and after drying is the mass of water (M_W)
7. Record Gravimetric Water Content ($w = M_w/M_s$)

(a) Wetting dry soil

(b) Rolling to 3 mm thick

Procedure to find Plastic Limit (ASTM):

1. Place approximately 20 grams of the prepared soil in an evaporating dish and thoroughly mix with water until the mass becomes plastic enough to be shaped into a ball.
2. Take approximately 8-12 grams of moistened soil and form into a uniform mass roughly elliptical in shape
3. Roll the ball of soil by hand on the rolling surface with just enough pressure to form an elongated thread as rolling proceeds.
4. If the soil can be rolled to a thread 3 mm thick without crumbling, it means that the water content is more than the plastic limit. Amass and re-roll it to reduce the water content
5. Repeat rolling and amassing until the soil crumbles under slight pressure required for rolling. Crumbling may occur when the soil has a diameter greater than 3 mm, however, this is considered a satisfactory end point, provided the soil has been previously rolled into a 3 mm thread.
6. Gather portions of the crumbled soil and place in a tared aluminium can and weigh, then oven dry at 100°C to a constant weight and weigh again after cooling. The measured water content difference is the water content of the plastic limit

Figure A.4: Determination of Sticky Limit

1. Dry a soil sample and pass it through a 0.5 mm sieve
2. Wet the soil sample near to its plastic limit and leave it to mature for 24 hours
3. Take 50% of the soil (about 100 grams) and run a nickel-plated spatula (or any flat tool) over the sample
4. If no sticking is observed, add 2 ml of water and draw the spatula over again
5. When sticking is observed, the sample is oven dried to determine the Sticky limit

(a) Cone Penetrometer

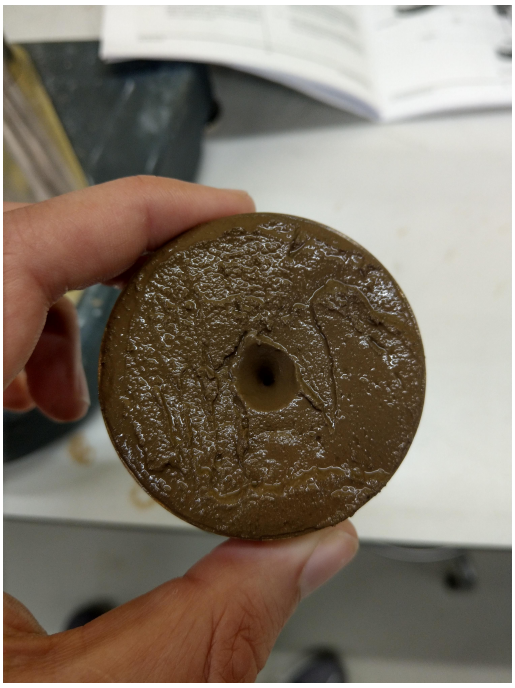

(b) Cone Penetrometer cavity in Clay 1 sample

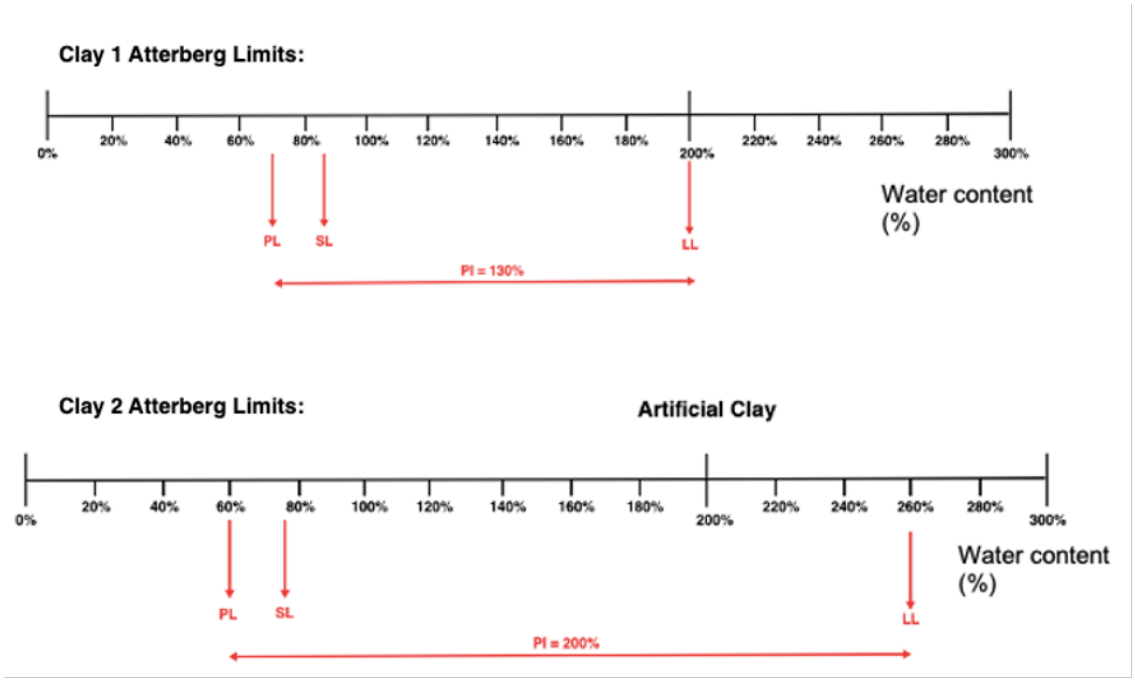

Figure A.6: Atterberg Results for Clay 1 (top) & Clay 2 (bottom)

A.2 Appendix B: Sample Consolidation

Figure A.7: Piston Consolidometer G&E Lab - TU Delft

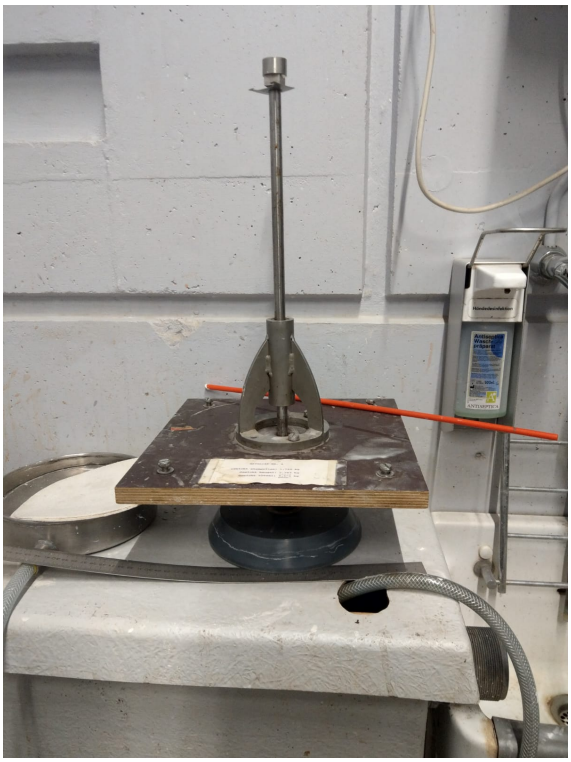

Figure A.8: Consolidometer Piston

Figure A.9: Consolidated Clay 1 Sample from Piston Consolidometer

Figure A.10: Rowe Cell Components

Figure A.11: Rowecell Set-up - G&E Lab TU Delft

Figure A.12: Consolidated Clay 2 Sample from Rowecell

A.3 Appendix C: Tensile Testing

Figure A.13: STICH Unit - G&E Lab TU delft

Figure A.14: Electrical Input volt box

Figure A.15: Manoeuvrable component views with Sensitive Load Cells

Figure A.16: Soil Container for STICH Unit test

Figure A.17: 500 g mass blocks

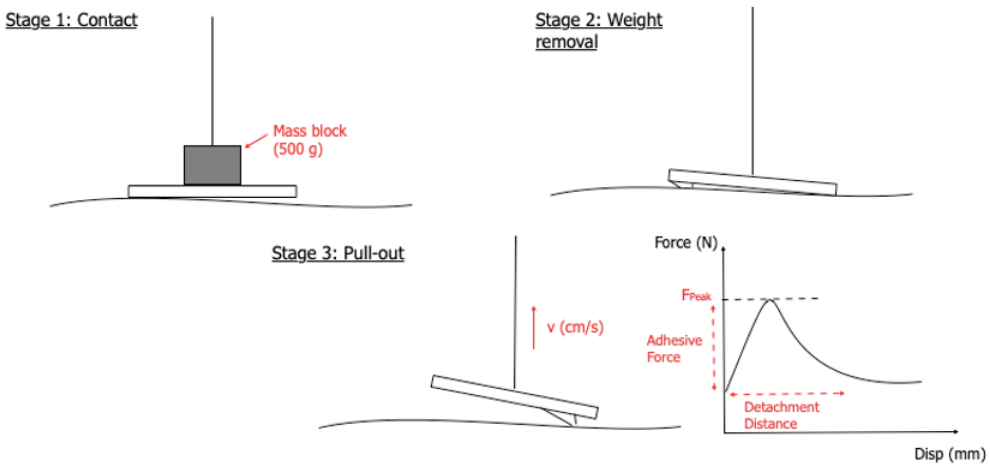

Figure A.18: Tensile Test Steps

A.4 Appendix E: Scaled Testing

Figure A.19: Displacement Sensor RU130U-M18ELIU2PN8x2T-H1151

Figure A.20: Tedea huntleigh model no.615 Load cell - 500 kg limit

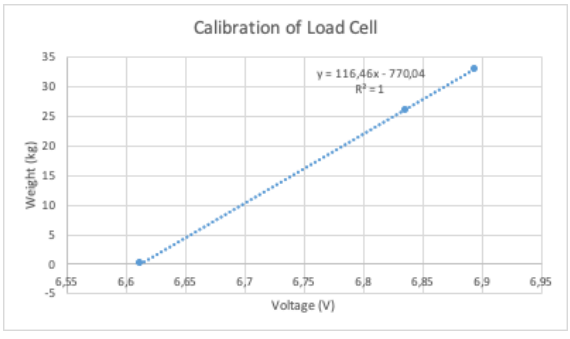

Figure A.21: Calibration line of Load Cell

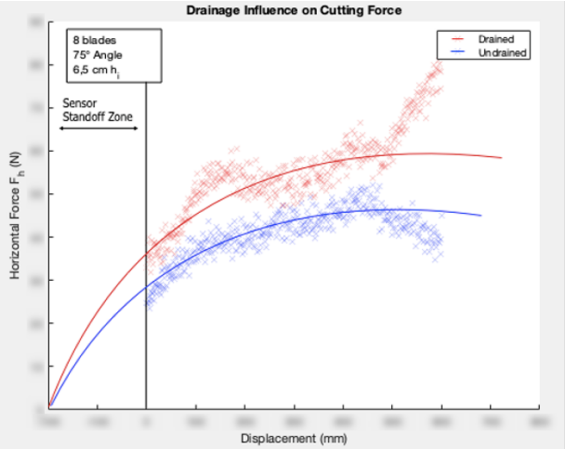

Figure A.22: Effect of Drainage Conditions on Test Runs